Aus dem Institut für Anatomie und Zellbiologie

Geschäftsführender Direktor: Prof. Dr. Ralf Kinscherf

des Fachbereichs Medizin der Philipps-Universität Marburg

# Atherosclerosis: The Role of Growth-Differentiation-Factor-15 (GDF-15) in Human THP-1 Macrophages

## Autophagy and Lipid Homeostasis

Inaugural Dissertation

Zur Erlangung des Doktorgrades der Naturwissenschaften

dem Fachbereich Medizin der Philipps-Universität Marburg

vorgelegt von

Kathrin Ackermann aus Koblenz

Marburg, 2020

Angenommen vom Fachbereich Medizin der Philipps-Universität Marburg

am: 13.08.2020

Gedruckt mit Genehmigung des Fachbereichs Medizin

Dekan: Herr Prof. Dr. H. Schäfer

Referent: Herr Prof. Dr. R. Kinscherf

1.Korreferent: Herr PD Dr. T. Adhikary

# Table of contents

# List of abbreviations

*Table 1:* **List of abbrevations in alphabetical order**

| | |
|---|---|
| % | Percent |
| °C | Degree celsius |
| µg | Microgram |
| µl | Microliter |
| µM | Micromolar |
| aqua dest. | Aqua destillata (destilled water) |
| ABCA-1 | ATP-binding cassette sub-family A member 1 |
| ABCG-1 | ATP-binding cassette sub-family G member 1 |
| ACAT-1 | Acetyl-CoA−Acetyltransferase |
| Actß | Actin-ß |
| AMBRA | Activating molecule in Beclin 1-regulated autophagy protein 1 |
| AMPK | Adenosine monophosphate-activated kinase |
| ApoE | Apolipoprotein-E |
| Ab | Antibody |
| ATG 5 / 12 | Autophagy-related proteins 5 / 12 |
| ATP | Adenosine triphosphate |
| BCA | Bicinchoninic acid |
| bp | Base pair |
| CD11b | Cluster of differentiation molecule 11B |
| CD14 | Cluster of differentiation molecule 14 |
| CD36 | Cluster of differentiation molecule 36 |
| cDNA | Complementary desoxyribonucleic acid |
| CE | Cholesteryl ester |
| CED | Cholesterol-enriched diet |
| CHD | Coronary heart disease |
| cm | Centimeter |
| $CuSO_4$ | Copper sulfate |
| CVD | Cardiovascular disease |
| dNTP | Deoxyribonucleotide triphosphate |
| dl | Deciliter |
| DPBS | Dulbecco's Phosphate-Buffered Saline |
| EC | Endothelial cell |

| | |
|---|---|
| ECM | Extracellular matrix |
| EDTA | Ethylendiaminetetraacetic acid |
| e.g. | Exempli gratia (for example) |
| ELISA | Enzyme-linked immunosorbent assay |
| ER | Endoplasmic Reticulum |
| FFA | Free fatty acids |
| FBS | Fetal bovine serum |
| FC | Free cholesterol |
| g | Gravitational force |
| gr | Gram |
| GDF-15 | Growth-Differentiation-Factor-15 |
| h | Hour |
| HDL | High-density lipoprotein |
| HFD | High-fat diet |
| ICAM-1 | Intercellular adhesion molecule 1 |
| IDL | Intermediate-density lipoprotein |
| IL-1ß | Interleukin-1 beta |
| IL-6 | Interleukin-6 |
| IL-10 | Interleukin-10 |
| IL-1 | Interleukin-1 |
| kDA | Kilo Dalton |
| l | Liter |
| LAL | Lysosomal acid lipase |
| Lamp-1 /2 | Lysosomal associated membrane protein-1 /2 |
| LC3 | Microtubule-associated proteins 1A/1B light chain 3A |
| LDL | Low-density lipoprotein |
| LOX-1 | Lectin-like oxidized low-density lipoprotein receptor-1 |
| M | Molar |
| MΦ | Macrophage |
| MCP-1 | Monocyte chemotactic protein-1 |
| MCSF | Macrophage colony-stimulating factor |
| MDC | Monodansylcadaverine |
| MES | 2-(N-Morpholino)ethansulfonic acid |
| min | Minute |
| ml | Milliliter |
| mM | Millimolar |

| | |
|---|---|
| MMP | Matrix metalloprotease |
| MOMA-2 | Monocyte + Macrophage antibody |
| mRNA | messenger Ribonucleic acid |
| mTOR | Mammalian target of rapamycin |
| mTORC1 | Mammalian target of rapamycin complex 1 |
| NaCl | Sodium chloride |
| nCEH-1 | Neutral cholesteryl ester hydrolase-1 |
| NO | Nitric oxide |
| oxLDL | Oxidized low-density Lipoprotein |
| p62 /Sequestosom-1 | Ubiquitin-binding protein p62 |
| PAD | Peripheral artery disease |
| PBS | Phosphate-buffered saline |
| PE | Phosphatidylethanolamine |
| P/S | Penicillin/Streptomycin (Supplement in culture medium) |
| PDGF | Platelet-derived growth factor |
| PI3K | Phosphatidylinositol 3-kinase |
| PI3P | Phosphatidylinositol 3-phosphate |
| PMA | Phorbol-12-myristate-13-acetate |
| RCT | Reverse cholesterol transport |
| RFU | Relative fluorescence unit |
| rGDF-15 | recombinant Growth-Differentiation-Factor-15 |
| rpm | Revolutions per minute |
| RT | Room temperature |
| RT-qPCR | Real Time-quantitative Polymerase-Chain reaction |
| RIN | RNA integrity number |
| RIPA-buffer | Radio immunoprecipitation assay-buffer |
| RNA | ribonucleic acid |
| rRNA | ribosomale RNA |
| ROS | Reactive oxygen species |
| s | Second |
| SDS | Sodium dodecyl sulfate |
| ssRNA | Single-stranded RNA |
| TC | Total cholesterol |
| ULK1 | Unc-51-like kinase 1 |

| | |
|---|---|
| SDS-PAGE | Sodium dodecyl sulfate polyacrylamide gel electrophoresis |
| SEM | Standard Error of the Mean |
| siRNA | Small interfering RNA |
| Sp-1 | Specificity protein-1 |
| SR-A1 | Scavenger-receptor A1 |
| TGF-β | Transforming growth factor-beta |
| TNF-α | Tumor necrosis factor-alpha |
| Tris | 2-Amino-2-hydroxymethyl-propane-1,3-diol |
| VCAM-1 | Vascular cell adhesion molecule-1 |
| VLDL | Very low-density lipoprotein |

# List of figures

# List of tables

# 1 Introduction

## 1.1 Atherosclerosis

In 2016, Cardiovascular diseases (CVD) were the cause of death of approximately 17.9 million people, representing 31% of all deaths worldwide (status 2017, World Health Organization). Atherosclerosis plays a decisive role in this regard. Atherosclerotic alterations can lead to stroke, coronary heart disease (CHD) or peripheral artery disease (PAD). As a growing number of people are exposed to multiple cardiovascular risk factors, such as obesity, arterial hypertension, hypercholesterolemia, diabetes, nicotine or alcohol abuse, the incidence of CVD is increased. The probability of developing cardiovascular disease also increases with age and the average life expectancy constantly rises. For these reasons, it is important to understand the exact molecular mechanisms and the interaction of the different cell types involved in atherosclerotic development and progression, in order to find new preventive or drug-based methods for treatment.

### 1.1.1 Development and Progression

Atherosclerosis is a disease concerning alterations in human arteries. Arterial vessels consist of three different layers. The tunica intima is the innermost layer, followed by the tunica media and the tunica adventitia as the external layer (reviewed in Tegos et al., 2001). The tunica intima consists of the endothelium, facing the vessel lumen with the circulating blood and the internal lamina elastica consisting of elastin, forming the outermost part. In between endothelium and lamina elastica, the so-called subendothelial space is composed of extracellular matrix molecules produced by a few resident smooth muscle cells (SMC) and also contains resident macrophages (MΦ) and pluripotent cells are present (reviewed in Bobryshev et al., 2016; Libby et al., 2011). Beneath the tunica intima lies the tunica media consisting of SMC, producing elastin, elastic and collagenous fibres. Thereafter, the external elastic lamina, composed of elastin is followed by the adventitia as the outer layer of the vessel. This layer of connective tissue consists of elastic and collagenous fibres with embedded small diameter blood and lymphatic vessels for nutrient supply, whereas the tunica intima and tunica media are nourished by diffusion of molecules from the blood in the arterial lumen (reviewed in Tegos et al., 2001).

Already in the 19th century, Rudolf Virchow described the pathology of atherosclerosis as inflammation (reviewed in Gisterå & Hansson, 2017). In 1913, Nikolai Antischow used rabbits to demonstrate the correlation between cholesterol feeding and atherosclerosis

development (reviewed in Gisterå & Hansson, 2017). More than 60 years later, Ross et al. (1977) published their „response-to-injury“-hypothesis, postulating that atherosclerotic lesion arises from „injury“ of the endothelium as the initiating event (Ross et al., 1977). This was a generally accepted postulation, since certain areas of arteries were found to be especially prone to atherosclerotic lesion development. This includes arterial branching points and bends, where the local disturbance in the blood flow is thought to cause endothelial dysfunction, leading to the invasion of circulating molecules into the subendothelial space (reviewed in Bobryshev et al., 2016). In 1995 Williams and Tabas postulated the alternative „response-to-retention“-hypothesis. Searching for a key event, which is absolutely required as the stimulus to induce atherosclerotic changes, they found that the endothelial injury is not a common feature, since atherogenesis can be initiated without endothelial denudation (Williams & Tabas, 1995). They refined the „response-to-injury“-hypothesis, stating that changes in the endothelium increases its permeability, leading to lipoprotein retention within the arterial wall as the common key event in atherogenesis (Williams & Tabas, 1995). Today, atherosclerosis is in general described as a chronic inflammatory disease triggered by the retention of lipoproteins in the arterial wall (reviewed in Bobryshev et al., 2016). There are several risk factors known to promote increased endothelial permeability such as smoking, hypertension, diabetes mellitus and dyslipidemia (reviewed in Libby et al., 2019).

Based on the present knowledge, the initiating event in atherosclerosis progression is the infiltration of circulating low-density lipoprotein (LDL) particles into the subendothelial space. The retention of these particles on proteoglycans leads to their trapping and biochemical modification through proteases and lipases, which promotes aggregation and further increases proteoglycan binding (reviewed in Gisterå & Hansson, 2017). One prominent LDL modification is the oxidation by myeloperoxidase, lipoxygenase and reactive oxygen species (ROS) found in the subendothelial space (reviewed in Gisterå & Hansson, 2017), but also by resident MΦ located in the arterial wall (reviewed in Glass & Witztum, 2001). The generated oxidized LDL (oxLDL) is internalized by endothelial cells (EC) through the lectin-like oxidized LDL receptor-1 (LOX-1) (reviewed in Pirillo et al., 2013). This initiates an intracellular signaling cascade in the EC, resulting in the expression of E-selectin, P-selectin, vascular cell adhesion molecule-1 (VCAM-1) and intracellular adhesion molecule-1 (ICAM-1) as well as the production of monocyte chemoattractant protein-1 (MCP-1) (reviewed in Pirillo et al., 2013). This leads to the recruiting, rolling, adhesion and finally migration of monocytes and leukocytes into the subendothelial space (reviewed in Bobryshev et al., 2016). Furthermore, oxLDL inhibits the production of nitric oxide (NO) in EC and inactivates NO by increasing cellular ROS production (reviewed in Pirillo et al., 2013). NO is a chemical mediator with anti-

atherogenic properties including vasorelaxation, inhibition of leukocyte-endothelial cell adhesion, platelet adhesion and SMC proliferation (reviewed in Pirillo et al., 2013). In the subendothelial space, the transmigrated monocytes proliferate and differentiate into MΦ in response to oxLDL (Frostegard et al., 1990) or in response to MΦ colony stimulating factor (MCSF) expressed by EC (reviewed in Gisterå & Hansson, 2017). Thereafter, the activated MΦ are polarized to a pro-inflammatory phenotype, called M1 MΦ (reviewed in Bobryshev et al., 2016). These M1 MΦ increasingly express scavenger receptors like SR-A1, cluster of differentiation 36 (CD36) or LOX-1, which account for 75 – 90% of the oxLDL internalization (reviewed in Moore et al., 2013). Unlike LDL-receptors, scavenger receptors are not downregulated in response to intracellular lipid accumulation, a protective mechanism to avoid foam cell formation (reviewed in Gisterå & Hansson, 2017). The uncontrolled uptake of oxLDL promotes an pro-inflammatory response induced by the assembly of toll-like receptors (TLRs) regulated by CD36 (reviewed in Park, 2014; Yu et al., 2013). Activated MΦ secrete pro-inflammatory cytokines such as tumor necrosis factor-α (TNF-α), interleukin-1β (IL-1β) and interleukin-6 (IL-6), which together with ROS further promote the inflammatory response as well as monocyte and T-lymphocyte recruitment (reviewed in Pirillo et al., 2013). Furthermore, the loss of MΦ-polarity is induced by oxLDL, inhibiting the ability to re-migrate into the blood stream (reviewed in Pirillo et al., 2013). This traps them in the subendothelial space, leading to the failure of inflammation resolution and promoting lesion progression (reviewed in Pirillo et al., 2013). Even though there is a large number of pro-inflammatory MΦ in atherosclerotic lesions, alternatively activated anti-inflammatory M2 MΦ are also detected in the more stable regions of the plaque (reviewed in Bobryshev et al., 2016). These type of MΦ are more resistant to foam cell formation and secrete anti-inflammatory factors such as interleukin-10 (IL-10) and interleukin-1 (IL-1) (reviewed in Bobryshev et al., 2016). The M1 phenotype is primarily found in progressing plaques, whereas the M2 phenotype is present in regressing plaques, where M2 MΦ are involved in tissue repair and remodelling (reviewed in Bobryshev et al., 2016). Therefore, the presence of the different phenotypes may reflect the plaque progression and stability (M1 subtype) or regression (M2 subtype) (reviewed in Bobryshev et al., 2016). During plaque progression, the unregulated uptake of oxLDL in MΦ renders them into foam cells, which increasingly produce ROS (reviewed in Pirillo et al., 2013). The oxLDL-derived cholesterol-accumulation in foam cells ultimately leads to the initiation of the apoptotic pathway by the protein p53 (Kinscherf et al., 1998). The released lipids and cell debris accumulate extracellular in the plaque (reviewed in Libby et al., 2011). The ineffective clearance of these residues by MΦ, called efferocytosis, further promotes the formation of a lipid-rich pool (reviewed Libby et al., 2011). This so-called necrotic core, consists of apoptotic and necrotic cells, cholesterol crystals and other extracellular

material (reviewed in Gisterå & Hansson, 2017). Not only dying MΦ, also apoptotic SMC and EC contribute to the necrotic core (reviewed in Pirillo et al., 2013). Upon oxLDL trapping, SMC from the media are stimulated to migrate into the subendothelial space (reviewed in Maiolino et al., 2013). The proliferation of these SMC is induced by oxLDL (reviewed in Pirillo et al., 2013), ROS and the platelet-derived growth factor (PDGF), secreted by MΦ and EC (reviewed in Maiolino et al., 2013).

SMC are able to take up oxLDL by LOX-1 receptors, inducing their proliferation and transdifferentiation into MΦ-like cells (reviewed in Gisterå & Hansson, 2017). Approximately 30% of the plaque SMC express MΦ-markers due to lipid-loading (reviewed in Gisterå & Hansson, 2017). The remaining plaque SMC produce an extracellular matrix composed of collagen, which forms a fibrous cap above the necrotic core and contributes to its stabilization (reviewed in Gisterå & Hansson, 2017). Thereby, enhanced cell migration and proliferation, as well as the formation of the necrotic core is shown in clinical manifestations such as flow-limiting stenosis, which leads to tissue ischemia or provoke thrombus, interrupting blood flow locally or embolizing arteries (reviewed in Libby et al., 2011). Generally, there are different stages during atherosclerotic progression. Early lesions, called fatty streaks, are identified by cholesterol-engorges MΦ in the subendothelial space. These fatty streaks are already found in the first decade of life, but they are not clinically significant, since they are reversible and asymptomatic (reviewed in Lusis, 2000). Fibrous lesions or fibrous plaques are characterized by a growing necrotic core consisting of mostly cholesterol esters and other cell debris from apoptotic or necrotic cells with an overlaying fibrous cap made of extracellular matrix from SMC (reviewed in Lusis, 2000). In advanced plaques, this fibrous cap is degraded by MMP, which are secreted by MΦ, EC and SMC (Galis et al., 1994; reviewed in Pirillo et al., 2013). This alters the lesion to a vulnerable plaque and decreases its ability to withstand the pulsatile forces from the blood, rendering it prone to rupture (reviewed in Gisterå & Hansson, 2017). Vulnerable plaques are characterized by a thin, collagen-poor fibrous cap with only a few SMC and abundant inflammatory cells (reviewed in Lusis, 2000). Rupture of a vulnerable plaque, commonly occurs at the lesion edges, so called plaque shoulders (reviewed in Lusis, 2000). This rupture exposes the necrotic core content to coagulation proteins in the blood, triggering thrombosis (reviewed in Libby et al., 2011).

The aforementioned processes are illustrated in Figure 1, showing the initial trapping and modification of LDL in the subendothelial space with the subsequent activation of EC, MΦ and SMC and following processes.

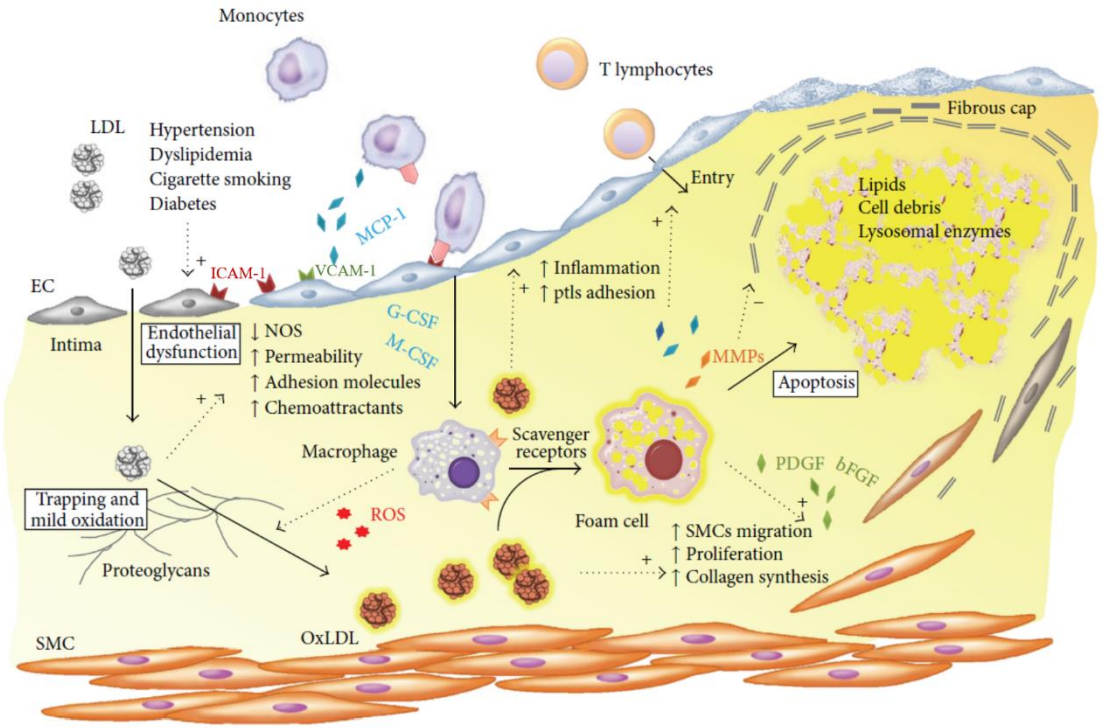


*Figure 1:* **Atherosclerosis development and progression.** Various risk factors can lead to endothelial dysfunction and allow lipoproteins to enter the subendothelial space, where they get trapped on proteoglycans and can be modified. The resulting expression of adhesion molecules on the ECs and the secretion of chemokines enable the adhesion and migration of monocytes and T-lymphocytes. Monocytes differentiate into MΦ upon oxLDL-exposure and cytokines, secreted by ECs. MΦ take up the oxLDL via their scavenger receptors and stimulate the migration and proliferation of SMCs from the media. SMCs secrete various extracellular matrix components and thus, contribute to the formation of a fibrous cap above the necrotic core consisting of dead foam cells. This fibrous cap may get weakened by its degradation through MMPs, secreted by MΦ, SMC and EC (Maiolino et al., 2013; modified).

### 1.1.2 Lipid metabolism in MΦ

In the literature, cholesterol and oxLDL are regularly mentioned, when referring to atherosclerosis and foam cell formation. Cholesterol is a sterol, which is an important plasma membrane component, ensuring membrane fluidity as well as lipid raft assembly and function (reviewed in McLaren et al., 2011). Also, it serves as a precursor for steroid hormones (reviewed in McLaren et al., 2011). Cholesterol can be produced de novo in the liver or is supplied by food intake. Since cholesterol is a hydrophobic molecule, it is transported in the bloodstream via lipoproteins. These particles can accommodate cholesteryl esters, triglycerides and other lipids in their hydrophobic core and are surrounded by a hydrophilic monolayer consisting of apolipoproteins and phospholipids (reviewed in McLaren et al., 2011; Moore & Tabas, 2011). The different lipoproteins are characterised according to their density and thus, their centrifugation behaviour, distinguishing chylomicrons, very low-density lipoprotein (VLDL), intermediate-density lipoprotein (IDL), low-density lipoprotein (LDL) and high-density lipoprotein (HDL)

(reviewed in Moore & Tabas, 2011). These different lipoproteins have different transport pathways within the body and possess different apolipoproteins, as they are the crucial recognition and docking molecule for the membrane receptors of the different target cells (reviewed in McLaren et al., 2011).

As mentioned before, one key initiating step in atherogenesis is the retention and oxidation of LDL in the subendothelial space, triggering the complex immune response described in the previous chapter. For clearance of this oxLDL from the intima, MΦ are the main cell type removing the subendothelially localized oxLDL by phagocytosis. Therefore, recruited monocytes undergo morphological and structural changes, while differentiating into MΦ. The intensification of metabolism, enhanced expression of surface receptors, altered sensitivity to signalling molecules and an increased lysosomal enzyme activity are induced in order to prepare the cells for active phagocytosis and digestion of engulfed material (reviewed Bobryshev et al., 2016). MΦ phagocytize oxLDL via the scavenger receptors like CD36, SR-A1 or LOX-1 (reviewed in Chistiakov et al., 2016). Thereafter, oxLDL is hydrolysed in lysosomes by the lysosomal acid lipase (LAL) (reviewed in Chistiakov et al., 2016). The emerging free cholesterol (FC) and free fatty acids (FFA) may be used for cellular needs, e.g. in cell membranes (reviewed in Fernandez-Ruiz et al., 2016). Esterification of free cholesterol, that is not immediately required, occurs at the endoplasmic reticulum (ER) and is catalysed by acetyl-CoA acetyltransferase-1 (ACAT-1). Thereafter, the lipid droplets (LDs) originate from the ER, composed of a hydrophobic lipid core containing triglycerides and cholesteryl esters (CE) to a varying extend (reviewed in Ouimet, 2013). When needed, these esterified lipids can be re-hydrolysed in the cytosol by neutral cholesteryl ester hydrolase-1 (nCEH-1) (reviewed in Chistiakov et al., 2016). Alternatively, lipolysis occurs by cargo-specific autophagy, in this case lipophagy, in the autophagolysosome by LAL (reviewed in Ouimet, 2013). In the case of excess lipid accumulation, FC is bound to HDL as acceptor, which transports the cholesterol to the liver for excretion (reviewed in Jeong et al., 2017). This reverse-cholesterol transport (RCT) is crucial for cell homeostasis, as most cells cannot catabolize excess cholesterol (reviewed in Remmerie & Scott, 2018). In MΦ the RCT depends on the lipoprotein HDL, as acceptor for FC as well as two members of the ABC transporter subfamily A and G, namely ABCA-1 and ABCG-1 (reviewed in Remmerie & Scott, 2018). These transporters are membrane proteins that are able to actively transport different substances across the cell membrane to various acceptors, by consuming adenosine-triphosphate (ATP) (reviewed in Vasiliou et al., 2009). When HDL is not available as acceptor, FC is re-esterified by ACAT-1 at the ER for further storage (reviewed in Ouimet, 2013). Furthermore, under physiological conditions CE in MΦ undergoes constitutive cycles of esterification and hydrolysis as a measure to control

cholesterol availability for cell membranes (reviewed in Ouimet, 2013). The re-esterification of FC by ACAT-1 functions as a protective response to excess FC accumulation, when the RCT-pathway is saturated (reviewed in Jeong et al., 2017). One rate-limiting step in the efflux of FC is the hydrolysis of neutral lipids from the LDs, since only FC, not CE can be exported to HDL (Ouimet, 2013). A special role in lipolysis and RCT was attributed to autophagy, since autophagosomes can deliver LDs for bulk degradation to the lysosome for hydrolysis, followed by ABC transporter-dependent efflux (reviewed in Jeong et al., 2017; Singh & Cuervo, 2012). This autophagy-dependent lipolysis for RCT is called lipophagy and was found to be activated in MΦ during excess lipid loading conditions, like in atherosclerotic plaque (Ouimet et al., 2011). The aforementioned phagocytosis, intracellular processing and RCT of oxLDL in MΦ is depicted in Figure 2.

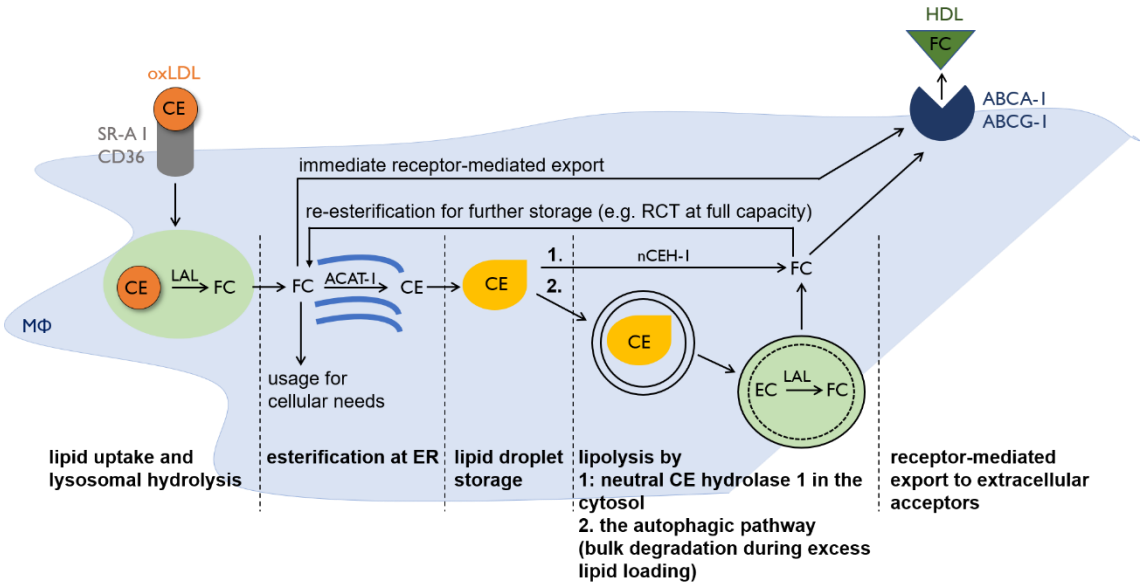


*Figure 2:* **MΦ cholesterol metabolism.** Cholesteryl esters are transported in the blood system bound to lipoproteins like LDL. In the subendothelial space, LDL is oxidized and binds with high affinity to scavenger receptors (SR-A1, CD36, LOX-1) expressed on MΦ. After phagocytosis, oxLDL is hydrolysed in the lysosome by LAL, generating FC. Thereafter, FC is used for cellular needs or can be exported out of the cell. Furthermore, MΦ can store lipids within lipid droplets (LDs) for later usage. Therefore, FC is esterified by ACAT-1 at the ER. For reverse cholesterol transport (RCT) out of the cell, CE, which is stored in LDs, is re-hydrolysed **1.** by neutral CE hydrolase-1 (nCEH-1) in the cytosol, or **2.** LDs in whole or in part can be degraded by autophagy, involving lysosomal hydrolyzation. Both ways are common under normal conditions, whereas the latter is especially important during excess lipid loading conditions. The anew emerging FC can be exported by the transporters ABCA-1 or ABCG-1 to extracellular acceptor HDL. When no acceptor is available or the transporters capacity is reached, FC is re-esterified for further storage.

The balance between hydrolysis and esterification to maintain cholesterol homeostasis, preventing foam cell formation is extremely sensitive and fragile (reviewed in Chistiakov et al., 2017). MΦ have different accommodation mechanisms during increased lipid

burden. The accumulation of cellular cholesterol activates different transcription factors in order to elevate ABCA-1 and ABCG-1 expression for increased RCT (reviewed in Remmerie & Scott, 2018). Additionally, the increased LAL activity upon elevated lipid influx also contributes to the regulation of ABCA-1 activity and expression (reviewed in Jeong et al., 2017). Nevertheless, in advanced lesions the dominating pro-inflammatory stimuli upregulate the expression of scavenger receptors, downregulate the ABCA-1 and ABCG-1 transporters, increase ACAT-1 activity and downregulate nCEH-1 activity, leading to a dysregulated MΦ lipid-handling, ultimately initiating apoptosis and necrotic core formation (reviewed in Chistiakov et al., 2017). Furthermore, for the efficient efferocytosis of apoptotic cells by surrounding MΦ, an intact lipid metabolism is required (reviewed in Moore et al., 2013). A dysfunctional lipid metabolism further increases apoptotic events in the atherosclerotic plaque and decreases efferocytosis, resulting in secondary necrosis, further contributing to the necrotic core expansion (reviewed in Moore et al., 2013). This seems to be a fatal cycle, since an increased plaque lipid burden not only contributes to the plaque volume, but also enhances the plaque associated inflammation (reviewed in Ghosh et al., 2010). With prolonged lipid burden, the protective mechanisms for lipid handling are overwhelmed, leading to the accumulation of FC in various cell- and organelle membranes (e.g. lysosomes and ER) (reviewed in Moore et al., 2013). This impairs their activity, ultimately inducing apoptosis by further triggering inflammation and stress responses (reviewed in Moore et al., 2013). Since lesional MΦ mainly accumulate CE-enriched lipid droplets (reviewed in Ouimet, 2013) and unmodified LDL was not found to cause CE-accumulations as massively as modified LDL in plaque MΦ (reviewed in Chistiakov et al., 2017), oxLDL still remains the primarily lipid causing foam cell formation in atherosclerosis.

As already mentioned, one protective mechanism during excess lipid loading is MΦ lipophagy (Figure 2). This pathway degrades LDs in bulk to avoid foam cell formation (reviewed in Ouimet et al., 2011). Besides MΦ lipophagy, autophagy was described to be activated in numerous cell types involved in atherosclerotic lesions (reviewed in De Meyer & Martinet, 2009). In the following chapter the autophagy process and autophagy in atherosclerosis are described in further detail.

## 1.2 Autophagy

Autophagy is an evolutionary conserved intracellular lysosomal pathway for degradation and recycling of various cellular constituents including excess or damaged organelles, misfolded or aggregate-prone proteins and infectious agents (reviewed in Bento et al., 2016; Cecconi & Levine, 2008). Generally, there are three forms of autophagy,

distinguished on basis of mechanism of cargo sequestration (reviewed in Hansen et al., 2018). Microautophagy describes the sequestration of cytoplasmic components directly into the lysosomes for acid hydrolase degradation (reviewed in Hansen et al., 2018). Chaperone-mediated autophagy is the selective degradation of proteins with the KFERQ-like motif, which are recognized by chaperones, then unfolded and translocated to the lysosome (reviewed in Hansen et al., 2018). Finally, macroautophagy refers to the degradation of cytosolic material via the sequestration into double-membrane vesicles, called autophagosomes, which fuse with lysosomes for cargo degradation (reviewed in Hansen et al., 2018). The fusion of the outer autophagosomal membrane with the lysosomal membrane, give rise to the autophagolysosome, where the formal inner autophagosomal membrane with its content is degraded by lysosomal hydrolases (reviewed in Christian et al., 2013). This described macroautophagy is hereafter referred to as autophagy.

Autophagy is a constitutive process, being active in most mammalian cells at basal levels, functioning as a homeostatic mechanism (reviewed in Christian et al., 2013). It gets increasingly activated during starvation and related cellular stress, degrading macromolecules to provide energy (reviewed in Bento et al., 2016). Nevertheless, it is also involved in cellular development, differentiation and aging (reviewed in Christian et al., 2013). Autophagy plays an important role in health and disease, since it can degrade aggregate-prone intracytoplasmic proteins causing various neurodegenerative disorders like Dementia, Parkinson- or Huntington-Disease (reviewed in Bento et al., 2016). Furthermore autophagy appears to have roles in metabolic and cardiac disease, stroke and hematopoiesis (reviewed in Bento et al., 2016). In the innate and adaptive immunity, autophagy acts protectively against infectious disease caused by pathogenic agents (reviewed in Bento et al., 2016; Christian et al., 2013).

### 1.2.1 Autophagic process

Autophagosomes are formed throughout the cytoplasm and are trafficked along microtubules via dynein to bring the double-membrane vesicles in proximity to lysosomes (reviewed in Bento et al., 2016). The autophagosomes originate from precursor structures, called the phagophore, which start growing from both ends sequestering bulk cytoplasm and organelles until it finally closes (reviewed in Cecconi & Levine, 2008). The first identification of autophagy-relevant genes (ATG) essential for autophagosomes formation was mostly carried out in yeast and later on the mammalian orthologs were identified (reviewed in Bento et al., 2016). The autophagic process can be distinguished in autophagy initiation, membrane nucleation, cargo recognition, membrane elongation

and closure, followed by autophagosome maturation through the fusion with the lysosome to form the autophagolysosome and finally the degradation (reviewed in Christian et al., 2013). The key upstream regulators in autophagy include the nutrient sensors mammalian target of rapamycin (mTOR) and adenosine monophosphate-activated kinase (AMPK) (reviewed in Hansen et al., 2018). The mTOR complex 1 (mTORC1) is a cell-growth regulator, integrating nutrient signals and cytokines from different pathways, acting as inhibitor for autophagy and promoting cell growth (reviewed in Li et al., 2016). Whereas AMPK is a conserved heterotrimeric protein kinase, acting as key energy sensor, maintaining the balance of ATP generation and consumption, thereby affecting cell growth and proliferation (reviewed in Zhu et al., 2017). Under normal physiological conditions, mTORC1 acts as kinase and inactivates the Unc-51-like kinase 1 (ULK1) complex, a conserved kinase, which serves as the key upstream initiator of autophagy (reviewed in Hansen et al., 2018). When nutrients are lacking, adenosine monophosphate increases, leading to the AMPK-mediated activation of the ULK1 complex for autophagy induction (reviewed in Cecconi & Levine, 2008). Simultaneously, AMPK represses the mTORC1 kinase activity (Kim, et al., 2011). ULK1 is a tetrameric kinase complex formed by ULK1, ATG13, ATG101 and FAK-family interacting protein of 200 kDa, FIP200 (reviewed in Bento et al., 2016). After activation, ULK1 phosphorylates activating molecule in Beclin-1-regulated autophagy (AMBRA) which activates the phosphatidylinositol 3-kinase (PI3K) III nucleation complex, composed of vacuolar protein sorting 15, VSP15, VPS34, ATG14 and Beclin-1 (reviewed in Li et al., 2016). Thereafter, the PI3K III complex marks a distinct ER membrane with phosphatidylinositol 3-phosphate (PI3P). This recruits two ubiquitin-like conjugation systems to the phagophore initiation site, essential for phagophore elongation and closure (reviewed in Chun & Kim, 2018). One is the ATG12 conjugation system, including ATG12, ATG5 and ATG16L1 (reviewed in Chun & Kim, 2018). Initially, this complex-formation is triggered by ATG7 in an ATP-dependent way, transferring ATG12 to the E2-like conjugating enzyme ATG10, forming the ATG12-ATG10 intermediate (reviewed in Li et al., 2016). Next, ATG12 is covalently attached to ATG5 and finally the interaction with the homodimer ATG16L1 creates the ATG12-ATG5-ATG16L1 conjugate, called the ATG12 conjugation system (reviewed in Li et al., 2016). This conjugate operates as a E3 ubiquitin ligase, playing a role in the phagophore membrane nucleation, elongation and closure (reviewed in Chun & Kim, 2018). Furthermore, the ATG12 conjugation system is involved in the procession and translocation of the microtubule associated protein light chain 3 (LC3) to the phagophore membrane (reviewed in Chun & Kim, 2018). LC3 is firstly cleaved by the cysteine protease ATG4 into LC3 I and further processed by ATG7 and ATG3 (reviewed in Chun & Kim, 2018). Finally, LC3 I is conjugated to the substrate phosphatidylethanolamine (PE), now called LC3 II, with the help of the ATG12

conjugation system and attached to the autophagosomal membrane (reviewed in Chun & Kim, 2018). Even if the phagophore originates from the ER membrane, the autophagosomal membrane is not entirely composed of ER-membrane fragments. Mitochondria, the trans-Golgi network, late endosomes and the plasma membrane also contribute to the phagophore elongation by providing parts of their membranes, orchestrated with the help of ATG9 (reviewed in Chun & Kim, 2018). LC3 II also participates in cargo recognition by interacting with various autophagy receptors or cargo receptors bound to proteins or organelles (reviewed in Hansen et al., 2018). One of these autophagy receptors is the protein sequestosome-1/p62, which recognizes ubiquitylated proteins and organelles targeted for degradation (reviewed in Hansen et al., 2018). These autophagy receptors are mandatory for selective autophagy and clearance of specifically marked cargo (reviewed in Hansen et al., 2018). After the LC3 II-orchestrated sequestration of p62 and its cargo into the autophagosome, the autophagosomal membrane closes. After closure, the ATG12 conjugation system dissolves from the outer autophagosomal membrane, being available for further autophagosome build-up (reviewed in Mehrpour et al., 2010). Since LC3 II is localized in both, the inner and outer autophagosomal membrane, it dissociates from the outer membrane, but remains on the inner membrane after autophagosome closure and is later on degraded in the autolysosome (reviewed in Chun & Kim, 2018). The newly formed autophagosome with its sequestrated cargo is now transported to lysosome, where the outer autophagosomal membrane fuses with the lysosomal membrane to form the autophagolysosome, regulated by the cytoskeleton and lysosomal membrane proteins like lysosomal associated membrane proteins-1 and -2 (Lamp-1 and Lamp-2) (reviewed in Li et al., 2016). This releases the now single-membrane autophagic vesicle into the lysosomal lumen with its acid enzymes and degrades the autophagic body including its cargo (reviewed in Dikic & Elazar, 2018). The emerging catabolic products are released in the cytoplasm for recycling or for export (reviewed in Li et al., 2016). These different stages in the autophagy process and the mentioned key regulators are depicted in Figure 3.

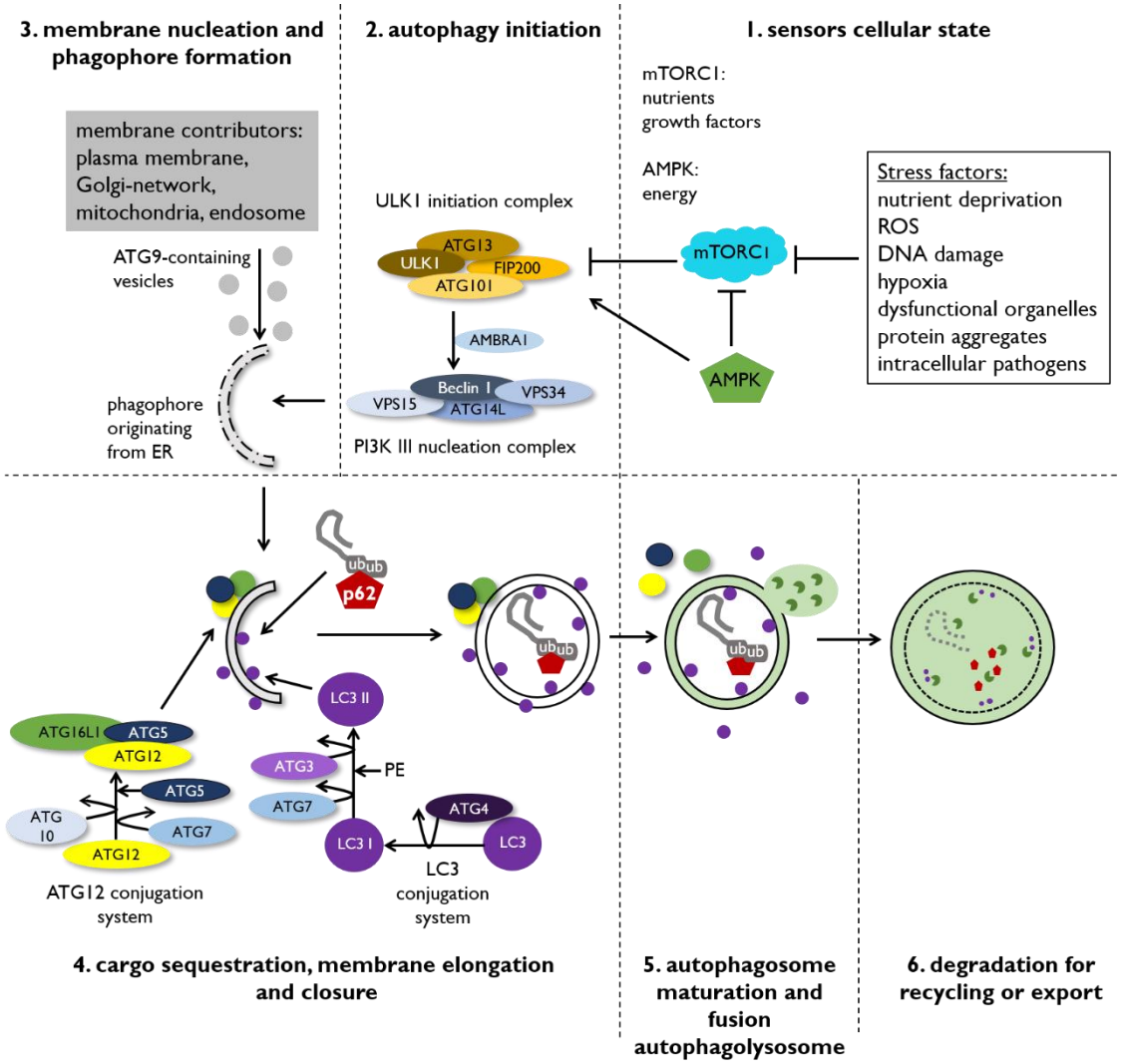


*Figure 3:* **Autophagy signaling pathway.** Upon cellular stress, autophagy is initiated by the activation of AMPK and by repressing the inhibitory effect of mTORC1 on the ULK 1 initiation complex. This leads to changes in the kinase activity of ULK1, recruiting AMBRA1 to activate the PI3K III nucleation complex. These complexes then translocate to the ER membrane, initiating membrane remodeling to give rise to the phagophore. Besides the ER membrane, other membrane contributors are the plasma membrane, the Golgi-network, mitochondria and endosome. Essential for the phagophore elongation and closure, as well as the cargo sequestration into the growing autophagosome, are the two ubiquitin-like conjugation systems composed of ATG12-ATG5-ATG16L1 and LC3 II. After autophagosome closure, ATG12-ATG5-ATG16L1 dissociate from the autophagosomal membrane, being available for further autophagosome formation. The LC3 II on the inner membrane remains with the sequestered, ubiquitinated cargo and its autophagy adaptor p62. After fusion of the outer autophagosomal membrane with the lysosome, the remaining autophagic vesicle is degraded by lysosomal enzymes. The emerging components can be re-used for cellular needs or exported out of the cell.

### 1.2.2 Autophagy in Atherosclerosis

While the autophagic process is constantly occurring at basal level in the cell, autophagy is more apparent in a wide range of diseases, including CVD (reviewed in Martinet & De Meyer, 2009). In numerous cell types, found in human atherosclerotic plaques,

autophagy activity was verified by transmission electron microscopy and immunohistochemical analysis (Liu et al., 2015). SMC and MΦ in the fibrous cap, as well as ECs of the plaque shoulders, increasingly expressed LC3 II as evidence for increased autophagic activity (Liu et al., 2015). An increased autophagic activity in atherosclerosis seems to be reasonable, since several autophagic triggers like inflammatory mediators, ROS and oxLDL are present in atherosclerotic plaques (reviewed in Maiuri et al., 2013). During lesion formation autophagy is thought to protect plaque cells against oxidative stress, inflammation, hypoxia and metabolic stress, promoting cell survival, decelerating plaque progression and promoting plaque stability (reviewed in De Meyer & Martinet, 2009; Maiuri et al., 2013). Though, excessively stimulated autophagy may cause cell death of SMC, leading to reduced collagen synthesis and plaque destabilization (reviewed in De Meyer & Martinet, 2009). Whereas autophagy-induced apoptosis of ECs can lead to acute clinical events by promoting lesional thrombosis (reviewed in De Meyer & Martinet, 2009).

In plaques of atherogenic mice, MΦ predominantly expressed autophagy-related proteins like ATG8, LC3 or p62 (Liao et al., 2012; Razani et al., 2012; Liu et al., 2016). In atherosclerotic plaques of $ApoE^{-/-}$ mice on western diet for <2 months, plaques in the aortic root showed high levels of LC3 expression and much of this LC3 was co-localized with p62 (Sergin, et al., 2017), indicating an intact autophagy. After 3-4 months on western diet, these mice still had high levels of p62, but the LC3 expression was reduced and the LC3 / p62 co-localization markedly vanished, indicating a declined autophagosome formation (Sergin, et al., 2017). Human atherosclerotic plaques, obtained from discarded carotid endarterectomy specimens were dissected, distinguishing regions with no, minimal or maximal atherosclerotic changes (Sergin et al., 2017). Areas lacking atherosclerotic changes only expressed LC3 and no p62, indicative for basal autophagy without accumulation of autophagic cargo (Sergin et al., 2017). In minimally diseased regions and advanced lesions p62 was detectable, whereas LC3 intensity was found to be reduced and p62 co-localized with polyubiquitin, indicative for marked cargo by autophagic degradation (Sergin et al., 2017). Furthermore, in advanced atherosclerotic plaques, increased p62 accumulations were found together with bigger lesion sizes and larger necrotic cores (Liao et al., 2012; Razani et al., 2012). Analyses on MΦ-specific ATG5-deficiency in atherogenic mice, compared with MΦ-specific ATG5-potent mice showed an increased plaque formation and inflammasome hyperactivation, indicated by elevated IL-1ß serum levels as well as aortic IL-1ß expression (Razani et al., 2012). Furthermore, in atherosclerotic mice models, MΦ autophagy-deficiency caused increased apoptosis and oxidative stress, ultimately promoting plaque necrosis and impairing lesional efferocytosis (Liao et al., 2012). As

already described, MΦ autophagy is an important mechanism to resolve the subendothelial accumulated oxLDL by aiding in MΦ lipid homeostasis (Ouimet et al., 2011). This protects from foam cell formation and furthermore ensures the efficient efferocytosis of death cells by MΦ (reviewed in Kurdi et al., 2016). However, the initial protective autophagy is impaired with lesion progression, since with increasing plaque burden p62- and ubiquitin-tagged protein inclusions increase, indicative for a compromised autophagic clearance (reviewed in Evans et al., 2017). A dysfunctional autophagy was shown to enhanced plaque formation by influencing multiple atherogenic aspects like foam cell, inflammasome hyperactivation, enhanced apoptosis with concomitant defects in efferocytosis and finally accumulation of cytotoxic organelles and proteins (reviewed in Sergin & Razani, 2014). Due to these anti-atherogenic properties and to rescue autophagy activity in atherosclerotic plaque, multiple groups experimented with rapamycin or rapamycin-derivates (e.g. Everolimus) to activate autophagy by mTOR inhibition. Inducing autophagy by mTORC1 inhibition indeed showed to attenuate atherosclerotic plaque progression (Baetta et al., 2009; Beutner et al., 2012; De Meyer et al., 2012; Martinet et al., 2007; Mueller et al., 2008; Verheye et al., 2007). Although this is a promising new therapeutic approach, there are still a lot of investigations required to establish this method of treatment.

## 1.3 Growth-Differentiation-Factor-15

### 1.3.1 The cytokine GDF-15

Growth-differentiation-factor-15 (GDF-15) was firstly described in a sequence analysis of activated MΦ by Walsh et al., 1995. Due to a seven cysteine domain in the protein sequence, GDF-15 was classified as cytokine divergently belonging to the transforming growth factor-β superfamily (TGF-β) (Fairlie et al., 1999). GDF-15 is synthesized as a 62 kDa dimeric propeptide and after cleavage by a furin-like protease, its secreted as a 25 kDa disulfide-linked dimeric protein (Fairlie et al., 1999). Various adult tissues e.g. brain, prostate, kidney, lung, liver and spleen, heart, thymus and pituitary gland express GDF-15 (Böttner, Suter-Crazzolara, et al., 1999; Böttner, Laaff, et al., 1999). In addition, GDF-15 expression is increased in human placenta (Lawton et al., 1997) and the developing brain (Schober et al., 2001). The cytokine GDF-15 is a useful marker for diagnostic and risk stratification, since it is expressed and secreted upon multiple stress factors (e.g. inflammation, oxidative stress, hypoxia, telomere erosion and oncogene activation) (reviewed in Brown et al., 2006; Wollert et al., 2016). Increased GDF-15 levels are associated with obesity, cancer, diabetes or CVD such as hypertrophy, heart failure, endothelial dysfunction and atherosclerosis (reviewed in Adela & Banerjee, 2015). Therefore, GDF-15 was attributed a role in metabolic, cardiovascular and chronic

diseases, as well as obesity and cancer, making it an useful biomarker (reviewed in Adela & Banerjee, 2015). Several studies investigated the relation between GDF-15 serum levels and various diseases. Healthy women with higher baseline GDF-15 serum levels were found to be at increased risk for cardiovascular events (Brown et al., 2002; Lin et al., 2014). In elderly individuals, GDF-15 was found to be a strong predictor of all-cause and non-cardiovascular mortality (Daniels et al., 2011). The cytokine GDF-15 is also described to influence metabolic processes (reviewed in Emmerson et al., 2018). In this context, GDF-15-deficient mice revealed an increased body weight and had increased adipose tissue due to increased food intake (Tsai et al., 2013). Furthermore, GDF-15-deficient mice were more prone to high-fat-diet (HFD)-induced obesity (Tran et al., 2018) and prone to increased lipid-deposition in the liver (Kim et al., 2018). Mice with diet-induced obesity, treated with GDF-15, showed weight loss due to lower food intake (Mullican et al., 2017; Tsai et al., 2018). Transgenic mice overexpressing GDF-15 had decreased body weight and less white adipose tissue (Kim et al., 2013; Macia et al., 2012), improved glucose tolerance, lower insulin levels and were reported to be resistant to dietary- and genetic-induced obesity (Chrysovergis et al., 2014; Macia et al., 2012).

### 1.3.2 GDF-15 in atherosclerosis

Several studies reported an elevated GDF-15 serum level as a strong predictor for cardiovascular events (reviewed in Adela & Banerjee, 2015). The expression of GDF-15 in mononuclear cells and MΦ is induced by various stimuli like IL-1β, IL-2, TNF-α, MCSF, Phorbol-12-myristate-13-acetate (PMA), ceramide, oxLDL or hydrogen peroxide, thus GDF-15 is associated with MΦ activation (Bootcov et al., 1997; Fairlie et al., 1999; Schlittenhardt et al., 2004; Schober et al., 2001). Furthermore, GDF-15 is increasingly expressed in the atherosclerotic artery wall, where it colocalizes with plaque MΦ (Bonaterra et al., 2012; de Jager et al., 2011). GDF-15 was found to influence MΦ lipid homeostasis (Wu et al., 2014), additionally, MΦ showed increased GDF-15 expression upon oxLDL-exposure. *In vitro* analyses revealed an impact of GDF-15 on the cholesterol efflux by increased expression of the ABCA-1 transporter, also known as the cholesterol efflux regulatory protein [CERP] (Wu et al., 2014). Furthermore, an elevated circulating level of GDF-15 is associated with endothelial activation and vascular inflammation (Eggers et al., 2012). A pro-atherogenic impact of GDF-15 has been reported by Bonaterra et al. (2012) and de Jager et al. (2011). The expression of the pro-inflammatory cytokine IL-6 was significantly decreased in peritoneal MΦ from GDF-15$^{-/-}$ / ApoE$^{-/-}$ mice compared to MΦ from ApoE$^{-/-}$ mice, when exposed to 100 µg/ml oxLDL for 12h (Bonaterra et al., 2012). Furthermore, peritoneal MΦ from GDF-15$^{-/-}$ / ApoE$^{-/-}$ mice incubated with 20 ng/ml rGDF-15 for 12h showed elevated IL-6 expression (Bonaterra

et al., 2012). GDF-15 mRNA and protein levels increased in peritoneal MΦ of ApoE$^{-/-}$ mice after 12 and 20 weeks on a cholesterol-enriched-diet (CED) (Bonaterra et al., 2012). Additionally, GDF-15-deficient mice, which had been fed a CED displayed an increased body weight, as well as blood triglyceride- and cholesterol levels (Bonaterra et al., 2012). Though, CED-fed GDF-15$^{-/-}$ / ApoE$^{-/-}$ mice revealed decreased lumen stenosis in the aortic arch compared to CED-fed ApoE$^{-/-}$ mice (Bonaterra et al., 2012). In agreement with this, de Jager et al. (2011) reported an upregulation of GDF-15 in murine atherosclerotic lesions with disease progression. They used LDLR$^{-/-}$ mice transplanted with bone marrow from GDF-15$^{-/-}$ mice, which received a western-diet for 4 to 12 weeks (de Jager et al., 2011). These double-knockout mice showed reduced MΦ infiltration, decreased necrotic core formation as well as improved plaque stability (de Jager et al., 2011). However, anti-atherogenic effects of GDF-15 were published by Johnen et al. (2012) and Preusch et al. (2013). LDLR$^{-/-}$ mice transplanted with bone marrow from GDF-15$^{-/-}$ mice with 24 weeks atherogenic-diet showed an increase of lesional-MΦ accumulation and thinner fibrous caps compared to control mice (Preusch et al., 2013). Johnen et al. (2012) investigated a model for advanced atherosclerosis, by keeping ApoE$^{-/-}$ mice, which also overexpressed GDF-15, on a high-fat-diet for 6 months. ApoE$^{-/-}$ mice overexpressing GDF-15 revealed smaller lesions in the aortic sinus and thoracic aorta, but showed no differences in lesion composition compared to ApoE$^{-/-}$ mice. Likewise, neither changes in the cytokine production nor in serum levels of lipids were detectable, comparing ApoE$^{-/-}$ mice overexpressing GDF-15 to ApoE$^{-/-}$ mice (Johnen et al., 2012). These studies attribute GDF-15 as an important, yet ambiguous role in atherosclerosis, especially in plaque MΦ. Though, the varieties concerning the used atherosclerotic mouse-models and the variability in the duration of atherogenic-diet should be considered, when comparing these findings.

## 1.4 Aim of this study

Autophagy was found being highly activated and acting protective in human atherosclerotic lesions (Liao et al., 2012; Razani et al., 2012). Especially in MΦ, autophagy is involved in RCT to prevent foam cell formation (Ouimet et al., 2011), lesion progression and necrotic core formation (Liao et al., 2012; Razani et al., 2012). The cytokine GDF-15 was also found to be implicated in MΦ lipid efflux (Wu et al., 2014) and is highly expressed in plaque MΦ (Schlittenhardt et al., 2004). Therefore, in this study the impact of the cytokine GDF-15 on MΦ autophagy and lipid homeostasis was investigated. By influencing MΦ autophagy, GDF-15 could be a valuable target in atherosclerosis by reducing plaque size or improving plaque stability through regulation of autophagy activity. In order to investigate the impact of GDF-15 on MΦ autophagy and lipid homeostasis, we examined the autophagy and lysosome activity, as well as the lipid loading and cholesterol levels using THP-1 MΦ with modified GDF-15 protein level.

# 2 Material and Methods

## 2.1 Material

### 2.1.1 Instruments/Equipment

*Table 2:* **Instruments/Equipment with producer in alphabetical order.**

| Instrument/Equipment | Producer |
|---|---|
| Autoklav Heratherm Oven OMS 100 | Fisher Scientific GmbH, Schwerte, Germany |
| Bench HERASafe® HS18 | Kendro Laboratory Products GmbH, Hanau, Germany |
| Bioanalyzer 2100 | Agilent Technologies Inc., Santa Clara, USA |
| Camera AxioCam MRm | Carl Zeiss AG, Oberkochen, Germany |
| Centrifuge Perfect Spin P | PEQLAB Biotechnologie GmbH, Erlangen, Germany |
| Centrifuge Pico 17 | Heraeus Holding GmbH, Hanau, Germany |
| Centrifuge Heraeus ™ Biofuge PrimoR | Thermo Fisher Scientific Inc. Waltham, USA |
| Chip Priming Station | Agilent Technologies Inc., Santa Clara, USA |
| Confocal laser scanning microscope Nikon Eclipse Ti | Nikon GmbH, Geschäftsbereich Mikroskope, Düsseldorf, Germany |
| Cytation™ 3 microplate reader | BioTek Instruments Inc., Winooski, VT, USA |
| FIREBOY plus safety Bunsen Burner | INTEGRA Biosciences GmbH, Fernwald, Germany |
| Fusion-SL 3500.WL Imaging System | PEQLAB Biotechnologie GmbH, Erlangen, Germany |
| Heracell™ 150 $Co_2$ Incubator | Thermo Fisher Scientific Inc. Waltham, USA |
| Hybridization Oven MK II | MWG-Biotech AG, Ebersberg, Germany |
| HydroFlex™ Microplate Washer | Tecan Group Ltd; Männedorf, Switzerland |
| Ice-crasher Scotsman AF103 | Kälte Kamrath GmbH & Co.KG, Linden, Germany |

| | |
|---|---|
| Kern KB 3600-2N Precision balance 0.01gr : 3600gr | Kern & Sohn GmbH, Balingen, Germany |
| Magnetic stirrer IKA® C-MAG MS4 | IKA®-Werke GmbH & Co. KG, Staufen, Germany |
| Mini Trans-Blot® Cell | Bio-Rad Laboratories Inc., Hercules, USA |
| MJ-Research PTC-200 Thermocycler | Global Medical Instrumentation Inc., Ramsey, USA |
| Multipipette® plus | Eppendorf AG, Hamburg, Germany |
| Mx3005P qPCR System | Agilent Technologies Inc., Santa Clara, USA |
| NanoDrop 200C, UV-Vis Spectrophotometer | Thermo Fisher Scientific Inc., Waltham, USA |
| Nikon Eclipse TS 100 Invert Microscope | Nikon GmbH, Düsseldorf, Germany |
| pH-Meter 761 Calimatic. | Knick Elektronische Messgeräte GmbH & Co.KG, Berlin, Germany |
| Pipetman Classic™ P10, P20, P100, P200, P1000 | Gilson Inc. Middleton, USA |
| Pipetus® 100-240 Volt | Hirschmann Laborgeräte GmbH & Co. KG, Eberstadt, Germany |
| Platform shaker Promax 1020 | Heidolph Instruments GmbH & Co.KG, Schwabach, Germany |
| PowerEase® 500 Power Supply | Life Technologies GmbH, Darmstadt, Germany |
| Tecan Sunrise Microplate Reader | Tecan Group Ltd; Männedorf, Switzerland |
| Microtube Thermoshaker PHMT-PSC-18 | Grant Instruments Ltd., Cambridge, UK |
| TKA GenPure with xCAD Dispenser | Thermo Electron LED GmbH, Niederelbert, Germany |
| Ultrasonic bath Sonorex | BANDELIN Electronic GmbH & Co.KG, Berlin, Germany |
| PCR Workstation Pro | PEQLAB Biotechnologie GmbH, Erlangen, Germany |
| Vakuum concentrator Bachhofer: BA-VC-300H | Mc Labor oHG, Albstadt, Germany |
| Vakuum pump BVC 21 NT | VACUUBRAND GmbH & Co. KG, Wertheim, Germany |

| | |
|---|---|
| Vortexer MS 3 | IKA®-Werke GmbH & Co. KG, Staufen, Germany |
| Vortexer VTX-3000L Uzusio | LMS Consult GmbH & Co. KG, Brigachtal, Germany |
| Zeiss Axiovert 135 (inverted epifluorescence microscop) | Carl Zeiss AG, Oberkochen, Germany |
| XCell SureLock™ Mini Cell Electrophoresis System | Life Technologies GmbH, Darmstadt, Germany |

### 2.1.2 Consumption items

*Table 3*: **List of consumption items with producer in alphabetical order.**

| **Consumption item** | **Producer** |
|---|---|
| 12-well, 24-well, 96-well CELLSTAR® Multiwell culture plates | Greiner Bio-One International GmbH, Kremsmünster, Austria |
| 96-well Immuno Plates, transparent, U96 MaxiSorp (GDF-15 Elisa) | Fisher Scientific GmbH, Schwerte, Germany |
| 96-well Polysterol Microplate, transparent (BCA-Protein-Assay) | Greiner Bio-One International GmbH, Kremsmünster, Austria |
| AriaMx 96-well skirted low profile plate (RT-PCR) | Agilent Technologies Inc., Santa Clara, USA |
| Amersham Protran® Premium 0,2µM NC Nitrocellulose Blotting Membran | GE Healtcare Life Science, Freiburg, Germany |
| C-Chip DHC-N01 Neubauer improved | Digital Bio, Hopkinton, USA |
| Cell flasks T25, T75, T175 Stand., Vent.Cap. | Sarstedt AG & Co, Nümbrecht, Germany |
| Cell Scraper 300mm | TPP techno Plastic Products AG, Trasadingen, Switzerland |
| Combitips advanced 0.5 ml, 5 ml | Eppendorf AG, Hamburg, Germany |
| Lumox® multiwell, 96-well plate | Sarstedt AG &Co., Nümbrecht, Germany |
| Microcentrifuge Tube w/lid, 0,5 ml | BrandTech Scientific Inc., Essex, UK |
| Nitrile gloves Nobaglove-Nitril | NOBA Verbandmittel Danz GmbH & Co. KG, Wetter, Germany |
| NuPAGE™ Novex™ 4-12% Bis-Tris Protein Gels, 1.0 mm, 12-well | Life Technologies GmbH, Darmstadt, Germany |

| | |
|---|---|
| Optical strip caps (12 strips) (RT-PCR) | Agilent Technologies Inc., Santa Clara, USA |
| PARAFILM® "M" | Pechiney Plastic packing, Chicago Il., USA |
| SafeSeal Tips Premium Cell Saver, 0.1-1000 µl, steril | Biozym Scientific GmbH, Hessisch Oldendorf |
| SafeSeal Microtubes, 0.5 ml,1.5 ml, 2 ml, transparent | Sarstedt AG & Co., Nümbrecht, Germany |
| Serological Pipette, with cottonplug, 5 ml, 10 ml, 25 ml | SARSTEDT AG & Co., Nümbrecht, Germany |
| Slide-A-Lyzer Dialysis Cassettes 7K MWCO (nLDL oxidation) | Thermo Fisher Scientific Inc., Waltham, USA |
| Tube, 15 ml and 50 ml | SARSTEDT AG & Co., Nümbrecht, Germany |
| TTP cell scraper 240mm | TPP Techno Plastic products AG, Trasadingen, Switzerland |
| Whatman ® Blotting Paper | GE Healthcare Life Science, Freiburg, Germany |

### 2.1.3 Reagents and Substances

Table 4: **Reagents and substances with producer in alphabetical order.**

| **Reagents/Substances** | **Producer** |
|---|---|
| Acetic acid 100% | Carl Roth GmbH & Co. KG, Karlsruhe, Germany |
| Agarose standard | Carl Roth GmbH & Co. KG, Karlsruhe, Germany |
| AllStars Negative Control siRNA | QIAGEN GmbH, Hilden, Germany |
| AllStars Hs Cell Death siRNA | QIAGEN GmbH, Hilden, Germany |
| Bovine Serum Albumin (BSA) Fraktion V | PAA Laboratories GmbH, Pasching, Austria |
| Calciumchlorid-Dihydrate | Merck KGaA, Darmstadt, Germany |
| Chloroform | Merck KGaA, Darmstadt, Germany |
| Coomassie Brilliant Blue G-250 dye | Thermo Fisher Scientific Inc., Waltham, USA |
| Crystal violet | Merck KGaA, Darmstadt, Germany |
| Cupper(II) sulfate pentahydrate ($CuSo_4$) | Merck KGaA, Darmstadt, Germany |

| | |
|---|---|
| DAPI | Carl Roth GmbH & Co. KG, Karlsruhe, Germany |
| Destilled Water, DNase/RNase free | Life Technologies GmbH, Darmstadt, Germany |
| DNase I, RNase-free | Fisher Scientific GmbH, Schwerte, Germany |
| dNTP-Mix | Agilent Technologies Inc., Santa Clara, USA |
| Dulbecco's Phosphate-Buffered Saline (PBS) (1x) (without Ca & Mg) | PAA Laboratories GmbH, Pasching, Austria |
| Ethylendiamintetraacetate (EDTA) | Fisher Scientific GmbH, Schwerte, Germany |
| EDTA Disodiumsalt Dihydrat (nLDL-Oxidation) | VWR International GmbH, Darmstadt, Germany |
| Ethanol 96% | Sigma-Aldrich Co. LLC, St.Louis, USA |
| Ethanol 70% | AppliChem GmbH, Darmstadt, Germany |
| Fetal bovine serum (FBS) | Capricorn Scientific GmbH, Ebsdorfergrund, Germany |
| Glycerin | Carl Roth GmbH & Co. KG, Karlsruhe, Germany |
| Glycine 99% PA | Carl Roth GmbH & Co. KG, Karlsruhe, Germany |
| Goat serum Batch: B11-035 | PAA Laboratories GmbH, Pasching, Austria |
| HiPerFect® Transfection Reagent | QIAGEN GmbH, Hilden, Germany |
| Isopropanol > 99,7% | AppliChem GmbH, Darmstadt, Germany |
| Methanol | Merck KGaA, Darmstadt, Germany |
| ß-Mercaptoethanol | Merck KGaA, Darmstadt, Germany |
| Native human low-density lipoprotein (nLDL) | RayBiotech Inc., Norcross, GA, USA |
| Sodium chloride (NaCl) 99,8% | Carl Roth GmbH & Co. KG, Karlsruhe, Germany |
| Sodium dodecyl sulfate (SDS) Pellets >99% | Carl Roth GmbH & Co. KG, Karlsruhe, Germany |
| Nonident™ P-40 (NP-40) | Sigma-Aldrich Co. LLC, St.Louis, USA |
| NuPAGE® Antioxidant | Invitrogen, Eugene, USA |
| NuPAGE® MES 20x (SDS Running Buffer) | Invitrogen, Eugene, USA |
| Oil-Red-O-Dye | Alfa Aeser GmbH & Co.KG, Karlsruhe, Germany |
| Oligo $(dt)_{15}$-Primer | Fisher Scientific GmbH, Schwerte, Germany |

| | |
|---|---|
| Paraformaldehyde (PFA) | Merck KGaA, Darmstadt, Germany |
| Penicillin/Streptomycin 100x | Capricorn Scientific GmbH, Ebsdorfergrund, Germany |
| Powdered Milk, blotting-grade, low-in-fat | Carl Roth GmbH & Co. KG, Karlsruhe, Germany |
| peqGOLD Trifast™ | PEQLAB Biotechnologie GmbH, Erlangen, Germany |
| Phosphate-buffered saline (PBS) 10x without $Ca^{2+}$, $Mg^{2+}$ | LONZA Group AG, Basel, Switzerland |
| Phosphate-buffered saline (PBS) 1x without $Ca^{2+}$, $Mg^{2+}$ | LONZA Group AG, Basel, Switzerland |
| Phorbol-12-myristate-13-acetate (PMA) | Sigma-Aldrich Co. LLC, St.Louis, USA |
| Protease/Phosphatase Inhibitor Cocktail 100x | Cell Signaling Technology Inc., Danvers, MA, USA |
| Reaction buffer with $MgCl_2$ (10x) | Fisher Scientific GmbH, Schwerte, Germany |
| recombinant GDF-15 protein<br>#1437 9580 20<br>species: human, source: CHO | provitro AG, Berlin, Germany |
| RIPA Lysis Puffer, 10x | Cell Signaling Technology Inc., Danvers, MA, USA |
| RNase Away | Molecular BioProducts Inc., San Diego, USA |
| RPMI-STA,<br>RPMI 1640 with stable Glutamine | Capricorn Scientific GmbH, Ebsdorfergrund, Germany |
| RPMI-XRXA<br>RPMI 1640, w/o L-Glutamine,<br>w/o Phenol Red | Capricorn Scientific GmbH, Ebsdorfergrund, Germany |
| Hydrochloric acid 1mol/l | Merck KGaA, Darmstadt, Germany |
| SigmaFAST™ OPD Peroxidase Substrate | Sigma-Aldrich Co. LLC, St.Louis, USA |
| Trinitrobenzene sulfonic acid (TNBSA) | Thermo Fisher Scientific Inc., Waltham, USA |
| Tris Base 99,9% PA | Carl Roth GmbH & Co. KG, Karlsruhe, Germany |
| Trypan blue 0,4% | Merck KGaA, Darmstadt, Germany |
| Triton X-100 | Sigma-Aldrich Co. LLC, St.Louis, USA |
| Tween® 20 | Carl Roth GmbH & Co. KG, Karlsruhe, Germany |

### 2.1.4 Buffers and Solutions

*Table 5:* **Buffers/Solutions in alphabetical order.**

| Buffers/Solutions | Ingredients |
|---|---|
| Blocking Solution (5% milk powder in TTBS) | 5 g milk powder<br>per 100 ml TTBS |
| Coomassie Blue dye solution (agarose gel) | 100 mg Coomassie Blue<br>25 ml Ethanol (100%)<br>5 ml acetic acid<br>ad 100 ml aqua dest. |
| Destain solution (destain Coomassie Blue dye solution for agarose gel) | 10 % Acetic acid (100%)<br>10 % Ethanol (96%)<br>in aqua dest. |
| Loading buffer (agarose gel) | 0.25 % (w/v) Bromphenol blue<br>30 % (v/v) Glycerin<br>ad 1 ml aqua dest. |
| NuPAGE® MES 1x (SDS Page Running Buffer) | 10 ml NuPAGE® 20x MES (SDS Page Running Buffer)<br>500 µl NuPAGE® Antioxidant<br>ad 200 ml aqua dest. |
| NuPAGE® 4x loading buffer (SDS Page) | 5,6 mM Tris Base<br>4,22 mM Tris HCL<br>2,77 mM SDS<br>20,53 mM EDTA<br>43,4 mM Glycerin<br>200 µl Bromphenol blue (1%)<br>ad 1 ml aqua dest.<br>pH 8,5<br>add before use 200 mg DTE/ml |
| Oil-Red-O stock solution | 3 mg/ml Oil-Red-O in 100% isopropanol |
| Oil-Red-O working solution | 3:2; stock solution:aqua dest. |
| RIPA (1x)<br>incl. Protease/Phosphatase Inhibitor | 1:10 10x RIPA in aqua dest.<br>1:100 Protease/Phosphatase-Inhibitor |
| RPMI 1640 culture medium for THP-1 cells | 445 ml RPMI 1640<br>50 ml FKB (10%)<br>5 ml P/S (1%) |
| Stripping buffer (after Amersham) | 62,5 mM Tris Base in 500 ml aqua dest.<br>2% SDS |

| | |
|---|---|
| | pH 6,7<br>add 139,5 µl ß-Mercaptoethanol<br>before use |
| TAE buffer (50x)<br>(agarose gel) | 242 g Tris-Base<br>57.1 ml acetic acid<br>100 ml 0.5 M EDTA<br>ad 1000 ml aqua dest. |
| TAE buffer (1x)<br>(agarose gel) | 5 ml TAE (50x)<br>245 ml aqua dest. |
| Transfer buffer (10x)<br>(SDS Page) | 0,25 M Tris Base<br>1,92 M Glycin<br>in 1l aqua dest. |
| Transfer buffer (1x)<br>(SDS Page) | 800 ml aqua dest.<br>100 ml 10x Transfer Puffer<br>100 ml Methanol |
| Washing buffer (5x)<br>(Western Blot) | 1,99 M Tris Base<br>2,49 M NaCl<br>29,55 mM EDTA<br>0,5% Tween 20<br>ad 2 l aqua dest.<br>pH 7,5 |

### 2.1.5 Used Kits

*Table 6:* **Used Kits in alphabetical order with ingredients and producer.**

| Kit | Ingredients | Producer |
|---|---|---|
| AceGlow™ Chemiluminescence Substrate | • Ace Glow Solution A (stabile Peroxid)<br>• Ace Glow Solution B (Luminol) | PEQLAB Biotechnology GmbH, Erlangen, Germany |
| Affinity Script Multiple Temperature Reverse Transcriptase | • Affinity Script Multiple Temperature Reverse Transcriptase<br>• 10x Affinity Script RT Puffer<br>• 100 mM DTT | Agilent Technologies Inc., Santa Clara, USA |

| | | |
|---|---|---|
| Agilent RNA 6000 Nano Kit | • Agilent RNA 6000 Nano Chips<br>• Electrode cleaners<br>• Spin filters<br>• Agilent RNA 6000 Ladder<br>• RNA Nano Dye Concentrate<br>• Agilent RNA 6000 Nano Marker<br>• Agilent RNA 6000 Nano Gel Matrix | Agilent Technologies Inc., Santa Clara, USA |
| Brilliant III Ultra-Fast SYBR® Green QPCR Master Mix | • 2x Brilliant III Ultra-Fast SYBR® Green QPCR Master Mix<br>• ROX Reference Dye (1mM) | Agilent Technologies Inc., Santa Clara, USA |
| Cell Meter™ Autophagy Assay Kit | • 500X Autophagy Blue™<br>• Stain Buffer<br>• Wash Buffer | AAT Bioquest® Inc. Sunnyval, CA, USA |
| Cholesterol / Cholesteryl Ester Quantification Assay Kit (Colorimetric / Fluorometric) | • Cholesterol Assay Buffer<br>• Cholesterol Probe<br>• Enzyme Mix<br>• Cholesterol Esterase | Abcam plc., Cambridge, UK |
| DuoSet® ELISA Human GDF-15 | • Human GDF-15 Capture Antibody<br>• Human GDF-15 Detection Antibody<br>• Human GDF-15 Standard<br>• Streptavidin-HRP | R&D Systems Inc., Minneapolis, USA |
| FlexiTube GeneSolution siRNA for GDF-15 | • Hs_GDF15_1<br>• Hs_GDF15_2<br>• Hs_GDF15_4<br>• Hs_GDF15_5 | QIAGEN GmbH, Hilden, Germany |
| LysoBrite™ Red | • 500X LysoBrite™ dye | AAT Bioquest® Inc. Sunnyval, CA, USA |

| | | |
|---|---|---|
| Pierce™ BCA Protein Assay Kit | • Pierce BCA Protein Assay Reagent A<br>• Pierce BCA Protein Assay Reagent B | Fisher Scientific GmbH, Schwerte, Germany |

### 2.1.6 Antibodies

*Table 7:* **Used Antibodies in alphabetical order.**

| Antibody | Description | Cat.no | Producer | Dilution | MW (kDa) |
|---|---|---|---|---|---|
| *Primary antibodies* | | | | | |
| anti-alpha tubulin | rabbit anti-alpha tubulin antibody | Ab4074 | Abcam plc., Cambridge, UK | 1:4000 | 50 |
| anti-ATG12 | monoclonal rabbit anti-ATG12 antibody | D88H11 | Cell Signaling Technology, Inc., Danvers, MA, USA | 1:1000 | 16 (free ATG12) 60 (ATG12 -ATG5) |
| anti-ATG5 | monoclonal rabbit anti-ATG5 antibody | D5F5U | Cell Signaling Technology, Inc., Danvers, MA, USA | 1:1000 | 56 |
| anti-Beclin-1 | monoclonal rabbit anti-Beclin-1 antibody | D40C5 | Cell Signaling Technology, Inc., Danvers, MA, USA | 1:1000 | 60 |
| anti-mTOR | rabbit anti-mTOR antibody | 2972 | Cell Signaling Technology, Inc., Danvers, MA, USA | 1:1000 | 289 |
| anti-p62 (SQSTM1) | monoclonal rabbit anti-p62 antibody | D5E2 | Cell Signaling Technology, Inc., Danvers, MA, USA | 1:1000 | 62 |
| anti-p62 (SQSTM1) IF preferred | monoclonal rabbit anti-p62 antibody | D10E10 | Cell Signaling Technology, Inc., Danvers, MA, USA | 1:400 (IF) | |
| anti-phospho-mTOR (Ser2448) | rabbit anti phosphor-mTOR (Ser2448) antibody | 2971 | Cell Signaling Technology, Inc., Danvers, MA, USA | 1:1000 | 289 |
| anti-Lamp-1/CD107a (IF) | polyclonal rabbit anti-Lamp-1/CD107a antibody | NB120-19294 | Novus Biologicals, LLC, Centennial, CO, USA | 1:100 (IF) | |
| *Secondary antibodies* | | | | | |
| anti-rabbit IgG | donkey anti-rabbit IgG, | NA9340 | GE Healthcare Life Science | 1:3000 | |

| | | | | |
|---|---|---|---|---|
| | HRP-linked $F(ab')_2$-fragment | | Freiburg, Germany | |
| anti-rabbit IgG (H+L) | goat anti-rabbit igG, (H+L) $F(ab')_2$-fragment Alexa Fluor® 488 conjugate | 4412 | Cell Signaling Technology, Inc., Danvers, MA, USA | 1:1000 |
| anti-rabbit IgG (H+L) | goat anti-rabbit igG, (H+L) $F(ab')_2$-fragment Alexa Fluor® 555 conjugate | 4413 | Cell Signaling Technology, Inc., Danvers, MA, USA | 1:1000 |

### 2.1.7 Primers

*Table 8:* **Used Primers.** All primers were purchased from Qiagen GmbH, Hilden, Germany**.**

| Gene symbol | detected transcript | amplicon length | Cat.no |
|---|---|---|---|
| *Reference gene* | | | |
| Actin β, Actβ | NM_001101 | 146 | QT00095431 |
| *Gene of interest* | | | |
| Growth-Differentiation-Factor 15, GDF-15 | NM_004864 | 114 | QT00082558 |

### 2.1.8 Software

*Table 9:* **Used Software.**

| Equipment | Software | Company |
|---|---|---|
| Chemiluminescence (Evaluation Western Blot) | Fusion Capture 1609B | PEQLAB Biotechnologie GmbH, Erlangen, Germany |
| Confocal laser scanning microscope Nikon Eclipse Ti | NIS Elements 4.30.01 64-bit 2014 | Nikon GmbH, Geschäftsbereich Mikroskope, Düsseldorf, Germany |
| Graphical Illustration | Microsoft Excel 2016 | Microsoft Corporation, Redmond, USA |
| Java-based image processing | Image J 1.52a | National Institutes of Health, Bethesda, USA |
| Light microscope images | AxioVision Release 4.8.2 | Carl Zeiss AG, Oberkochen, Germany |
| Real Time PCR | MxPro QPCR Software | Agilent Technologies Inc., Santa Clara, USA |

| | | |
|---|---|---|
| Statistical analyses | Sigma Plot 12.0 | Systet Software Inc., Chicago, USA |

### 2.1.9 THP-1 cells

| | |
|---|---|
| Cell line: | THP-1 |
| DSMZ no.: | ACC 16 |
| Species: | human (Homo sapiens) |
| Cell type: | acute monocytic leukemia |
| Origin: | established from the peripheral blood of a 1-year-old boy with acute monocytic leukemia (AML) at relapse in 1978; the cells can be used for induction of differentiation studies;<br>the cells were described to produce lysozyme and to be phagocytic; carries t(9;11)(p21;q23) leading to MLL-MLLT3 (MLL-AF9) fusion gene |
| Reference(s): | 14493, 15021, 15022, 18187 |
| | |
| Biosafety level: | 1 |
| Permissions and Restrictions: | A |
| Morphology: | round, single cells in suspension, partly in clusters |
| Medium: | 90% RPMI 1640 + 10% heat-inactivated FBS<br>+ 1% Pen/Strep |
| Incubation: | at 37 °C with 5% $CO_2$ |
| Doubing Time: | ca. 35-50 hours |
| Harvest: | saturation density at about 1.0 x 106 cells/ml |
| Storage: | frozen with 70% medium, 20% FBS, 10% DMSO |

Source: DSMZ, 2020

## 2.2 Methods

### 2.2.1 Cell Culture

All experiments were performed under a sterile working bench.

#### *2.2.1.1 Defrosting and culturing of THP-1 monocytes*

THP-1 cells, which were stored in liquid nitrogen, were quickly defrosted by placing them in the cell incubator at 37°C. Then, the cells were resuspended in 10 ml RPMI 1640 cell medium with L-Glutamine, which was supplemented with 10% heat-inactivated FBS, 100

U/ml Penicillin and 0.1 mg/ml Streptomycin. After centrifugation at 250 x g for 10 min at room temperature (RT), the supernatant was removed, the cell pellet resuspended in 1 ml fresh medium and transferred into a 25 $cm^2$ flask containing 9 ml medium. Thereafter the cell culture was maintained at 37°C in a humified cell incubator at an atmosphere with 5% $CO_2$.

#### *2.2.1.2 Cell splitting and cell counting*

THP-1 cells were cultivated until they reached 1x$10^6$ cells/ml. Then, the cell suspension was transferred into a 50 ml tube and centrifuged for 10 min at 250 x g and RT. After discarding the supernatant, the cells were resuspended in 10 ml medium. For further cultivation or experimental implementation, the exact cell number in the suspension was determined using a C-Chip Neubauer-improved disposable counting chamber. Therefore, 10 µl cell suspension was mixed with trypan blue (1:10) and incubated for 1 min at RT. This diazo dye stains dead cells blue, while living cells do not absorb the dye. Subsequently, 10 µl of the mixture was placed in a disposable counting chamber (C-Chip Neubauer improved) and the cell count was determined under the light microscope. For the determination of the cell count, living cells (trypan blue negative) were counted in the four corner squares and the cell concentration was calculated with the following formula:

$$\frac{\text{living cells in 4 squares}}{4\ [\text{squares}]}\ \text{x}\ 10\ [\text{dilution fator}]\ \text{x}\ 10.000\ [\text{chamber factor}] = \text{cells/ml}$$

Thereafter, the appropriate cell number could be calculated and used for experiments. For further cultivation, the amount of 1x$10^5$ cells/ml were suspended in 1 ml medium and put into a new cell culture flask (75$cm^2$) together with 30 ml fresh medium, cultivated at 37°C and 5% $CO_2$.

#### *2.2.1.3 Differentiation of THP-1 monocytes into THP-1 MΦ*

To investigate the influence of GDF-15 on THP-1 MΦ, THP-1 monocytes were differentiated into MΦ. The differentiation was induced by exposing THP-1 monocytes to 80 nM PMA for 72h. Therefore, 3.5x$10^5$ cells/ml were seeded in 96-well, 24-well or 12-well plates, depending on the experiment to be performed. Then, the cells were cultured in culture medium (RPMI 1640 + 10% FKS + 1% P/S) supplemented with 80nm PMA for 72h. Afterwards, a 24h resting-period was performed in culture medium. The differentiated cells now adhered to the bottom of the culture plate and usually showed an elongated, flattened morphology. Non-adherent and therefore, non-differentiated cells were removed during medium change.

#### *2.2.1.4 Transfection of THP-1 MΦ*

To investigate the GDF-15 dependent MΦ autophagy and lipid homeostasis, the GDF-15 protein level was decreased in THP-1 MΦ by transfecting the cells with small interfering RNA (siRNA) against GDF-15. After the resting period, the differentiated THP-1 MΦ were transfected with 4 different siRNAs directed against 4 different sequences of the GDF-15 mRNA to increase the efficacy of GDF-15 mRNA degradation. The AllStars Negative Control siRNA (Qiagen) was used as negative control. Since this siRNA has no known homologies to any mammalian gene, the gene expression should not be affected by this siRNA. The AllStars Hs Cell Death siRNA (Qiagen) was used as positive control, degrading mRNA of ubiquitously expressed survival genes and thus, inducing cell death. 50nM of the corresponding siRNA were dissolved in 200 µl medium without supplements per well (for a 24-well plate) together with 3 µl HiPerFect transfection reagent (transfection-solution). After vortexing for 10 s, the solutions were incubated at RT for 5-10 min. Before transfection, the cells were washed with medium without supplements. Thereafter transfection-solution was added to the cells dropwise. Afterwards, the transfected THP-1 MΦ were incubated for 6h at 37°C and 5% $CO_2$. After 6h, 300 µl medium per well, supplemented with FBS, but without P/S were added. Thereafter, the cells remained in the incubator for 48h. Afterwards, the cells transfected with AllStars Hs Cell Death siRNA were evaluated by light microscopy to verify the successful transfection by identifying dead cells. Subsequently, the cells transfected with i) siRNA against GDF-15 or ii) siRNA negative control were washed and further exposed to oxLDL, described in the next chapter.

#### *2.2.1.5 Lipoprotein- and rGDF-15-exposure*

After transfection, cells were washed with medium to remove the transfection reagents. Thereafter, THP-1 MΦ were exposed to 50 µg/ml oxLDL to induce foam cell formation or cells were left in culture medium for 4h. Another experimental approach to investigate GDF-15 dependent MΦ autophagy and lipid homeostasis was the augmentation of the GDF-15 protein level with recombinant GDF-15 (rGDF-15). In this experimental setting, THP-1 MΦ were exposed to 50 µg/ml oxLDL and/or rGDF-15 for 4h, immediately after PMA-induced differentiation and the 24h resting-period. After 4h exposure-time, the cells were harvested or fixed, depending on the following experiments. An overview of the experimental setting is depicted in Figure 4.

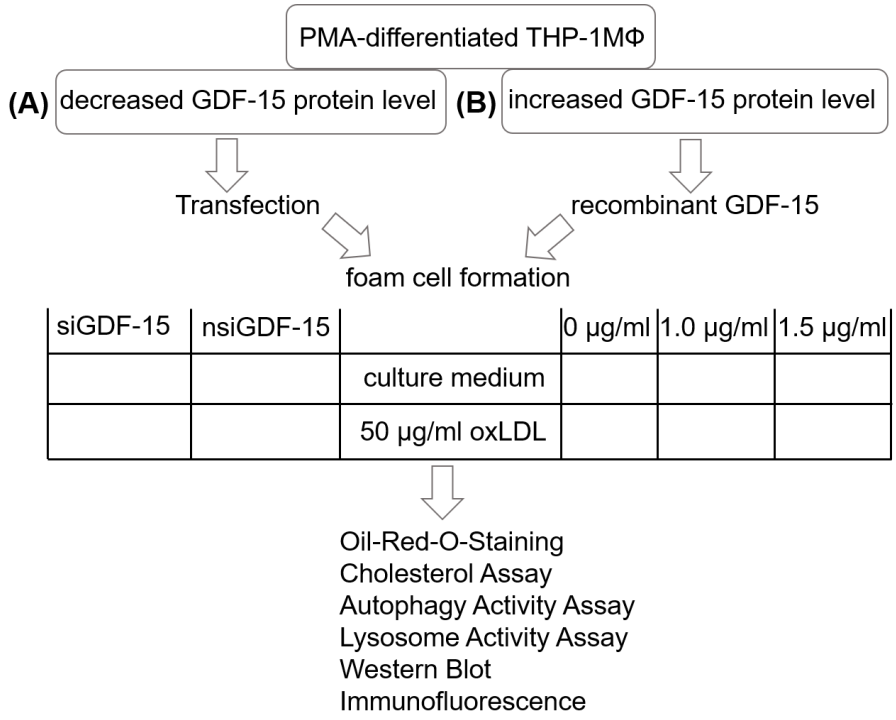


*Figure 4:* **Experimental Setting.** (A) To decrease the GDF-15 protein level, PMA-differentiated THP-1 MΦ were transfected with siRNA against GDF-15 (siGDF-15) or negative control (nsiGDF-15). Thereafter, THP-1 MΦ remained in culture medium or were exposed to 50 µg/ml oxLDL to induce foam cell formation. (B) In order to increase the GDF-15 protein level, THP-1 MΦ were exposed to 1.0 µg/ml or 1.5 µg/ml recombinant (r)GDF-15. To induce foam cell formation in THP-1 MΦ with elevated GDF-15 protein levels, cells were incubated with the combination of 1.0 µg/ml or 1.5 µg/ml rGDF-15 and 50 µg/ml oxLDL. As controls, THP-1 MΦ were incubated with 50 µg/ml oxLDL alone or cells were left in culture medium (0 µg/ml rGDF-15). Thereafter, THP-1 MΦ were.harvested or fixed, depending on the further experimental procedure.

### 2.2.2 Molecular Biology

#### *2.2.2.1 RNA preparation with PeqGold Trifast*

After transfection and lipoprotein-exposure, THP-1 MΦ were harvested and the RNA was isolated. In order to avoid contamination and degradation of the RNA, the tools used and the working surface were firstly cleaned with RNase AWAY. After removal of the supernatant, 200 µl Trifast per well (12-well-plate) was added under a fume hood. After an incubation period of 2-3 min on ice, the cells were scraped off with a cell scraper and transferred to an RNase free tube on ice. After 5 min incubation at RT, 40 µl chloroform were added and the tube was repeatedly inverted for 15s. By centrifugation at 4°C and 13 000 rpm for 5 min (Heraeus ™ Biofuge PrimoR) the homogenate was separated into 3 phases. The aqueous, upper phase contained the RNA, the interphase contained the DNA and the organic, lower phase contained the proteins. After transferring the upper phase into a new tube, 100 µl isopropanol was added. After thorough mixing, the

samples were left on ice for 15 min, followed by centrifugation for 30 min at 13 000 rpm and 4°C to precipitate the RNA. The RNA pellet was carefully freed from the supernatant and washed twice with 500 µl 70% ethanol. After addition of ethanol, the samples were centrifuged again for 5 min at 13 000 rpm and 4°C (Heraeus ™ Biofuge PrimoR). After the last washing step and removal of the supernatant, the pellet was air dried under the fume hood. As soon as the residual ethanol completely evaporated the pellet was carefully dissolved by pipetting up and down several times with 15 µl $H_2O$ including RiboLock (1 µl RiboLock added to 100 µl $H_2O$). For complete dissolution of the RNA the samples were incubated for 10 min at 60°C on the heating block. After dissolution the RNA was stored at -80°C until further processing.

#### *2.2.2.2 RNA concentration measurement with NanoDrop*

The RNA concentration was determined by absorption measurement at 260 nm wavelength, using NanoDrop 200C. Since the absorption unit corresponds to 40 µg ssRNA/ml, the concentration was determined using the following formula:

$$c\left[\frac{\mu g\ RNA}{ml}\right] = A(260)\ x\ 40$$

For measurement, 1µl RNA was applied and measured twice in a row. Furthermore, the absorption ratio A260/A280 provides information about the purity of the sample. For pure RNA the ratio should be between 1.9-2.1.

#### *2.2.2.3 RNA integrity-control with Bioanalyzer*

The integrity of the isolated RNA was determined using the Agilent RNA 6000 Nano Kit with the Agilent 2100 Bioanalyzer. With this technique, based on the principle of capillary electrophoresis, the RNA samples are separated according to their fragment size by the molecular sieve effect, using a polymer. Based on the ratio of the ribosomal subunit 28s to 18s rRNA, the software determines a RIN value between 1 (completely degraded RNA) and 10 (completely intact RNA). For the nanochip analysis, all RNA samples (1µl) previously had to be adjusted with RNase-free water to a concentration between 5 ng/µl and 500 ng/µl. Additionally, the RNA Ladder was heat-denatured for 2 min at 70°C and stored in 1.3 µl portions at -80°C until usage. Furthermore, 550 µl of the Agilent 6000 Nano Gel Matrix were centrifuged through a filter for 10 min at 1500 x g. Thereafter, the Matrix was aliquoted in 65 µl portions and stored at 4°C for up to 4 weeks. Before loading, the chip, the solutions (RNA Nano Dye Concentrate (in the dark), Agilent RNA 6000 Nano Marker and the gel matrix) were equilibrated at RT. Immediately before

loading of the chip, 1 µl dye solution was pipetted onto 65 µl gel matrix and centrifuged for 10 min at 13.000 rpm. After the Gel-Dye-Mix was pipetted into the chip, an evenly distribution of the solution was achieved by using the Priming Station. Thereafter, 5 µl RNA Nano Marker were pipetted into each sample well. Then 1 µl RNA Ladder or 1 µl RNA sample were added. After vortexing the loaded chip for 1 min at 2000 rpm, the analysis was performed with the Bioanalyzer and evaluated with the included software. Only RNA samples with a RIN value >7 were used for subsequent experiments.

#### *2.2.2.4 DNA digestion with DNAse I*

In order to remove any residual DNA from the RNA samples, a DNA digestion using the enzyme DNase I was performed. For this purpose, 1 µg of isolated RNA was used and a digestion-mix was prepared according to the pipetting scheme in Table 10. The reaction buffer together with DNase I was prepared as a master mix and pipetted to the 1 µg RNA sample. After mixing and a short centrifugation, the samples were incubated for 30 min at 37°C. To stop the reaction, 1 µl EDTA per sample was added and heated to 65°C for 10 min.

*Table 10:* **Pipetting scheme for a DNAse digestion.**

| **Volume** | **components** |
|---|---|
| 1 µg | isolated RNA |
| 1 µl | 10x reaction buffer with $MgCl_2$ |
| 1.5 µl | DNase I enzyme |
| Ad 10 µl | $H_2O$ |

#### *2.2.2.5 cDNA synthesis*

For further analysis, the RNA was transcribed into cDNA. The pool of copies produced in this way is much more stable and the cDNA molecules can subsequently serve as templates for a polymerase. This enables the amplification of specific cDNA molecules and provides information on gene expression. The standard pipetting scheme of a 20 µl mix is shown in Table 11. In order to avoid concentration variations, master mixes (I. and II.) were prepared, which contained all reagents except RNA and $H_2O$.

*Table 11:* **Pipette scheme for a cDNA synthesis.**

| | **volume** | **components** |
|---|---|---|
| I. | 1 µg | RNA |
| | 1 µl | Oligo $dT_{18}$ |
| | ad 13.7 µl | $H_2O$ |
| mix – centrifuge shortly – 5 min at 65°C 10 min at 24°C | | |
| II. | 2 µl | 10x A.Script Buffer |
| | 2 µl | 100 mM DTT |
| | 0,8 µl | 100 mM dNTP-Mix |
| | 1 µl | A. Script Reverse Transcriptase |
| | 0,5 µl | RiboLock |
| mix – centrifuge shortly – 1h at 42°C heat-deactivate at 70°C for 15 min | | |

*2.2.2.6 Real Time-quantitative Polymerase Chain Reaction (RT-qPCR)*

Real Time-quantitative PCR is an amplification method for nucleic acids, that allows the quantification of the cDNA obtained. The quantification is performed by fluorescence measurements, which are recorded in real time during a PCR cycle. The fluorescent dye used (here SYBR Green) intercalates into the double helix by binding into the small groove between the bases. Since the amount of amplified cDNA increases from cycle to cycle, the increase in stained cDNA correlates with the increase in fluorescence, which is measured at the end of the elongation phase. Elongation is followed by denaturation, whereby the SYBR Green I dye is released from the DNA. The free dye molecules emit a low background fluorescence, which is later subtracted from the actual signal by the PCR software. To control the product specificity of the SYBR Green I PCR, a melting temperature analysis is performed after each PCR. Thereby, the amplifications are melted by a continuous temperature increase, where the melting temperature is determined by the length, sequence and GC-content of the DNA double strand. If the melting temperature curve shows more than one peak, usually at a lower temperature than that of the target gene, non-specific products or primer dimers were amplified. Since only under optimal conditions, a constant doubling of the initial amount of cDNA takes place in the exponential (log-linear) phase of each cycle, it is possible to calculate the product amount (N) using the initial amount (N0) and the PCR efficiency (E), as well as the number of PCR cycles (CT):

$$N = N_0 * E^{cT}$$

This equation can be linearized by logarithmization:

$$\log N = \log N_0 + C_T * \log E$$

After further reshaping, the equation of the standard curve is obtained:

$$C_T = -\frac{1}{\log E} * \log N_0 + \frac{\log N}{\log E}$$

The preparation of a 96-well PCR plate was carried out under a PCR workstation, previously irradiated with UV light. The cDNA was first diluted 1:10 with $H_2O$. The cDNA pool, which served as the standard for the PCR, was diluted 1:10 - 1:320 in a serial dilution. After pipetting 10 µl of the master mix (Table 12) per well, 5 µl cDNA sample was added in duplicate.

*Table 12:* **Master mix for PCR analysis.**

| Volume | Reagent |
|---|---|
| 7,5 µl | SYBR Green Mix |
| 1,5 µl | Primer-Mix |
| 1 µl | $H_2O$ |

After sealing, the PCR plate was briefly centrifuged. For PCR the following thermal profile was used (Table 13).

*Table 13:* ***Thermal profile for a RT-qPCR.***

| Time | Temperature | |
|---|---|---|
| 3 min | 95°C | |
| 10 s | 95°C | x 40 |
| 20 s | 60°C | |
| Dissociation curve | | |
| 1 min | 95°C | |
| 30 s | 55°C | |
| 30 s | 95°C | |

Using the MxPro qPCR software (Agilent Technologies), an average value was calculated from the double determination of the $C_T$ value. Thereafter, the corresponding value was normalized with the determined actin-ß value of the cDNA sample. For calculations, the value of the nsiGDF-15 MΦ remaining in culture medium for 4h were set as 100% GDF-15 expression, in order to detect any expression differences in the differently treated samples.

### 2.2.3 Biochemistry

#### *2.2.3.1 Protein extraction with RIPA*

All subsequent steps were performed on ice. After exposing (transfected) THP-1 MΦ to oxLDL (and/or rGDF-15), the supernatant was removed and the cells were washed with ice cold 1x PBS. Thereafter, cell lysis was performed with 150 µl 1x RIPA (incl. protease/phosphatase inhibitor) (12-well plate). After 5 min incubation on ice, the cells were carefully scraped off with a cell scraper and transferred to a fresh tube. The cell lysates were homogenized for 3 min in an ultrasonic bath in ice water. After centrifugation at 13 000 rpm and 4°C for 10 min (Heraeus ™ Biofuge PrimoR), the protein-containing supernatant was removed from the pellet, consisting of cell debris. After protein extraction, the protein concentration was determined by BCA and proteins could be stored at -20°C.

#### *2.2.3.2 Protein concentration measurement with BCA*

The bicichoninic acid assay is a spectrophotometric method for determining protein concentrations in solution, due to the reduction of a cupric cation ($Cu^{2+}$ to $Cu^{1+}$) initiated by proteins in an alkaline medium. The arisen cuprous cations ($Cu^{1+}$) can be colorimetric detected by bicichoninic acid, which binds to the emerging copper cations ($Cu^{1+}$) and induce a colorimetric switch. Thereby, the total protein concentration can be determined by comparison to a protein standard. First, copper chelates with the peptide bonds in an alkaline medium to a light blue complex, called biuret reaction. The bicichoninic acid then chelates with the reduced $Cu^{1+}$ ions, resulting in a reddish colour change. The newly formed BCA-$Cu^{1+}$ complex has a strong linear absorption with increasing protein concentration, which can be measured at 562 nm wavelength. For protein quantification, the absorbance of sample and BSA standard was measured in duplicates on a 96-well plate. Therefore 10 µl samples or BSA standard (0, 25, 125, 250, 500, 1000, 1500 and 2000 µg/ml), together with 200 µl BCA working reagent (50:1, Reagent A:B) were incubated for 30 min in the dark at 37°C. Thereafter, the measurement was performed in the Tecan Sunrise Microplate Reader at 562 nm, with reference 0 nm. The

generated BSA standard curve (Figure 5) was used to determine the protein concentration by linear interpolation.

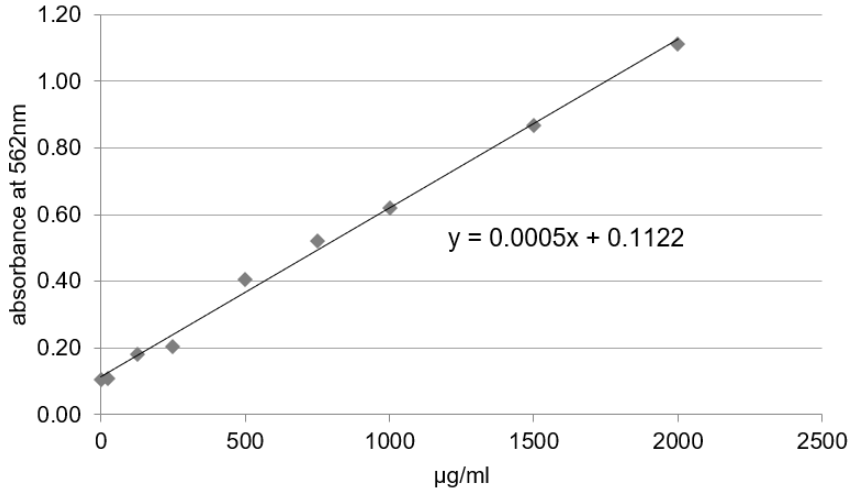


*Figure 5:* **BCA standard curve.** Representative BCA standard curve. With the protein standard (0, 25, 125, 250, 500, 1000, 1500 and 2000 µg/ml) the generated standard curve can be used to calculate the protein concentration of the samples.

### *2.2.3.3 GDF-15 Elisa*

To quantify the amount of GDF-15 protein in the protein samples, a DuoSet® ELISA for human GDF-15 was used. Therefore, the GDF-15 antigen specific capture antibody was diluted to a working concentration of 4.0 µg/ml in 1xPBS and 100 µl/well were pipetted into a MaxiSorp 96-well plate and incubated over night at 4°C. After washing three times with 400 µl 0.05% Tween-20® in 1xPBS (washing buffer) using the HydroFlex Elisa-Washer, blocking of unspecific binding sites of the capture antibody was performed with 1% BSA in PBS for 1h at RT. Thereafter, three washing steps (washing buffer) were performed. Samples were prepared, using 5 µg total protein in 100 µl 1xRIPA. The standard was prepared according to the manufacturer's instructions in 1xRIPA. After washing, the samples or standard were applied (100 µl/well) and incubated for 2h at RT. Another three washing steps were followed by incubation with 100 µl detection antibody, prepared according to the manufacturer's' instructions for 2h at RT. Since the detection antibody is biotinylated, streptavidin was used to bind to the biotin of the detection antibody and streptavidin (1:200 diluted in 1% BSA in PBS; 100 µl/well) is covalently bound to the horse radish peroxidase (HRP). After 20 min incubation in the dark, three washing steps were followed by two washes with 300 µl distilled water. To detect the peroxidase activity, 100 µl of the soluble substrate (Sigma Fast OPD tablets dissolved in 50 ml distilled water) was added and incubated for 30 min in the dark at RT. During this time the substrate is oxidized by the HRP, causing a characteristic change in the

substrates' structure, which is now photometrically detectable. This reaction was stopped using 25 µl/well 3M HCL, thereafter the absorbance was measured at 490 nm wavelength, with a reference at 655 nm. The generated standard curve (Figure 6), was used to determine the GDF-15 protein concentration by linear interpolation.

.

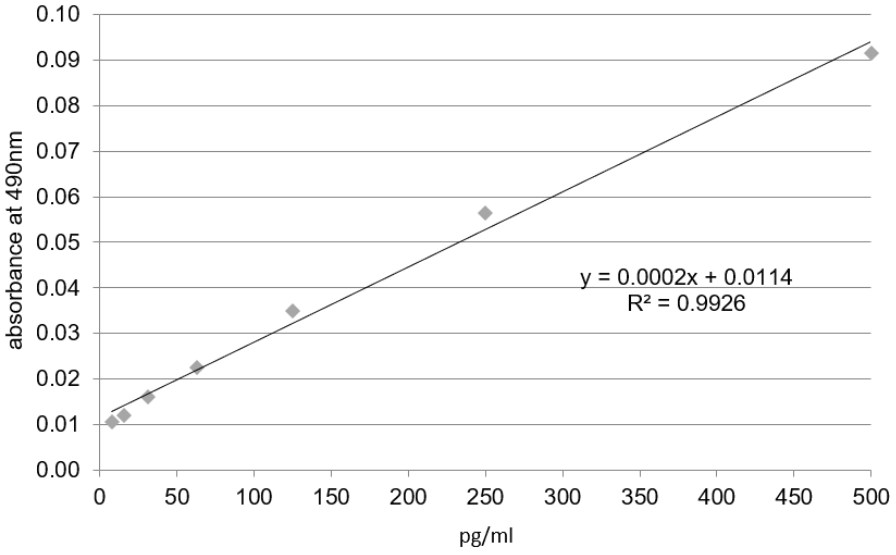


*Figure 6:* **GDF-15 Elisa standard curve.** Representative GDF-15 Elisa standard curve. With the protein standard (8, 16, 32, 64, 125, 250 and 500 pg/ml) the generated standard curve can be used to calculate the GDF-15 protein concentration of the samples.

### *2.2.3.4 SDS PAGE*

Using a 4-12% Bis-Tris SDS-PAGE, proteins can be separated according to their molecular weight. The used gel consists of polymerized acrylamide, where cross-linked polymers form a tight network, through which the proteins move to the anode, when voltage is applied. By adding SDS, an anionic detergent, the samples are uniformly negatively charged, so that the movement of the proteins in the electric field towards the anode is exclusively influenced by their molecular weight. Besides SDS, the sample buffer also contains DTE to reduce disulfide bridges and bromophenol blue to make the running front of the proteins more visible. In this work, 20 µg protein were mixed with 1x NuPAGE® sample buffer and denatured for 5 min at 95°C on a heating block, then put on ice for 5 min for renaturation. As running buffer, 1x MES (Table 5), including NuPAGE® antioxidant (ratio 1:4), was used. The renatured samples or the peqGOLD marker (IV or VI) were pipetted into the gel pockets and were separated in the gel at 200 V for 30-45 min.

*2.2.3.5 Western Blot Analysis*

After protein separation, the proteins were transferred from the gel to a 0.45 µm nitrocellulose membrane through an electric field. Therefore, two Whatman-Papers (8cm x 9cm), previously soaked in 1x transfer buffer (Table 5), were inserted into the blotting cassette (white side). Then, the moistened (1x transfer buffer) nitrocellulose membrane (7cm x 8cm) was applied, followed by the SDS gel and finally two more moistened Whatman-Papers were added and the blotting cassettes closed (black side). The blotting cassette was placed into the Mini Trans-Blot® Cell and filled with 1x transfer buffer. The transfer was carried out at 35 mA overnight.

Subsequently, protein detection was performed using specific antibodies (Table 7). For this purpose, the membrane was blocked twice for 30 min at RT in blocking solution (Table 5). The incubation of the membrane with primary antibody (diluted in blocking solution) was performed overnight at 4°C (Table 7). After incubation, the membrane was washed three times for 10 min in 1x washing buffer. Then, the incubation with the corresponding secondary antibody (diluted in blocking solution) (Table 7) was performed for 1h, followed by another three washing steps for 10 min.

The specific protein bands could be detected using HRP, which is coupled to the secondary antibody. HRP catalyses the oxidation of luminol by hydrogen peroxide. The end product of this reaction causes chemiluminescence. The strength of the emitted light is proportional to the amount of bound antibody and thus to the amount of protein. AceGlow Chemiluminescence Reagent A and B were added 1:1 to the membrane and incubated in the dark for 5 min. The detection of the protein bands was carried out using the Fusion-SL Advanced™ Imaging System according to the manufacturer's specifications. The protein band-intensity was quantified using ImageJ software (National Institutes of Health, USA) and normalized against α-tubulin.

*2.2.3.6 Membrane stripping*

After protein detection, the membrane was washed again three times for 10 min with washing buffer. Then, 7 µl ß-mercaptoethanol per 1 ml stripping buffer was mixed and added to the membrane (total volume 20 ml). The membrane was then freed from bound antibodies for 30 min at 60°C in the Hybridization Oven MK II. After another wash cycle (3 x 10 min) the membrane was used for further protein detection. Per membrane a maximum of two stripping-cycles were performed.

*2.2.3.7 Immunofluorescence*

To quantify p62 and Lamp-1 accumulation in THP-1 MΦ, immunofluorescence staining was performed. For this purpose, THP-1 cells were seeded in a 96-well plate, differentiated, transfected and stimulated for 4h (Figure 4). Subsequently, the medium was aspirated and cells were washed with 1xPBS. MΦ were fixed with ice-cold methanol (200 µl/well) for 10 min. After washing the cells with 1xPBS, MΦ were permeabilized with 0.1% Triton X-100 in 1xPBS (100 µl/well) for 15 min. After another washing step with 1xPBS, blocking was carried out with 2% goat serum in 1xPBS (200 µl/well) for 30 min at RT. Thereafter, the primary antibody against p62 or Lamp-1 was diluted in 1xPBS as indicated in Table 7 (100 µl/well). Incubation was carried out over night at 4°C. Subsequently, cells were washed with 0.1% Triton X-100 in 1xPBS (100 µl/well). The respective secondary antibody conjugated with AlexaFluor® 488 or Alexafluor® 555 was diluted in 1xPBS, also containing Dapi (1:1000) or DNA staining. After incubation for 1h in the dark at RT, cells were washed with 0.1% Triton X-100 in 1xPBS (100 µl/well) and finally left in 1xPBS (100 µl/well) during fluorescence detection with the confocal laser scanning microscope Nikon Eclipse Ti. The quantification of the Lamp-1 or p62 accumulation was performed using ImageJ software (National Institutes of Health, USA).

*2.2.3.8 Oil-Red-O-Staining*

To quantify the lipid storage of MΦ after exposure to lipoproteins, an ORO staining was performed. For this purpose, THP-1 cells were seeded in a 96-well plate, differentiated into MΦ and incubated as depicted in Figure 4. Subsequently, the medium was aspirated and the cells were washed three times with 300 µl medium to remove the respective stimulants. The cells were then fixed with 100 µl 10% PFA and incubated for 20 min at RT. Afterwards cells were washed twice (300 µl/well) with 1xPBS and once with aqua dest. (300 µl/well). Oil-Red-O working solution (Table 5) (100 µl/well), a red staining azo dye, was used to stain intracellular triglycerides. After 5 min incubation, the dye was removed and the cells were washed three times with 300 µl distilled water. Before removing the distilled water for the last time, the staining was verified with the Nikon Eclipse TS 100 Invert Microscope. After removal of the distilled water, the dye was eluted again with 100% isopropanol (100 µl/well) and absorbance was determined, using the Tecan Sunrise Microplate Reader at 595 nm with reference at 655 nm wavelength. As blank 100 µl/well 100% isopropanol was applied as triplicate to wells without cells. Thereafter, the cells were washed twice with 1x PBS (300 µl/well), twice with 0.1% Triton X-100 in 1x PBS (200 µl/well) and twice with aqua dest. (200 µl/well) and dried for 5 min at RT Afterwards, the cells were stained with previously filtered crystal

violet (100 µl/well). After 30 min incubation at room temperature, the cells were stained twice with 1x PBS (200 µl/well) and six times with Aqua dist. (200 µl/well) six times. The dye was dissolved from the cells with 1% SDS in 1x PBS (100 µl/well) for 30 min. The amount of eluted dye was then measured in the Elisa Microplate Reader at 595nm with a reference at 655nm. The blank value was measured with 1% SDS in PBS. The data of the ORO staining were normalized with the values of the crystal violet staining. The percentage of lipid deposition was then calculated by reference to the control as 100% value.

#### *2.2.3.9 Autophagy activity assay*

To measure the autophagy activity in THP-1 MΦ with enhanced or decreased GDF-15 protein level, cells were seeded in a Lumox® 96-well plate. After exposure of (transfected) THP-1 MΦ to oxLDL (and/or rGDF-15) for 4h, the cells were washed with RPMI culture medium. The Cell Meter™ Autophagy Assay Kit (AAT Bioquest®) was used to measure autophagy activity. Since the included Autophagy Blue™ accumulates in autophagosomes, its fluorescence intensity correlates with the number of intracellular autophagosomes and thereby the autophagy activity can be measured. The Autophagy Blue™ working solution was prepared according to the manufacturer's instructions and 100 µl were added into each well. Thereafter, the cells were incubated at 37°C and 5% $CO_2$ for 20 min, followed by washing the cells with the manufacturer washing buffer for four times. For the measurement, the cells remained in the washing buffer. The fluorescence intensity was determined using the Cytation™ 3 microplate reader with Ex/Em at 333/518 nm wavelength. As a blank, washing buffer was applied in triplicate to wells without cells. After subtracting the mean blank from each well, the autophagy activity of nsiGDF-15 THP-1 MΦ or THP-1 MΦ, which remained in culture medium for 4h was set as 100% autophagy activity.

#### *2.2.3.10 Lysosome activity assay*

To measure the lysosome activity of THP-1 MΦ with enhanced or decreased GDF-15 protein level, cells were seeded in a Lumox® 96-well plate. The dye LysoBrite™ Red (AAT Bioquest®) was used to measure lysosome activity. Since this dye selectively accumulates in lysosomes, its fluorescence intensity correlates with the number of intracellular lysosomes and thereby the lysosome activity can be measured. The dye working solution was prepared by diluting 20 µl of the 500 X LysoBrite™ stock in 10 ml RPMI medium without Phenol Red and without L-Glutamine. After exposure of (transfected) THP-1 MΦ to oxLDL (and/or rGDF-15) for 4h, the supernatant was removed

and 100 µl/well of the working solution were applied. Thereafter, the cells were incubated at 37°C, 5% $CO_2$ for 30 min, followed by washing the cells twice with RPMI medium without Phenol Red and without L-Glutamine. For the measurement, the cells remained in the RPMI medium without Phenol Red and without L-Glutamine. The fluorescence intensity was determined using the Cytation™ 3 microplate reader with Ex/Em at 575/605 nm wavelength. As a blank, RPMI medium without Phenol Red and without L-Glutamine was applied in triplicate to wells without cells. After subtracting the mean blank from each well, the lysosome activity of nsiGDF-15 THP-1 MΦ or THP-1 MΦ, which remained in culture medium for 4h was set as 100% lysosome activity.

*2.2.3.11 Cholesterol Assay*

To measure the amount of total cholesterol (TC), cholesteryl esters (CE) and free cholesterol (FC), a Cholesterol / Cholesteryl Ester Quantification Assay Kit (Abcam) was used. To measure the TC level, cholesterol is oxidized using cholesterol oxidase to produce $H_2O_2$, which reacts with a sensitive cholesterol probe to produce fluorescence. Based on the same principle, the CE level is measured. Prior to the cholesterol oxidation, CE is hydrolysed to cholesterol, using cholesterol esterase. The amount of FC is obtained by subtraction of CE from TC. Therefore, THP-1 MΦ were seeded in 6-well plates and differentiated as described. After exposure of (transfected) THP-1 MΦ to oxLDL (and/or rGDF-15) for 4h, cells were washed with ice cold 1xPBS. Afterwards, 150 µl ice cold 1xPBS were applied and cells were thoroughly scraped off with a cell scraper and transferred to a fresh 1.5 ml tube. After centrifugation at 250 x g and 4°C for 10 min, the supernatant was discarded. The remaining pellet was thoroughly resuspended in 100 µl chloroform: isopropanol: NP-40 in the relation 7: 11: 0.1. After centrifugation at 15 000 x g and 4°C for 10 min, the supernatant was discarded and the pellet was dried overnight. To remove any residual organic solvents, the samples were centrifuged in the vacuum concentrator for 30 min. In the meantime, the Cholesterol Standard, TC Reaction Mix and FC Reaction Mix were prepared for a duplicate reading, according to the manufacturer's instructions. After removing all solvents, the samples were resuspended in 200 µl Assay Buffer. Thereafter, the standard and samples were pipetted as duplicate for the TC Mix and for the FC Mix into a 96-well plate. Finally, 50 µl Total Cholesterol Mix was added to the standard and to the Total Cholesterol samples. 50 µl of the Free Cholesterol Mix was only added to the Free Cholesterol samples. After incubation at 37 °C for 60 min in the dark, the fluorescence intensity was determined using the Cytation™ 3 microplate reader with Ex/Em at 575/587 nm wavelength. The generated standard curve (Figure 7) was used to determine the Total and Free Cholesterol concentrations by linear interpolation. In subtracting the sample

concentration of Free Cholesterol from the concentration of Total Cholesterol, the concentration of Cholesteryl esters was determined.

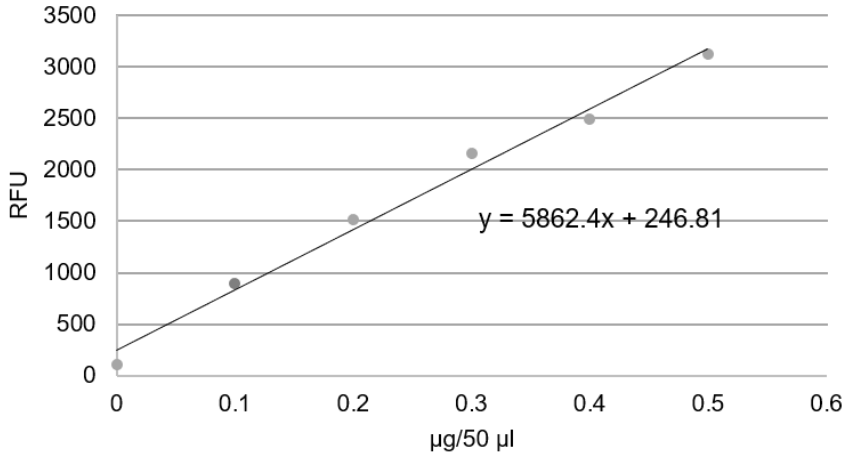


*Figure 7:* **Cholesterol Assay standard curve.** Representative Cholesterol Assay standard curve. With the cholesterol concentrations (0, 0.1, 0.2, 0.3, 0.4, and 0.5 µg/50 µl), the generated standard curve can be used to calculate the Total and Free Cholesterol concentration of the samples.

*2.2.3.12 LDL oxidation*

For oxLDL-generation, nLDL was suspended in endotoxin-free 1x PBS without $Ca^{2+}$ and $Mg^{2+}$ to a final concentration of 1 mg protein/ml. Dialyzing of nLDL was performed using Slide-A-Lyzer Dialysis Cassettes 7K MWCO in 500 ml endotoxin-free 1x PBS without $Ca^{2+}$ and $Mg^{2+}$ under constantly stirring for 72 h at 4°C in the dark for removal of EDTA. For nLDL oxidation, the Slide-A-Lyzer Dialysis Cassettes 7K MWCO was placed into 500 ml endotoxin-free 1x PBS without $Ca^{2+}$ and $Mg^{2+}$ containing 50 µM $CuSO_4$ and constantly stirred for 24 h at RT in the dark. To stop the oxidation, Slide-A-Lyzer Dialysis Cassettes 7K MWCO were stirred in endotoxin-free 1xPBS without $Ca^{2+}$ and $Mg^{2+}$ containing 50 µM EDTA for 6 h. Thereafter, oxLDL was sterile filtered by using a 0.2 µm filter and the concentration was determined using a BCA protein assay as described above. The grade of nLDL oxidation was verified using relative electrophoretic mobility (REM) shift by agarose gel with nLDL and BSA as reference (Figure 8 A) (Lougheed & Steinbrecher, 1996). Furthermore, the free amino groups of oxLDL and nLDL were compared, using trinitrobenzene sulfonic acid (TNBSA, Thermo Fisher Scientific, Inc.) according to the manufacturer's instruction (Figure 8B) (Foxx et al., 2008). Also, spectrophotometric analysis was performed generating an absorbance spectrum for nLDL and oxLDL between 400 nm and 700 nm (Tecan Sunrise Microplate Reader) (Figure 8C) (Galle & Wanner, 1998.). OxLDL was approved for further experimental usage, if at least 40.4% ± 0.65% amino groups were blocked compared to nLDL, an increased

REM of 17.5 % ± 3.34% compared to nLDL and the disappearance of the characteristic nLDL absorption peaks at 460 and 485 nm were attested.

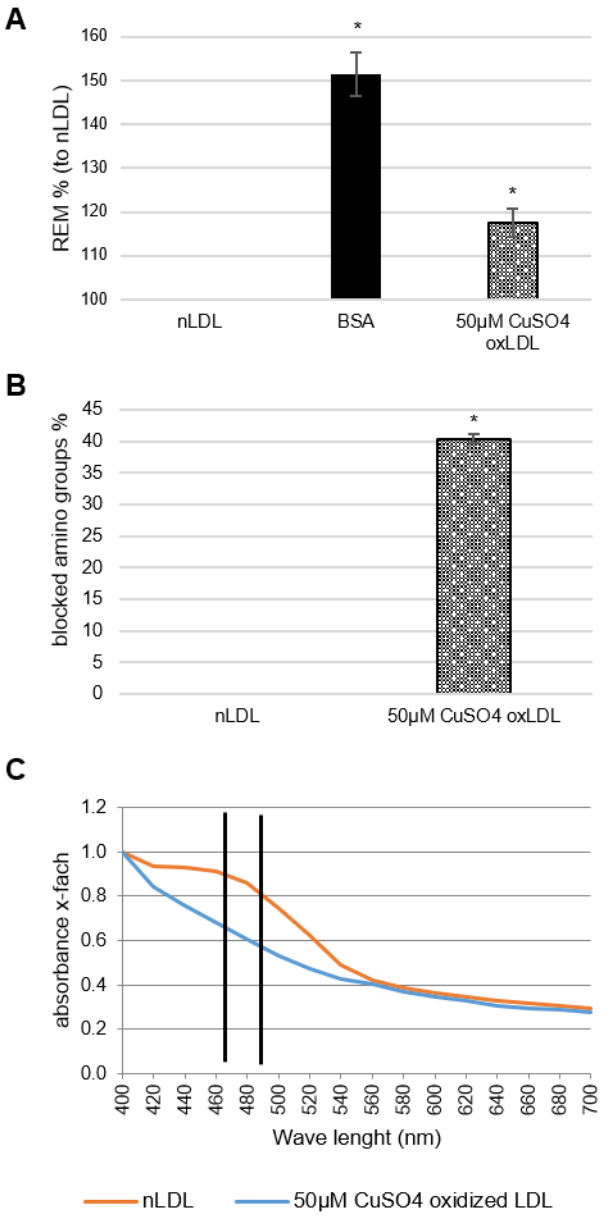


*Figure 8:* **Methods used to verify nLDL oxidation.** (A) Relative electrophoretic mobility (REM) was performed by agarose gel electrophoresis with nLDL, BSA and oxLDL (oxidized with 50µM $CuSO_4$). The agarose gel was dyed in Coomassie Blue for visualising the different bands. Thereafter the running length of every band was measured and compared to the running length of nLDL as reference. (B) Number of blocked amino acids in nLDL and oxLDL (oxidized with 50 µM $CuSO_4$) were determined using trinitrobenzene sulfonic acid (TNBSA, Thermo Fisher Scientific, Inc.) according to the manufacturer's instructions. (C) Spectrophotometric analysis was performed generating an absorbance spectrum for nLDL and oxLDL (oxidized with 50 µM $CuSO_4$) between 400 nm and 700 nm (Tecan Sunrise Microplate Reader). nLDL shows a characteristic peak in the absorbance between 460 nm and 485 nm, this peak is lacking when nLDL is oxidized.

*2.2.3.13 Agarose gel electrophoresis (for oxLDL)*

To verify oxidation grad of LDL, agarose gel electrophoresis was performed. Therefore, a 1 % agarose gel was prepared by dissolving agarose in 1x TAE buffer. After heating the solution for better dissolving, the solution was poured into a gel electrophoresis chamber. After cooling, the gel was loaded with oxLDL (8 µl oxLDL with 2 µl loading buffer), nLDL (4µl nLDL dialyzed with 4 µl aqua dest. and 2 µl loading buffer) as well as BSA (2 µl BSA with 6 µl aqua dest. and 2 µl loading buffer). The gel run at 200 V for 30 min. Thereafter, the gel was dyed in Coomassie Blue dye solution for at least 1 h and destained in destain solution for at least 24 h. Thereafter, the running length of the samples was measured and compared. Typically, nLDL shows the shortest, followed by oxLDL and BSA runs the furthest, depending on their electrical charge (Figure 9).

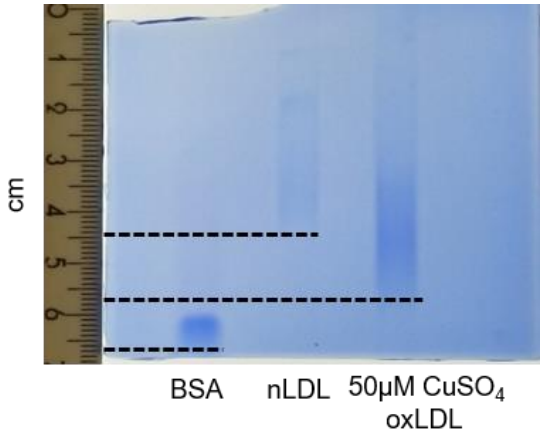


*Figure 9**: 1% agarose gel to verify oxidation grade of oxLDL.*** 1% agarose gel was loaded with BSA, nLDL and oxLDL (oxidized with 50µM $CuSO_4$) and ran at 200 V for 30 min. After dyeing with Coomassie Blue and destaining, the running length of the probes was measured and compared with BSA set as 100%.

# 3 Results

Interested in investigating a potential role of GDF-15 in MΦ autophagy we approached bidirectionally. First, a knock-down of GDF-15 in human THP-1 MΦ was assessed using small interfering RNAs. Second, THP-1 MΦ were treated with recombinant GDF-15 (rGDF-15) in concentrations of 1.0 µg/ml and 1.5 µg/ml to elevate the intracellular GDF-15 protein level. Foam cell formation was induced by treatment with 50 µg/ml oxLDL for 4h. Thereafter, the expression and accumulation of different autophagy-relevant markers as well as the lipid accumulation was assessed.

## 3.1 GDF-15 silencing impairs lipid accumulation and autophagic flux in human THP-1 MΦ

### 3.1.1 Transfection of human THP-1 MΦ with siRNA

PMA-differentiated human THP-1 MΦ were transfected with siRNA complementary to GDF-15 mRNA (siGDF-15). As negative control (nsiGDF-15) siRNA with no known homology to any human gene was used. Transfection efficiency was verified by using THP-1 MΦ transfected with a cell death-inducing siRNA as positive control. After 48h, successful transfection of THP-1 MΦ was assessed via light microscopy. THP-1 MΦ showing a round-like shape with intact cell membrane (black arrows) displayed healthy cells with no cell death-induction, indicating non-transfected cells. Apoptotic cells (white arrows), as indication for successfully induced cell death via transfection, were identified by a dissolved cell membrane, releasing cellular debris into the medium (Figure 10).

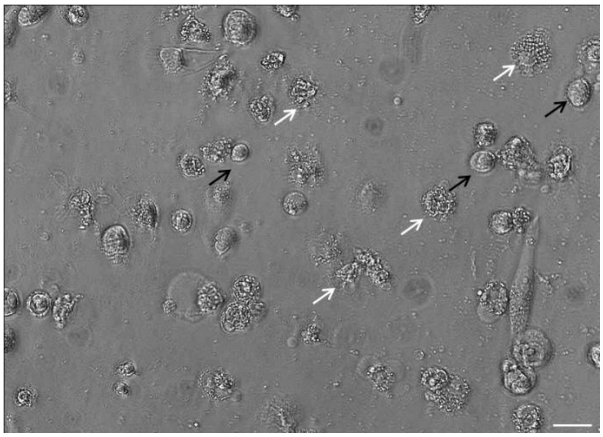

*Figure 10:* **Light microscopy image of THP-1 MΦ after transfection with AllStars HS Cell Death.** PMA-differentiated THP-1 MΦ were transfected (48h) with AllStars HS Cell Death small interfering RNA, used as positive control for assessing transfection efficiency. Black arrows indicate healthy cells, white arrows indicate apoptotic cells. Scale bars 20µM.

After 48h transfection, foam cell formation was induced by exposing siGDF-15 MΦ and nsiGDF-15 MΦ to 50 µg/ml oxLDL for 4h. As control, siGDF-15 MΦ or nsiGDF-15 MΦ were incubated in medium alone. siGDF-15 MΦ incubated in medium showed a significant ($p < 0.001$) -75% decreased GDF-15 mRNA level, whereas siGDF-15 MΦ incubated with oxLDL showed a -104% ($p < 0.001$) decreased GDF-15 mRNA level compared to equally incubated nsiGDF-15 MΦ (Figure 11 A). OxLDL upregulated the GDF-15 mRNA expression in nsiGDF-15 MΦ (35%, $p = 0.037$), whereas this effect was not found in siGDF-15 MΦ (Figure 11 A).

After incubation of nsiGDF-15 MΦ in medium the GDF-15 protein level was similar to that after incubation of nsiGDF-15 MΦ with oxLDL (Figure 11 B). In siGDF-15 MΦ incubated in medium, we found a -53% ($p = 0.026$) reduction of intracellular GDF-15 protein in comparison to nsiGDF-15 MΦ incubated in medium (Figure 11 B). Furthermore, after incubation of siGDF-15 MΦ with oxLDL, the intracellular GDF-15 protein level was -58% ($p = 0.001$) decreased compared to oxLDL-incubated nsiGDF-15 MΦ (Figure 11 B).

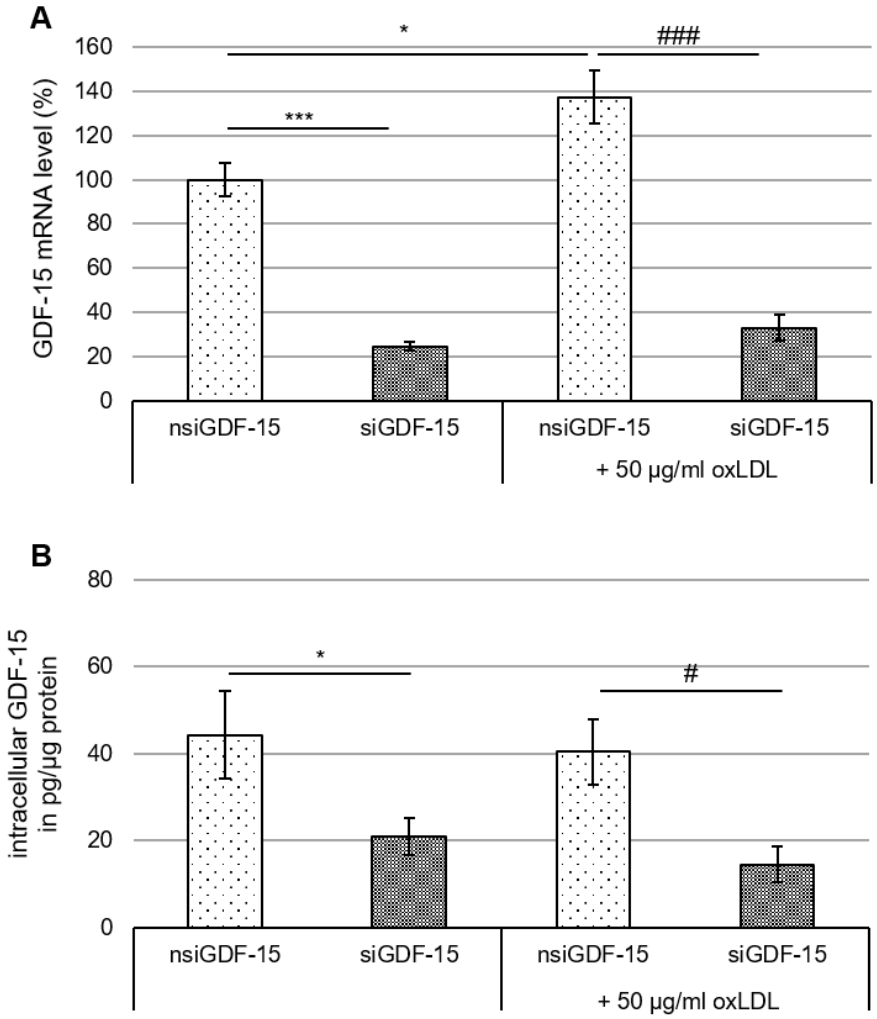


*Figure 11:* **GDF-15 mRNA and protein levels in nsiGDF-15 and siGDF-15 THP-1 MΦ after exposure to oxLDL or after incubation in medium.** (A) GDF-15 mRNA level (in % of nsiGDF-15 MΦ incubated in medium = 100%) in nsiGDF-15 / siGDF-15 MΦ was determined using RT-qPCR and normalized against GAPDH. Three independent experiments were performed. **(B)** Intracellular GDF-15 levels (pg/µg total protein) determined by ELISA [$OD_{490/655}$]. Six independent experiments were performed. Data are presented as mean ± SEM. *$p < 0.05$, ***$p < 0.001$ significance vs. nsiGDF-15 MΦ incubated in medium, $^{\#}p < 0.05$, $^{\#\#\#}p < 0.001$ significance vs. nsiGDF-15 MΦ + 50 µg/ml oxLDL. Student-Newman-Keuls test. Data published in Ackermann et al., 2019b.

### 3.1.2 GDF-15 silencing decreases lipid burden although cellular cholesterol levels remain unaltered

Modified LDL, such as oxLDL, is assumed as the main lipoprotein to cause foam cell formation, a critical step in the initiation of atherosclerosis (reviewed in Chistiakov et al., 2017). The induction of foam cell formation was examined using Oil-Red-O-staining, detecting neutral cell lipids. The successful lipid staining was controlled by light microscopy, showing red-colored lipid droplets within the cells (Figure 12 A-D). Exposure

to oxLDL caused an increase of 29% ($p < 0.05$) in the lipid content of nsiGDF-15 MΦ compared to nsiGDF-15 MΦ incubated in medium (Figure 12 E). Additionally, treatment of siGDF-15 MΦ with oxLDL increased the lipid content about 30% ($p < 0.05$) in comparison to siGDF-15 MΦ incubated in medium (Figure 12 E). Analyzation of the lipid content in siGDF-15 MΦ incubated in medium showed a -19% ($p < 0.05$) decrease compared to nsiGDF-15 MΦ incubated in medium, whereas siGDF-15 MΦ exposed to oxLDL showed -18% ($p < 0.05$) reduction in the lipid content compared to nsiGDF-15 MΦ exposed to oxLDL (Figure 12 E).

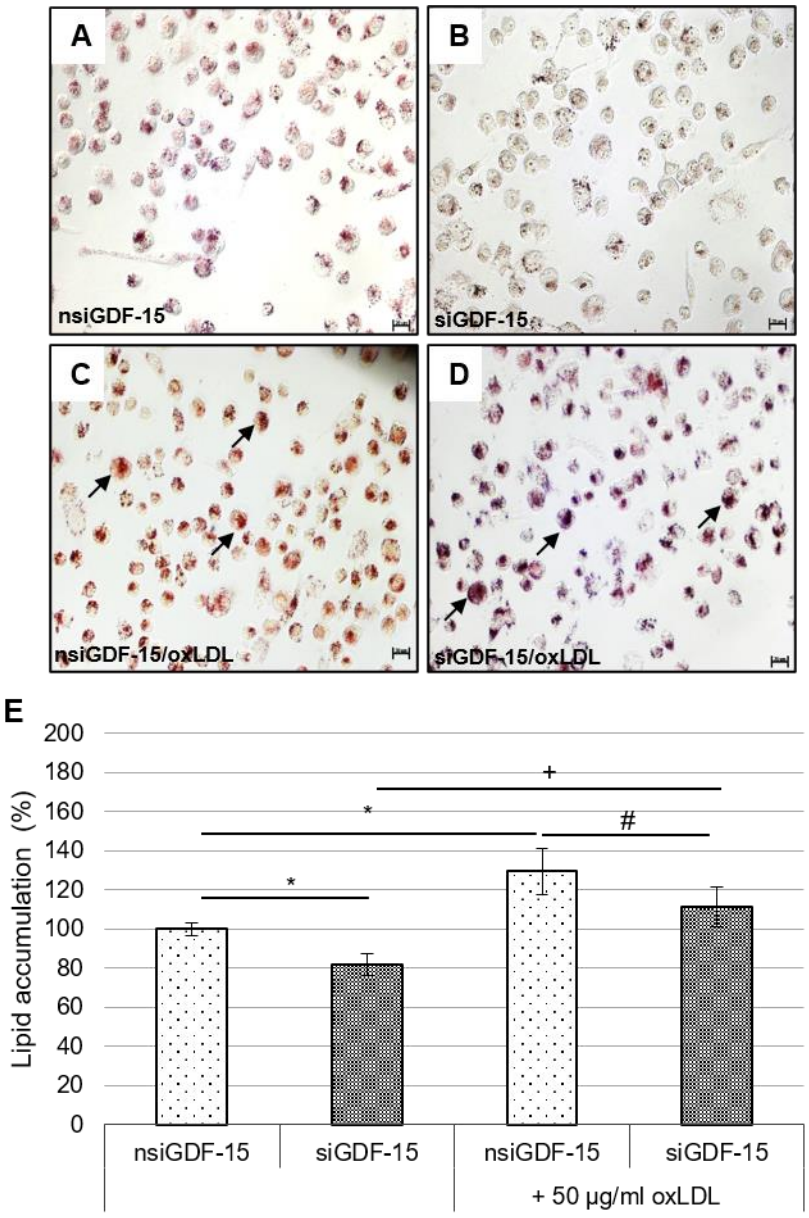


*Figure 12:* **Lipid accumulation in nsiGDF-15 and siGDF-15 THP-1 MΦ after exposure to oxLDL or after incubation in medium.** (A-D) Representative images of Oil-Red-O-stained nsiGDF-15 / siGDF-15 THP-1 MΦ. Black arrows indicate lipid-loaded cells. Scale bars 20µm. (E) Lipid accumulation (in % of nsiGDF-15 MΦ incubated in medium = 100%) measured by Oil-Red-O-staining after isopropanol elution [$OD_{510}$]. Seven independent experiments were performed. Data are presented as mean ± SEM. *$p < 0.05$ significance vs. nsiGDF-15 MΦ incubated in medium, $^{\#}p < 0.05$ significance vs. nsiGDF-15 MΦ + 50 µg /ml oxLDL, $^{+}p < 0.05$ significance vs. siGDF-15 MΦ incubated in medium. Student-Newman-Keuls test. Data published in Ackermann et al., 2019b.

Beside the measurement of the influence of GDF-15 on lipid content, the cholesterol export was examined by measuring the intracellular cholesterol level (Figure 13). Here, total cholesterol (TC), free cholesterol (FC) or cholesteryl ester (CE) levels were similar in nsiGDF-15 MΦ or siGDF-15 MΦ with or without 50 µg/ml oxLDL exposure (Figure 13).

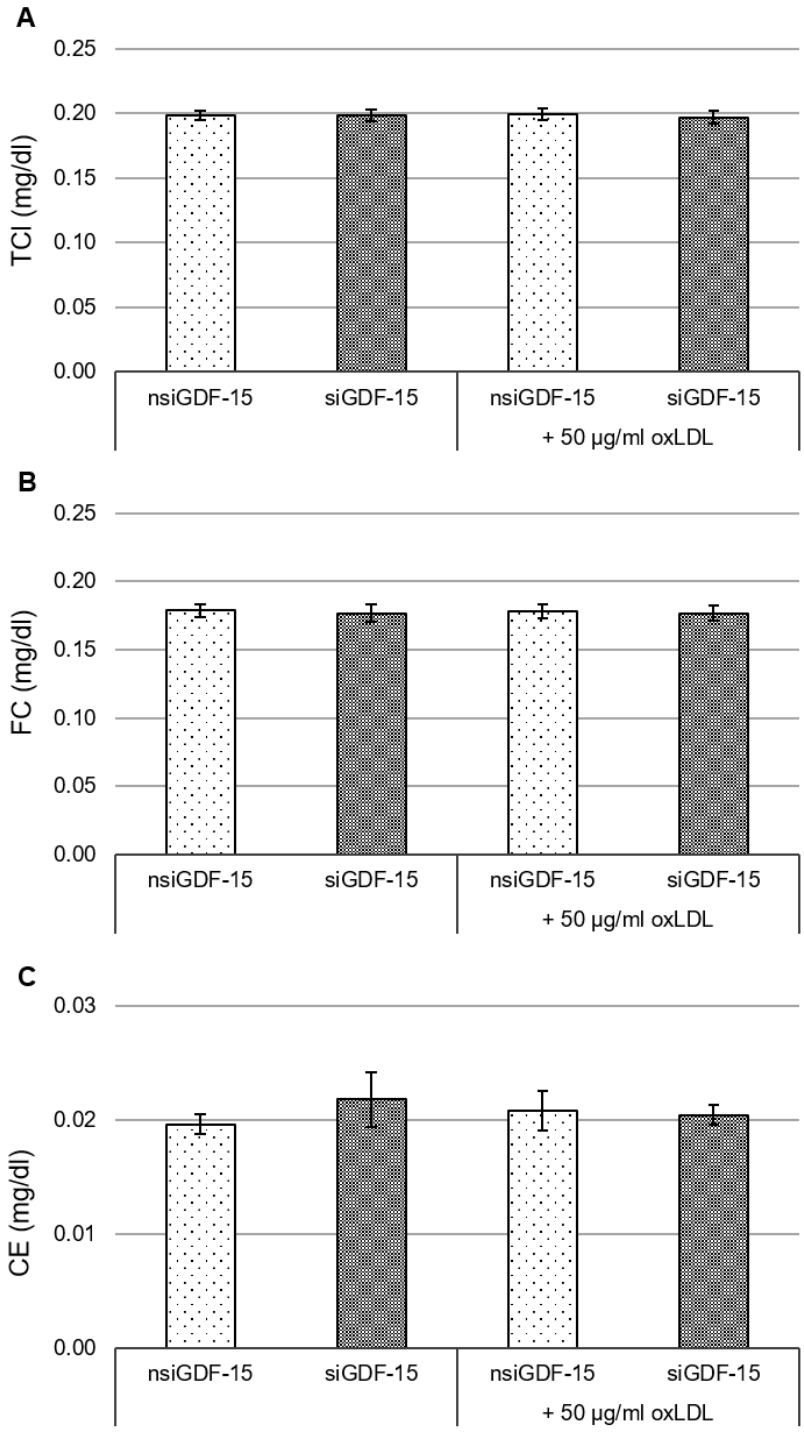


*Figure 13:* **Cholesterol levels in nsiGDF-15 and siGDF-15 THP-1 MΦ after exposure to oxLDL or incubation in medium.** (A) Total cholesterol (TC); (B) free cholesterol (FC); (C) cholesteryl ester (CE) in nsiGDF-15 / siGDF-15 THP-1 MΦ. Results are expressed in mg/dl. Four independent experiments were performed. Data are presented as mean ± SEM. Data published in Ackermann et al., 2019b.

### 3.1.3 GDF-15 silencing impairs autophagosome formation and reduces autophagic activity

Aiming to investigate a possible impact of GDF-15 on MΦ autophagy, the autophagy-relevant proteins ATG5 and ATG12, essential for the phagophore expansion, were analyzed. In siGDF-15 MΦ incubated in medium, the ATG5 protein level was significantly ($p < 0.05$) -36% decreased compared to nsiGDF-15 MΦ incubated in medium. Also, siGDF-15 MΦ incubated with oxLDL showed a -36% ($p < 0.05$) reduced ATG5 protein level compared to oxLDL-incubated nsiGDF-15 MΦ (Figure 14 A, C). OxLDL itself caused no significant changes in the ATG5 protein levels in siGDF-15 MΦ or nsiGDF-15 MΦ compared to medium-incubated siGDF-15 MΦ or nsiGDF-15 MΦ (Figure 14 A, C). The ATG12 / ATG5-complex protein level decreased about -20% ($p = 0.003$) in siGDF-15 MΦ incubated in medium compared to nsiGDF-15 MΦ incubated in medium (Figure 14 B, C). Exposure to oxLDL did not influence the ATG12 / ATG5-complex protein level in nsiGDF-15 MΦ or siGDF-15 MΦ compared to siGDF-15 MΦ or nsiGDF-15 MΦ incubated in medium (Figure 14 B, C).

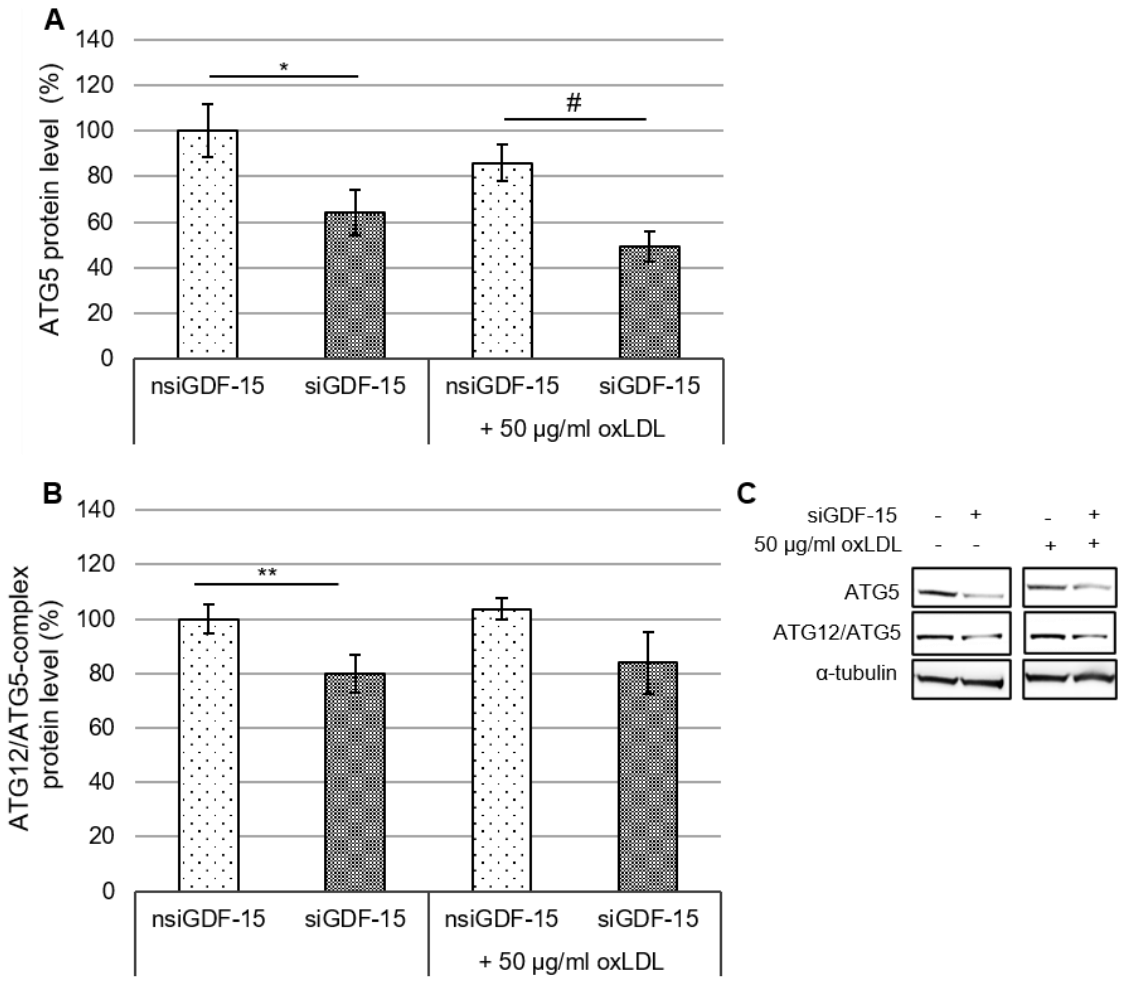


*Figure 14:* **ATG5 protein and ATG12 / ATG5-complex protein levels in nsiGDF-15 and siGDF-15 THP-1 MΦ after exposure to oxLDL or incubation in medium.** (A) ATG5 and (B) ATG12 / ATG5-complex protein levels (in % of nsiGDF-15 MΦ incubated in medium = 100%) in nsiGDF-15 / siGDF-15 THP-1 MΦ. ATG5 and ATG12 / ATG5-complex protein was normalized against α-tubulin and quantified with ImageJ. (C) Representative Western Blot images. Four (ATG5) and six (ATG12 / ATG5-complex) independent experiments were performed. Data are presented as mean ± SEM. *$p < 0.05$, **$p < 0.01$ significance vs. nsiGDF-15 MΦ incubated in medium, $^{\#}p < 0.05$ significance vs. nsiGDF-15 MΦ + 50 µg/ml oxLDL. Holm-Sidak test (ATG5) and Mann-Whitney-U test (ATG12 / ATG5-complex). Data published in Ackermann et al., 2019b.

Autophagic flux was measured by determination of the p62 protein level (Figure 15 A, B). In siGDF-15 MΦ incubated in medium, the p62 protein level decreased significantly ($p < 0.05$) about -23% compared to nsiGDF-15 MΦ incubated in medium. Incubation of nsiGDF-15 MΦ or siGDF-15 MΦ with oxLDL significantly ($p < 0.05$) increased the p62 protein level about 60% and 65% compared to nsiGDF-15 MΦ or siGDF-15 MΦ incubated in medium (Figure 15 A).

For additional validation of the autophagic status the intracellular p62 accumulation in THP-1 MΦ was measured (Figure 15 C, E-J). After incubation of siGDF-15 MΦ in medium, p62 accumulation was reduced by -56% ($p < 0.001$) compared to medium-incubated nsiGDF-15 MΦ (Figure 15 C). Incubation of siGDF-15 MΦ with oxLDL decreased the p62 accumulation about -67% ($p < 0.029$) compared to nsiGDF-15 MΦ incubated with oxLDL (Figure 15 C). Upon exposure to oxLDL, the p62 accumulation increased about 78% ($p < 0.009$) in nsiGDF-15 MΦ and 67% ($p < 0.001$) in siGDF-15 MΦ compared to nsiGDF-15 MΦ or siGDF-15 MΦ incubated in medium (Figure 15 C). As positive control for autophagy activity induction and therefore p62 accumulation initiation, THP-1 MΦ were starved for 4h. Upon starvation THP-1 MΦ showed a significantly ($p < 0.05$) 107% enhanced p62 accumulation compared to nsiGDF-15 MΦ incubated in medium (Figure 15 C). Besides the amount of p62 accumulations, the diameter of these intracellularly accumulated p62 was measured to draw conclusions regarding changes in the autophagosome-size (Figure 15 D). Here, the diameter of intracellularly accumulated p62 varied from 1.7 to 1.9 µm with no significant changes in the accumulation size in medium-incubated or oxLDL-incubated nsiGDF-15 MΦ and siGDF-15 MΦ (Figure 15 D).

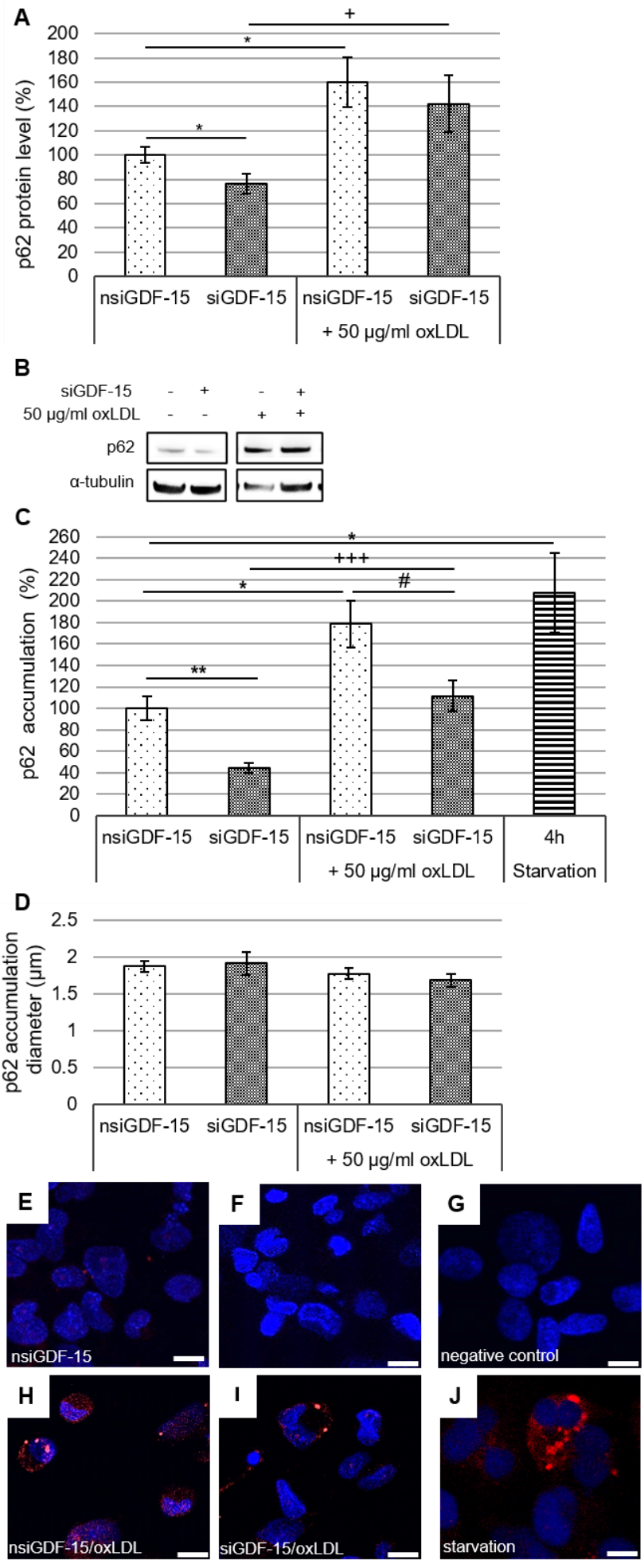
A
p62 protein level (%)
200
180
160
140
120
100
80
60
40
20
0
*
*
+
nsiGDF-15
siGDF-15
nsiGDF-15
siGDF-15
+ 50 µg/ml oxLDL
B
siGDF-15 - + - +
50 µg/ml oxLDL - - + +
p62
α-tubulin
C
p62 accumulation (%)
260
240
220
200
180
160
140
120
100
80
60
40
20
0
*
+++
*
#
**
nsiGDF-15
siGDF-15
nsiGDF-15
siGDF-15
+ 50 µg/ml oxLDL
4h
Starvation
D
p62 accumulation diameter (µm)
2.5
2
1.5
1
0.5
0
nsiGDF-15
siGDF-15
nsiGDF-15
siGDF-15
+ 50 µg/ml oxLDL
E
nsiGDF-15
F
G
negative control
H
nsiGDF-15/oxLDL
I
siGDF-15/oxLDL
J
starvation

*Figure 15:* **p62 protein level and intracellular p62 accumulation in nsiGDF-15 and siGDF-15 THP-1 MΦ after exposure to oxLDL or incubation in medium.** (A) p62 protein level (in % of nsiGDF-15 MΦ incubated in medium = 100%) in nsiGDF-15 / siGDF-15 THP-1 MΦ. Expression was normalized against α-tubulin and quantified with ImageJ. Ten independent experiments were performed. (B) Representative Western Blot images for p62 and α-tubulin. (C) p62 accumulations (in % of nsiGDF-15 MΦ incubated in medium = 100%) were analyzed with Fiji ImageJ and normalized against DAPI (D) Diameter of intracellularly accumulated p62 was measured in µm using Fiji ImageJ. Six independent experiments were performed. Data are presented as mean ± SEM. (E-J) Representative immunofluorescence images of p62 accumulations (red) and DAPI (blue) double staining, visualized with laser scanning microscopy (Nikon Eclipse). (I) The negative control shows DAPI-stained THP-1 MΦ without primary antibody against p62. Scale bars 50 µM. *$p < 0.05$, **$p < 0.01$ significance vs. nsiGDF-15 MΦ incubated in medium, $^{\#}p < 0.05$ significance vs. nsiGDF-15 MΦ + 50 µg/ml oxLDL, $^{+}p < 0.05$, $^{+++}p < 0.001$ significance vs. siGDF-15 MΦ incubated in medium. Student-Newman-Keuls test (p62 total protein), TTest and Mann-Whitney-U test (p62 accumulation). Data (A-C; E-J) published in Ackermann et al., 2019b.

Additionally, to the measurement of the p62 protein status, we performed an autophagy activity assay in combination with a lysosomal activity assay to determine, whether the autophagic flux is intact or impaired. In siGDF-15 MΦ incubated in medium, we found a decreased autophagic activity by -22% ($p = 0.035$) in comparison to nsiGDF-15 MΦ incubated in medium (Figure 16 A). This autophagic activity-reduction in siGDF-15 MΦ compared to nsiGDF-15 MΦ was not seen after exposure to 50 µg/ml oxLDL. However, incubation of nsiGDF-15 MΦ or siGDF-15 MΦ with oxLDL significantly decreased the autophagic activity by -41% ($p < 0.001$) in nsiGDF-15 MΦ and -21% ($p = 0.011$) in siGDF-15 MΦ compared to nsiGDF-15 MΦ or siGDF-15 MΦ incubated in medium (Figure 16 A). The lysosomal activity showed no significant changes in medium-incubated siGDF-15 MΦ compared to medium-incubated nsiGDF-15 MΦ (Figure 16 B). After incubation with oxLDL the lysosomal activity was reduced by -20% ($p < 0.05$) in nsiGDF-15 MΦ and siGDF-15 MΦ compared to medium-incubated nsiGDF-15 MΦ or siGDF-15 MΦ (Figure 16 B). Starvation, was used as positive control for an induction of autophagic and lysosomal activity (Zhou et al., 2013). THP-1 MΦ starved for 4h showed a 34% ($p = 0.038$) increase in the autophagic activity (Figure 16 A) and 18% ($p = 0.006$) increase in the lysosomal activity (Figure 16 B) compared to nsiGDF-15 MΦ incubated in medium. It is of note, that starvation was induced in non-transfected THP-1 MΦ, which were starved for 4h in medium not supplemented with fetal-bovine-serum, followed by normalization against medium-incubated nsiGDF-15 MΦ

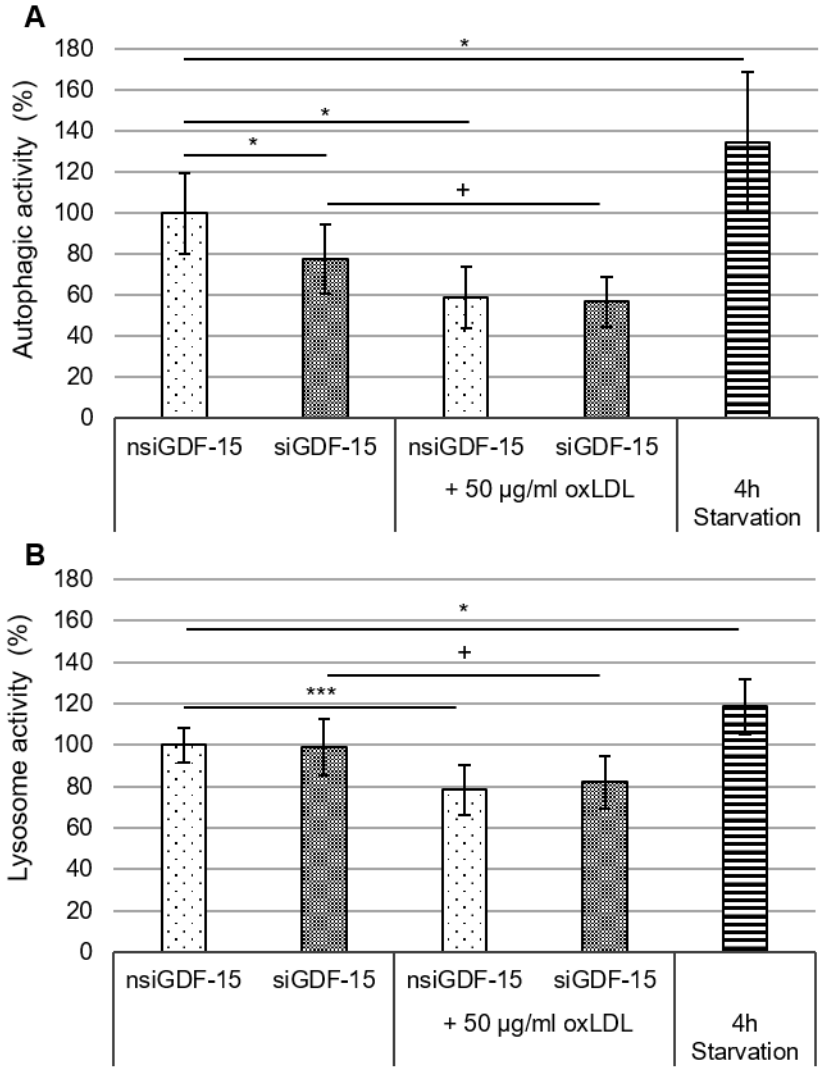


*Figure 16:* **Autophagic and lysosomal activity in nsiGDF-15 and siGDF-15 THP-1 MΦ after exposure to oxLDL or after incubation in medium.** (A) Autophagic activity (in % of nsiGDF-15 MΦ incubated in medium = 100%) in nsiGDF-15 / siGDF-15 THP-1 MΦ determined using fluorescent Cell Meter™ Autophagy Assay Kit [$OD_{333/518}$]. Five independent experiments were performed. Data are presented as mean ± SEM. (B) Lysosomal activity (in % of nsiGDF-15 MΦ incubated in medium = 100%) in nsiGDF-15 / siGDF-15 THP-1 MΦ determined using LysoBrite™ Red [$OD_{575/597}$]. Four independent experiments were performed. Data are presented as mean ± SEM. *$p < 0.05$, ***$p < 0.001$ significance vs. nsiGDF-15 MΦ incubated in medium, $^{+}p < 0.05$ significance vs. siGDF-15 MΦ incubated in medium. Student-Newman-Keuls test.

## 3.2 rGDF-15 enhances autophagosome formation and amplifies oxLDL-induced autophagic flux impairment

### 3.2.1 THP-1 MΦ ingest rGDF-15

In order to investigate the effect of extracellular GDF-15 on MΦ autophagy and lipid homeostasis, further experiments were performed using rGDF-15 produced in *Escherichia Coli.* After incubation of PMA-differentiated THP-1 MΦ with 1.0 µg/ml or 1.5 µg/ml rGDF-15 for 4h, the cellular GDF-15 protein level was determined using a GDF-15 Elisa Kit. As control, THP-1 MΦ were incubated for 4h in medium alone. In medium-incubated THP-1 MΦ, the GDF-15 protein level was 35.7 pg/µg protein. Incubation of THP-1 MΦ with 1.0 µg/ml or 1.5 µg/ml rGDF-15 increased the cellular GDF-15 protein level about 82% ($p = 0.029$) to 65.2 pg/µg protein and 99% ($p = 0.014$) to 71.2 pg/µg protein compared to THP-1 MΦ incubated in medium (Figure 17). THP-1 MΦ exposed to 50 µg/ml oxLDL had 28.4 pg/µg cellular GDF-15 protein level after 4h, showing no significant changes compared to medium-incubated THP-1 MΦ (Figure 17). Additionally, after co-incubation of THP-1 MΦ with 1.0 µg/ml rGDF-15 / oxLDL and 1.5 µg/ml rGDF-15 / oxLDL cellular GDF-15 levels increased about 93% ($p = 0.002$) to 61.7 pg/µg protein and 122% ($p = 0.002$) to 72.2 pg/µg protein compared to oxLDL-exposed THP-1 MΦ (Figure 17).

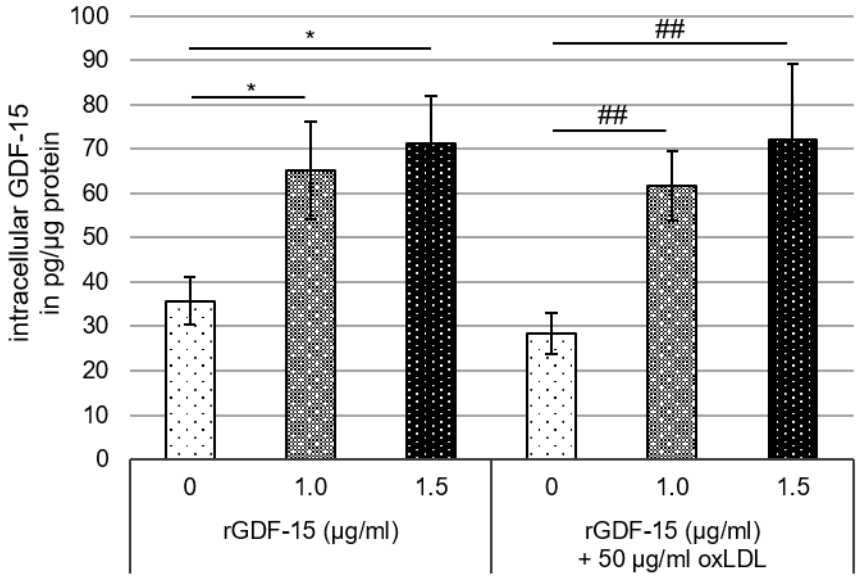


*Figure 17:* **Intracellular GDF-15 protein level in THP-1 MΦ after exposure to rGDF-15 with / without oxLDL.** ELISA [$OD_{490/655}$] was used to determine intracellular GDF-15 levels (pg/µg protein). Eleven independent experiments were performed. Data are presented as mean ± SEM. *$p < 0.05$ significance vs. THP-1 MΦ incubated in medium, $^{\#\#}p < 0.01$ significance vs. THP-1 MΦ + 50 µg/ml oxLDL. Student-Newman-Keuls test and Dunn's test. Data published in Ackermann et al., 2019b.

### 3.2.2 rGDF-15 enhances lipid accumulation in human THP-1 MΦ

The oxLDL-induced foam cell formation and the rGDF-15-effect on lipid accumulation were determined by Oil-Red-O-staining (Figure 18). Light microscopy pictures were taken to control the successful lipid uptake (Figure 18 A-D). THP-1 MΦ incubated with rGDF-15 showed an increase of neutral lipid content of about 10% (1.0 µg/ml rGDF-15; $p < 0.05$) and of 17% (1.5 µg/ml rGDF-15; $p < 0.05$) compared to THP-1 MΦ incubated in medium alone (Figure 18 E). Exposure of THP-1 MΦ to oxLDL resulted in a 37% ($p < 0.05$) increased lipid accumulation compared to THP-1 MΦ incubated in medium. The co-incubation of THP-1 MΦ with rGDF-15 / oxLDL did not significantly influence the lipid accumulation compared to THP-1 MΦ treated with oxLDL alone, but enhanced the lipid content about 43% (1.0 µg/ml rGDF-15 / oxLDL, $p < 0.05$) and 42% (1.5 µg/ml rGDF-15 / oxLDL, $p < 0.05$) compared to THP-1 MΦ treated with rGDF-15 alone (without oxLDL) (Figure 18 E).

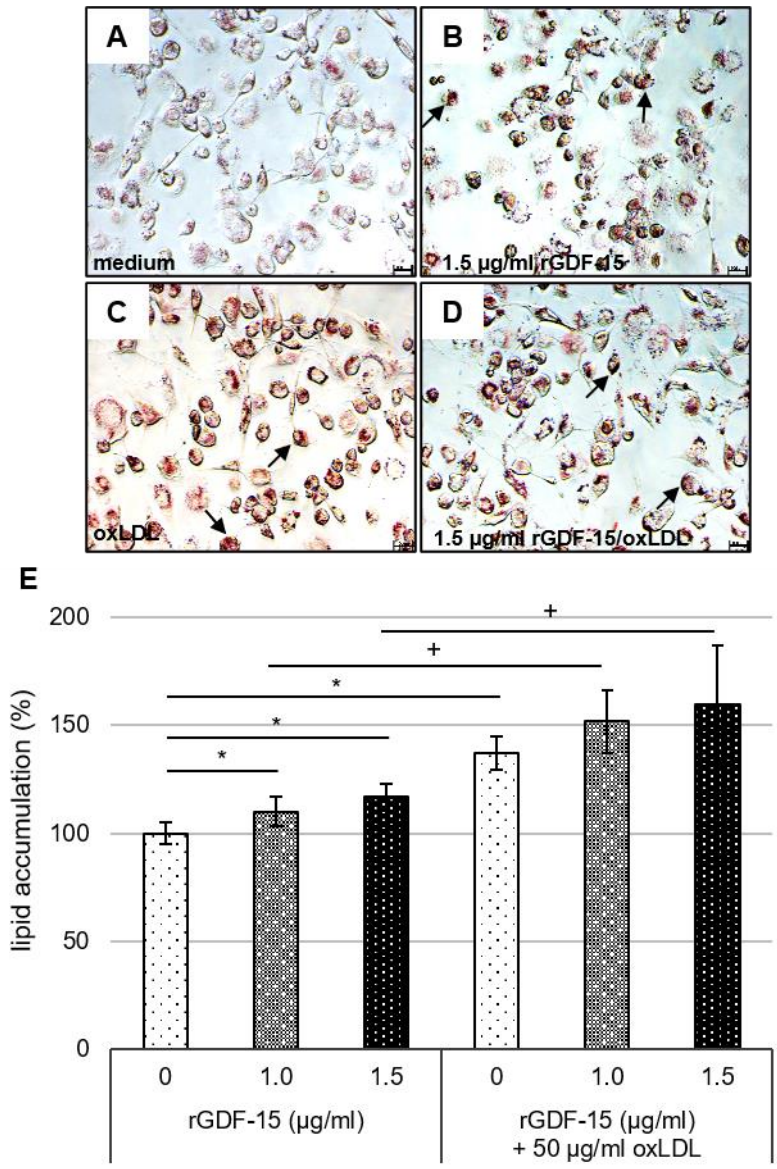


*Figure 18:* **Lipid content in THP-1 MΦ after exposure to rGDF-15 with / without oxLDL.**
(A-D) Representative photos of Oil-Red-O-stained THP-1 MΦ. Black arrows indicate lipid loaded cells. Scale bars 100µm. (E) Lipid accumulation (in % of THP-1 MΦ incubated in medium = 100%) measured by Oil-Red-O-staining after isopropanol elution [$OD_{510}$]. Data are presented as mean ± SEM. Six independent experiments were performed. *p < 0.05 significance vs. THP-1 MΦ incubated in medium, $^{+}$p < 0.05 significance vs. THP-1 MΦ incubated without 50 µg/ml oxLDL. Student-Newman-Keuls test. Data published in Ackermann et al., 2019b.

To evaluate, if the changes in the lipid accumulation are due to altered cholesterol levels, a cholesterol assay was performed, measuring the levels of total cholesterol (TC), free cholesterol (FC) and cholesteryl ester (CE) (Figure 19). After exposure of THP-1 MΦ to rGDF-15, oxLDL or in combination rGDF-15 / oxLDL, the levels of TC, FC or CE were similar as in THP-1 MΦ incubated in medium alone (Figure 19 A-C).

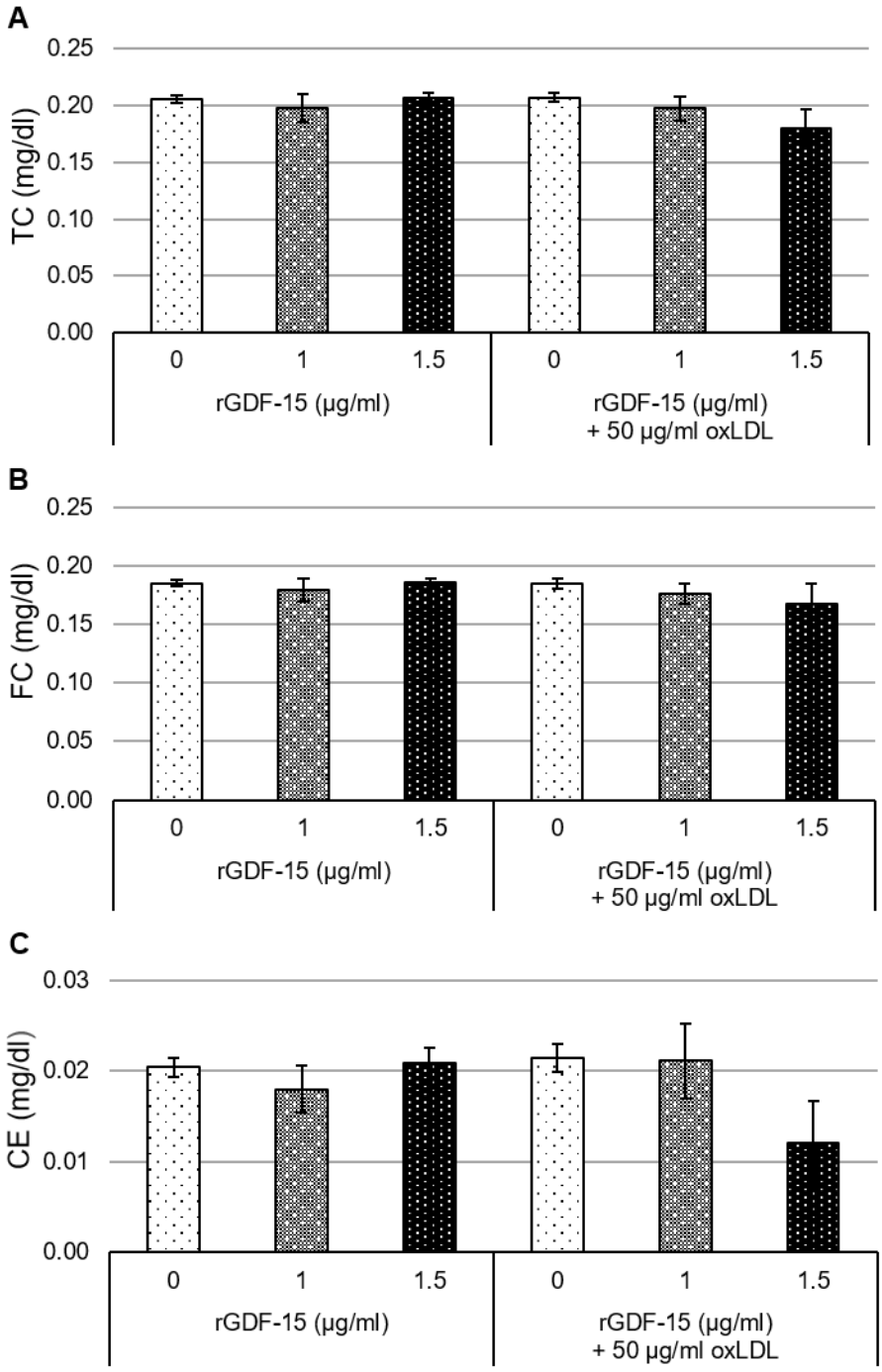


*Figure 19:* **Cholesterol levels in THP-1 MΦ after exposure to rGDF-15 with / without oxLDL.** (A) TC, total cholesterol, (B) FC, free cholesterol, (C) CE, cholesteryl ester in THP-1 MΦ after exposure to rGDF-15 with / without oxLDL. Results are expressed in mg/dl. Four independent experiments were performed. Data are presented as mean ± SEM. Data published in Ackermann et al., 2019b.

### 3.2.3 rGDF-15 affects basic autophagy by increasing autophagosome formation and aggravates the oxLDL-induced autophagy impairment

To confirm a GDF-15-silencing-dependent impairment of the autophagic process, we analyzed the protein levels of ATG5 and ATG12 / ATG5-complex using THP-1 MΦ exposed to rGDF-15 with and without oxLDL. Incubation of THP-1 MΦ with rGDF-15 or 50 µg/ml oxLDL alone did not affect the protein level of ATG5 (Figure 20 A,C) and of the ATG12 / ATG5-complex compared to THP-1 MΦ incubated in medium (Figure 20 B,C) . The co-incubation of THP-1 MΦ with rGDF-15 / oxLDL increased the ATG5 protein level about 48% (1.0 µg/ml rGDF-15 / oxLDL; $p = 0.029$) and 47% (1.5 µg/ml rGDF-15 / oxLDL; $p < 0.001$) compared to THP-1 MΦ exposed to rGDF-15 alone (without oxLDL) (Figure 20 A,C). Furthermore, a 38% ($p = 0.004$) increase in the ATG5 protein level was induced by the co-incubation of THP-1 MΦ with 1.5 µg/ml rGDF-15 / oxLDL compared to THP-1 MΦ incubated with oxLDL alone (Figure 20 A, C). Additionally, co-incubation of THP-1 MΦ with rGDF-15 / oxLDL increased the ATG12 / ATG5-complex protein level about 107% (1.0 µg/ml rGDF-15 / oxLDL, $p < 0.001$) and 140% (1.5 µg/ml rGDF-15 / oxLDL, $p < 0.001$) compared to THP-1 MΦ exposed to rGDF-15 alone (without oxLDL) (Figure 20 B,C). Moreover, incubation of THP-1 MΦ with 1.0 µg/ml rGDF-15 / oxLDL increased the ATG12 / ATG5-complex protein level about 59% ($p = 0.012$) and 1.5 µg/ml rGDF-15 / oxLDL about 85% ($p = 0.007$) compared to THP-1 MΦ incubated with oxLDL alone (Figure 20 B, C).

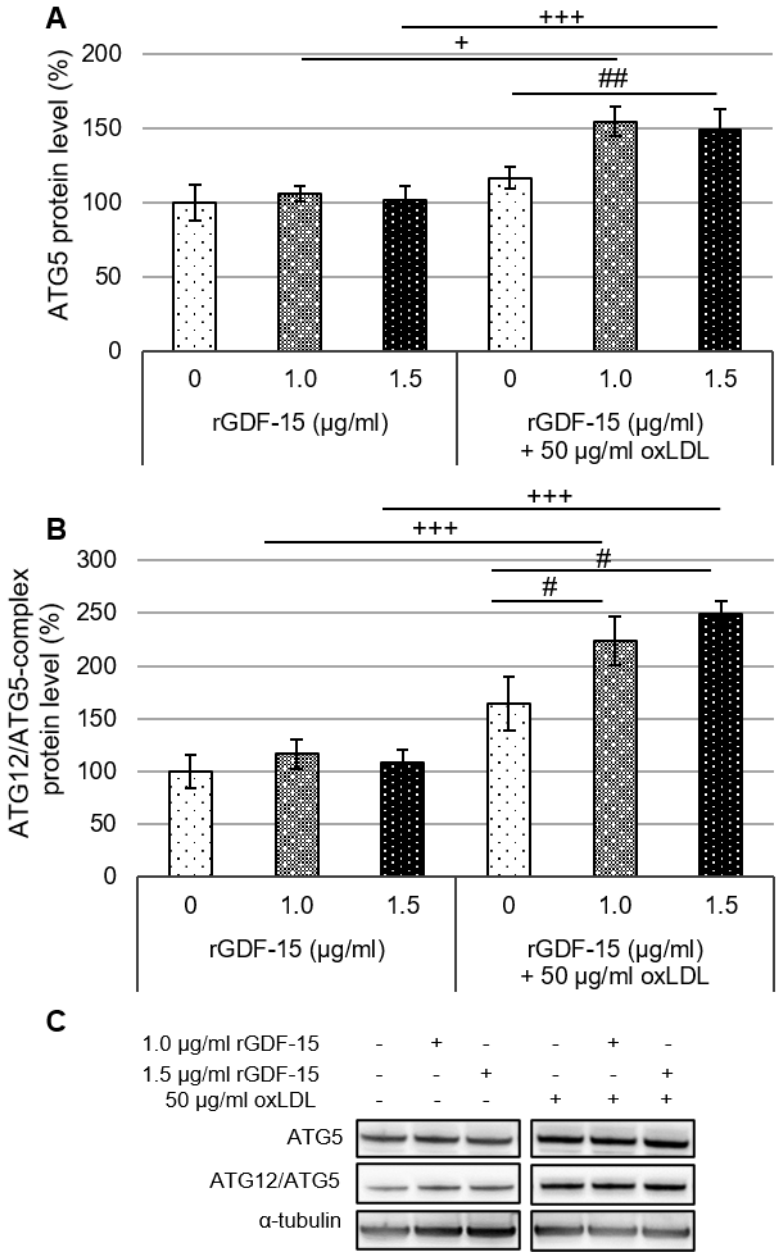


*Figure 20:* **ATG5 protein and ATG12 / ATG5-complex protein levels in THP-1 MΦ after exposure to rGDF-15 with / without oxLDL.** (A) ATG5 and (B) ATG12 / ATG5-complex protein levels (in % of THP-1 MΦ incubated in medium = 100%) in THP-1 MΦ. Expression was normalized against α-tubulin and quantified with ImageJ. (C) Representative Western Blot images for ATG5, ATG12/ATG5-complex and α-tubulin. Six (ATG5) to four (ATG12 / ATG5-complex) independent experiments are presented as mean ± SEM. $^{\#}p < 0.05$, $^{\#\#}p < 0.01$ significance vs. THP-1 MΦ + 50 µg/ml oxLDL, $^{+}p<0.05$, $^{+++}p < 0.01$ significance vs. THP-1 MΦ incubated without 50 µg/ml oxLDL. Student-Newman-Keuls test (ATG5) and Holm-Sidak test (ATG12 / ATG5-complex). Data published in Ackermann et al., 2019b.

The impact of rGDF-15 with and without oxLDL on the autophagic flux of THP-1 MΦ was once again verified by observing p62 status (Figure 21). Incubation of THP-1 MΦ with 1.0 µg/ml rGDF-15 or 1.5 µg/ml rGDF-15 had no effect on the p62 protein level compared to medium-incubated THP-1 MΦ (Figure 21 A, B). Whereas exposing THP-1 MΦ to 50 µg/ml oxLDL increased the p62 protein level about 31% ($p = 0.065$) compared to medium-incubated THP-1 MΦ. Co-incubation of THP-1 MΦ with 1.5 µg/ml rGDF-15 / oxLDL increased the p62 protein level about 80% ($p < 0.05$) compared to THP-1 MΦ exposed to 1.5 µg/ml rGDF-15 alone. Additionally, THP-1 MΦ exposed to 1.5 µg/ml rGDF-15 / oxLDL showed a 66% ($p < 0.05$) enhanced p62 protein level in comparison to THP-1 MΦ incubated with 50 µg/ml oxLDL alone (Figure 21 A, B). Furthermore, after incubation of THP-1 MΦ with 1.5 µg/ml rGDF-15 p62 accumulation significantly ($p < 0.05$) increased about 26% compared to THP-1 MΦ incubated in medium (Figure 21 C). Incubation of THP-1 MΦ with 50 µg/ml oxLDL enhanced the p62 accumulation about 49% ($p < 0.05$) compared to medium-incubated THP-1 MΦ (Figure 21 C). The co-incubation of THP-1 MΦ with 1.5 µg/ml rGDF-15 / oxLDL elevated the p62 accumulation about 60% ($p < 0.05$) compared THP-1 MΦ exposed to 1.5 µg/ml rGDF-15 alone and 37% ($p < 0.05$) in comparison to THP-1 MΦ exposed to oxLDL (Figure 21 C). Once again, as a positive control for autophagy activity induction, THP-1 MΦ were starved for 4h. Upon starvation THP-1 MΦ showed a significantly ($p = 0.006$) 112% enhanced p62 accumulation compared to THP-1 MΦ incubated in medium.

Regarding the diameter of intracellularly accumulated p62, rGDF-15 and oxLDL increased the diameter in THP-1 MΦ (1.0 µg/ml rGDF-15: 0.15 µm, $p = 0.048$; 1.5 µg/ml rGDF-15: 0.14 µm, $p < 0.0001$; oxLDL: 0.11 µm, $p = 0.039$) compared to medium-incubated THP-1 MΦ (Figure 21 D). Upon co-incubation of THP-1 MΦ with 1.0 µg/ml rGDF-15 / oxLDL or 1.5 µg/ml rGDF-15 / oxLDL diameter of intracellularly accumulated p62 expanded about 0.28 µm ($p < 0.001$) and 0.14 µm ($p < 0.001$) compared to incubation with 50 µg/ml oxLDL alone (Figure 21 D).

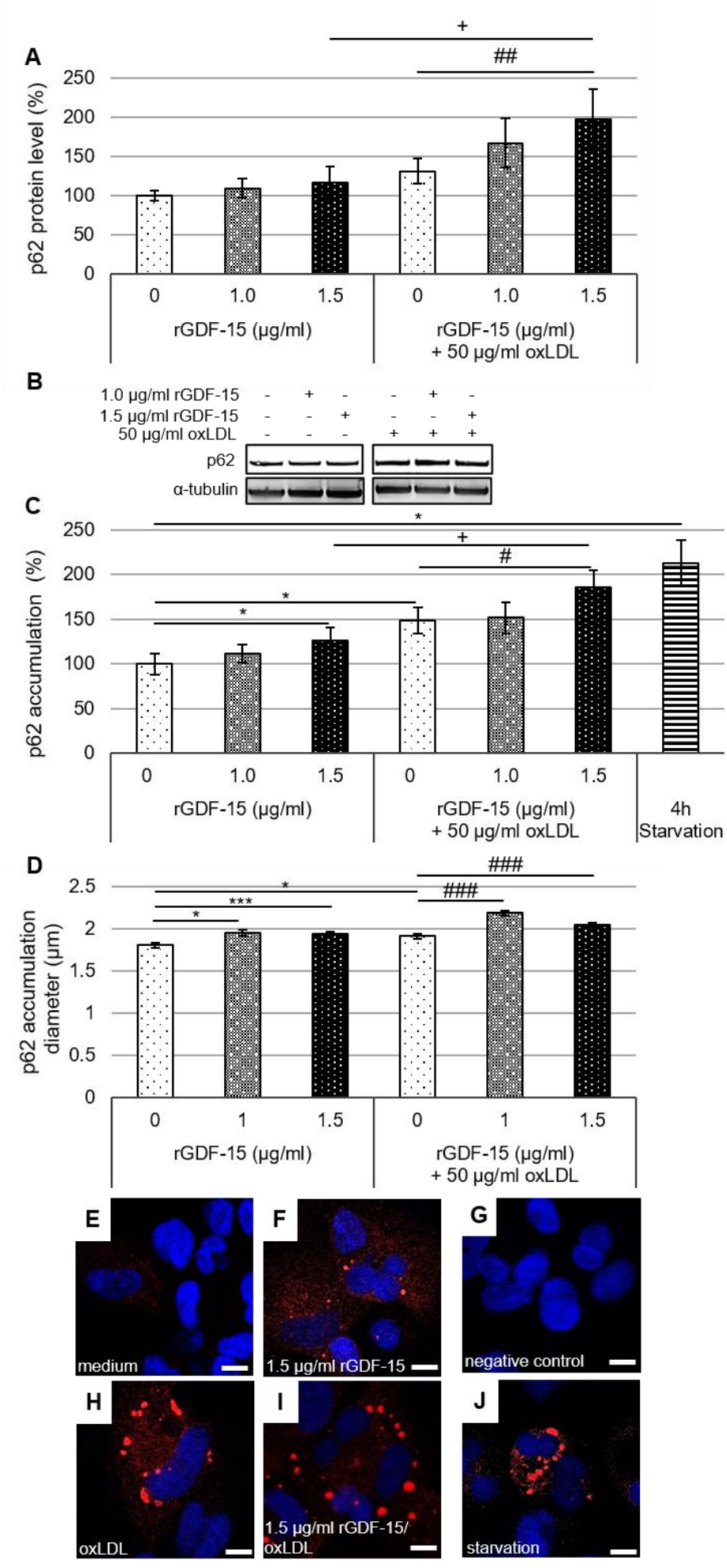
A
p62 protein level (%)
250
200
150
100
50
0
+
##
0
1.0
1.5
0
1.0
1.5
rGDF-15 (µg/ml)
rGDF-15 (µg/ml)
+ 50 µg/ml oxLDL
B
1.0 µg/ml rGDF-15 - + - - + -
1.5 µg/ml rGDF-15 - - + - - +
50 µg/ml oxLDL - - - + + +
p62
α-tubulin
C
p62 accumulation (%)
250
200
150
100
50
0
*
+
#
*
*
0
1.0
1.5
0
1.0
1.5
rGDF-15 (µg/ml)
rGDF-15 (µg/ml)
+ 50 µg/ml oxLDL
4h
Starvation
D
p62 accumulation diameter (µm)
2.5
2
1.5
1
0.5
0
*
***
*
###
###
0
1
1.5
0
1
1.5
rGDF-15 (µg/ml)
rGDF-15 (µg/ml)
+ 50 µg/ml oxLDL
E
medium
F
1.5 µg/ml rGDF-15
G
negative control
H
oxLDL
I
1.5 µg/ml rGDF-15/
oxLDL
J
starvation

*Figure 21:* **p62 protein level and p62 accumulation in THP-1 MΦ after exposure to rGDF-15 with / without oxLDL.** (A) Total p62 protein level (in % of THP-1 MΦ incubated in medium = 100%) in THP-1 MΦ. Expression was normalized against α-tubulin and quantified with ImageJ. Six independent experiments were performed (B) Representative Western Blot images for p62 and α-tubulin. (C) p62 accumulation (in % of THP-1 MΦ incubated in medium= 100%) was analyzed with Fiji ImageJ and normalized against DAPI. (D) Diameter of intracellularly accumulated p62 were measured in µm using Fiji ImageJ. Seven independent experiments were performed. Data are presented as mean ± SEM. (E-J) Representative immunofluorescence images of p62 accumulations (red) and DAPI (blue) double staining, visualized with laser scanning microscopy (Nikon Eclipse). (G) The negative control shows THP-1 MΦ DAPI stained without primary antibody against p62. Scale bars 50 µM. *$p < 0.05$, **$p < 0.01$ significance vs. THP-1 MΦ incubated in medium, $^{\#}p < 0.05$, $^{\#\#}p < 0.01$, $^{\#\#\#}p < 0.001$ significance vs. THP-1 MΦ + 50 µg/ml oxLDL, $^{+}p < 0.05$ significance vs. THP-1 MΦ incubated without 50 µg/ml oxLDL. Student-Newman-Keuls test (p62 total protein and p62 accumulation), Dunn's test (p62 accumulation diameter. Data (A-C; E-J) published in Ackermann et al., 2019b.

In order to investigate the autophagic process in more detail, the expression and accumulation of lysosomal-associated membrane protein-1 (Lamp-1), a marker for lysosomes, was determined to quantify fusion of autophagosomes with lysosomes (Biazik et al., 2015).

The exposure of THP-1 MΦ to 1.0 µg/ml or 1.5 µg/ml rGDF-15 resulted in a -22% decrease ($p \leq 0.04$) in the Lamp-1 protein level compared to THP-1 MΦ incubated in medium (Figure 22 A). Incubation of THP-1 MΦ with oxLDL led to -23% ($p = 0.003$) reduced Lamp-1 protein level in comparison to medium-incubated THP-1 MΦ. Additionally, Lamp-1 protein level in THP-1 MΦ was reduced after co-incubation with rGDF-15 / oxLDL (1.0 µg/ml rGDF-15 / oxLDL: -23%; 1.5 µg/ml rGDF-15 / oxLDL: -25%; $p = 0.001$) compared to medium-incubated THP-1 MΦ (Figure 22 A). Exposure of THP-1 MΦ to 1.0 µg/ml and 1.5 µg/ml rGDF-15 increased the Lamp-1 accumulation about 79% ($p = 0.037$) and 70% ($p = 0.029$) compared to THP-1 MΦ incubated in medium (Figure 22 B). THP-1 MΦ incubated with 50 µg/ml oxLDL showed 91% ($p = 0.026$) enhanced Lamp-1 accumulation compared to medium-incubated THP-1 MΦ. Co-incubation of THP-1 MΦ with 1.5 µg/ml rGDF-15 / oxLDL raised the Lamp-1 accumulation about 95% ($p = 0.029$) compared to 1.5 µg/ml rGDF-15 alone and about 74% ($p = 0.054$) compared to 50 µg/ml oxLDL alone (Figure 22 B). Additionally, starvation served as positive control for enhanced Lamp-1 accumulation (Zhou et al., 2013) and showed a 141% ($p = 0.003$) increase of Lamp-1 accumulation compared to THP-1 MΦ incubated in medium. Together with the number, the size of the Lamp-1 accumulations was evaluated (Figure 22 C). THP-1 MΦ co-incubated with rGDF-15 / oxLDL increased the diameter of intracellularly accumulated Lamp-1 about 0.15 µm (1.0 µg/ml rGDF-15, $p < 0.001$) , 0.25 µm (1.5 µg/ml rGDF-15, $p < 0.001$) and

0.16 µm (50 µg/ml oxLDL, $p < 0.001$) compared to medium-incubated THP-1 MΦ. Comparing exposure of THP-1 MΦ to 1.0 µg/ml rGDF-15 with 1.5 µg/ml rGDF-15, the diameter of Lamp-1 accumulation rose 0.13 µm ($p < 0.001$). Upon co-incubation of THP-1 MΦ with 1.0 µg/ml rGDF-15 / oxLDL the diameter of accumulated Lamp-1 decreased about 0.08 µm ($p=0.002$) compared to exposure with 50 µg/ml oxLDL (Figure 22 C).

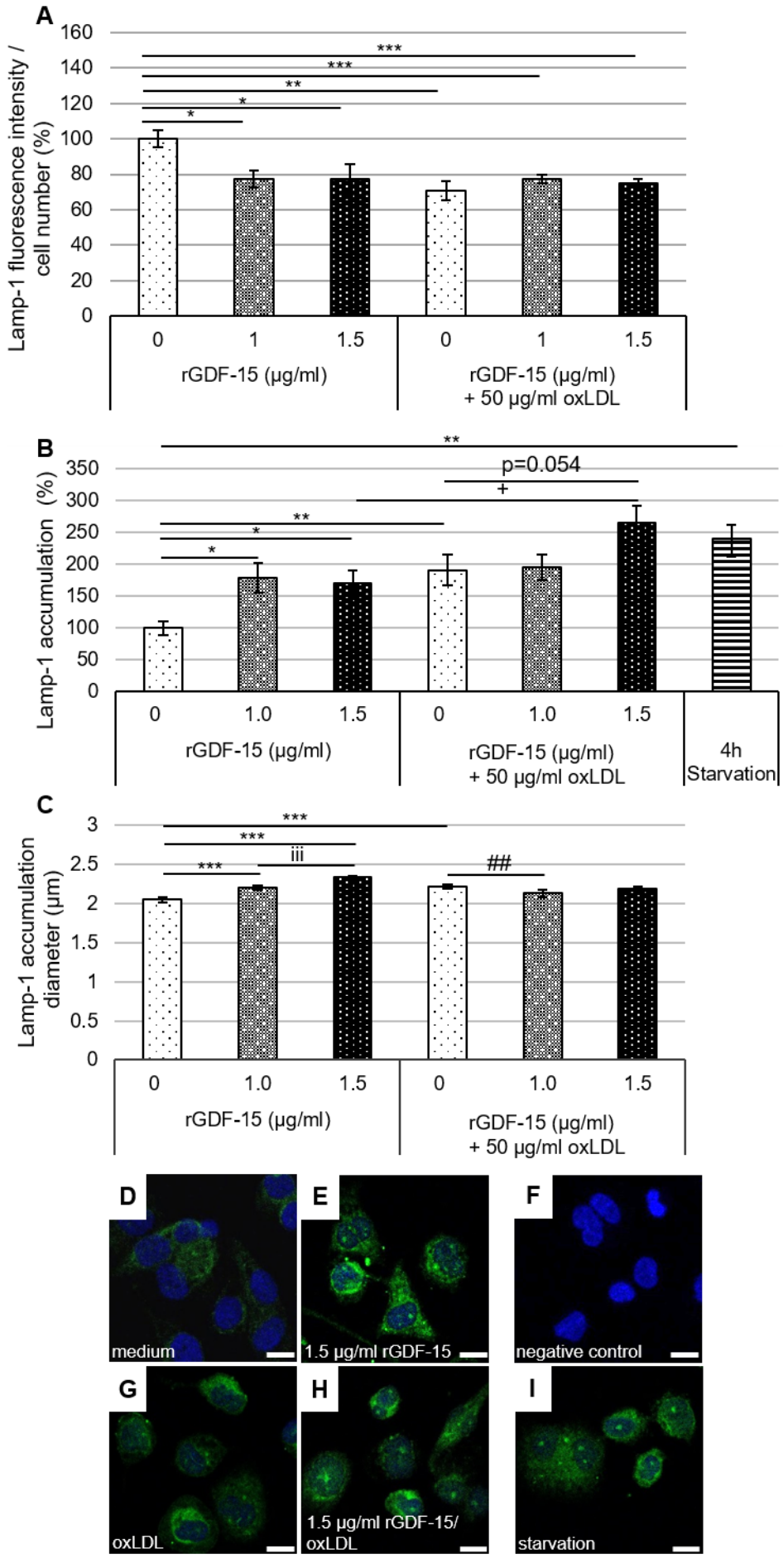
A
Lamp-1 fluorescence intensity / cell number (%)
160
140
120
100
80
60
40
20
0
***
***
**
*
*
0
1
1.5
0
1
1.5
rGDF-15 (µg/ml)
rGDF-15 (µg/ml)
+ 50 µg/ml oxLDL
B
Lamp-1 accumulation (%)
350
300
250
200
150
100
50
0
**
p=0.054
+
**
*
*
0
1.0
1.5
0
1.0
1.5
rGDF-15 (µg/ml)
rGDF-15 (µg/ml)
+ 50 µg/ml oxLDL
4h
Starvation
C
Lamp-1 accumulation diameter (µm)
3
2.5
2
1.5
1
0.5
0
***
***
***
iii
##
0
1.0
1.5
0
1.0
1.5
rGDF-15 (µg/ml)
rGDF-15 (µg/ml)
+ 50 µg/ml oxLDL
D
medium
E
1.5 µg/ml rGDF-15
F
negative control
G
oxLDL
H
1.5 µg/ml rGDF-15/
oxLDL
I
starvation

*Figure 22:* **Lamp-1 protein level and Lamp-1 accumulation in THP-1 MΦ after exposure to rGDF-15 with / without oxLDL.** (A) Lamp-1 protein level (in % of THP-1 MΦ incubated in medium = 100%) in THP-1 MΦ. Expression was measured using Alexafluor 488 conjugated antibody against Lamp-1 [$OD_{488/518}$] and normalized against total cell count (DAPI) [$OD_{405/455}$]. Six independent experiments were performed. (B) Lamp-1 accumulation (in % of THP-1 MΦ incubated in medium = 100%) was analyzed with Fiji ImageJ and normalized against DAPI. Six independent experiments were performed. (C) Diameters of intracellularly accumulated Lamp-1 were measured in µm using Fiji ImageJ. Seven independent experiments were performed. Data are presented as mean ± SEM. (D-I) Representative immunofluorescence images of Lamp-1 accumulations (green) and Dapi (blue) double staining, visualized with laser scanning microscopy (Nikon Eclipse). (E) The negative control shows Dapi-stained THP-1 MΦ without primary antibody against Lamp-1. Scale bars 50 µM. *$p < 0.05$, **$p < 0.01$, ***$p \leq 0.001$ significance vs. THP-1 MΦ incubated in medium, $^{\#\#}p < 0.01$ significance vs. THP-1 MΦ + 50 µg/ml oxLDL, +$p < 0.05$ significance vs. THP-1 MΦ incubated without 50 µg/ml oxLDL, $^{iii}p \leq 0.001$ significance vs. 1.0 µg/ml rGDF-15. Student-Newman-Keuls test (Lamp-1 total protein and Lamp-1 accumulation), Dunn's test (Lamp-1 accumulation diameter).

In order to analyze the effects on the autophagic flux caused by rGDF-15 and oxLDL, an autophagy activity assay (Figure 23 A) and a lysosome activity assay (Figure 23 B) were performed. THP-1 MΦ exposed to 1.0 µg/ml or 1.5 µg/ml rGDF-15 showed an enhanced autophagic activity by about 20% ($p = 0.039$) and 16% ($p = 0.018$) compared to medium-incubated THP-1 MΦ (Figure 23 A). Whereas incubation of THP-1 MΦ with 50 µg/ml oxLDL diminished the autophagic activity about -26% ($p = 0.013$) compared to THP-1 MΦ incubated in medium. Moreover, co-incubation of THP-1 MΦ with 1.0 µg/ml / 50 µg/ml oxLDL or 1.5 µg/ml rGDF-15 / 50 µg/ml oxLDL reduced the autophagic activity about -15% and -23% ($p < 0.001$) compared to medium-incubated THP-1 MΦ (Figure 23 A). Upon starvation, used as a positive control for autophagy-induction, the autophagic activity in THP-1 MΦ was significantly ($p = 0.024$) increased by 16% compared to medium-incubated THP-1 MΦ (Figure 23 A).

Together with the autophagic activity a lysosome activity assay was performed. The lysosomal activity in THP-1 MΦ was not influenced upon exposure to rGDF-15 (Figure 23 B), whereas 50 µg/ml oxLDL diminished the activity about -9% ($p = 0.039$) in comparison to medium-treated THP-1 MΦ. After the co-incubation of THP-1 MΦ with 1.0 µg/ml rGDF-15 / oxLDL or 1.5 µg/ml rGDF-15 / oxLDL a decreased lysosomal activity of about -10% ($p < 0.001$) and -13% ($p = 0.002$) was detectable compared to THP-1 MΦ exposed to rGDF-15 alone (without oxLDL) (Figure 23 B). THP-1 MΦ on starvation showed no changes in the lysosome activity compared to medium-incubated THP-1 MΦ.

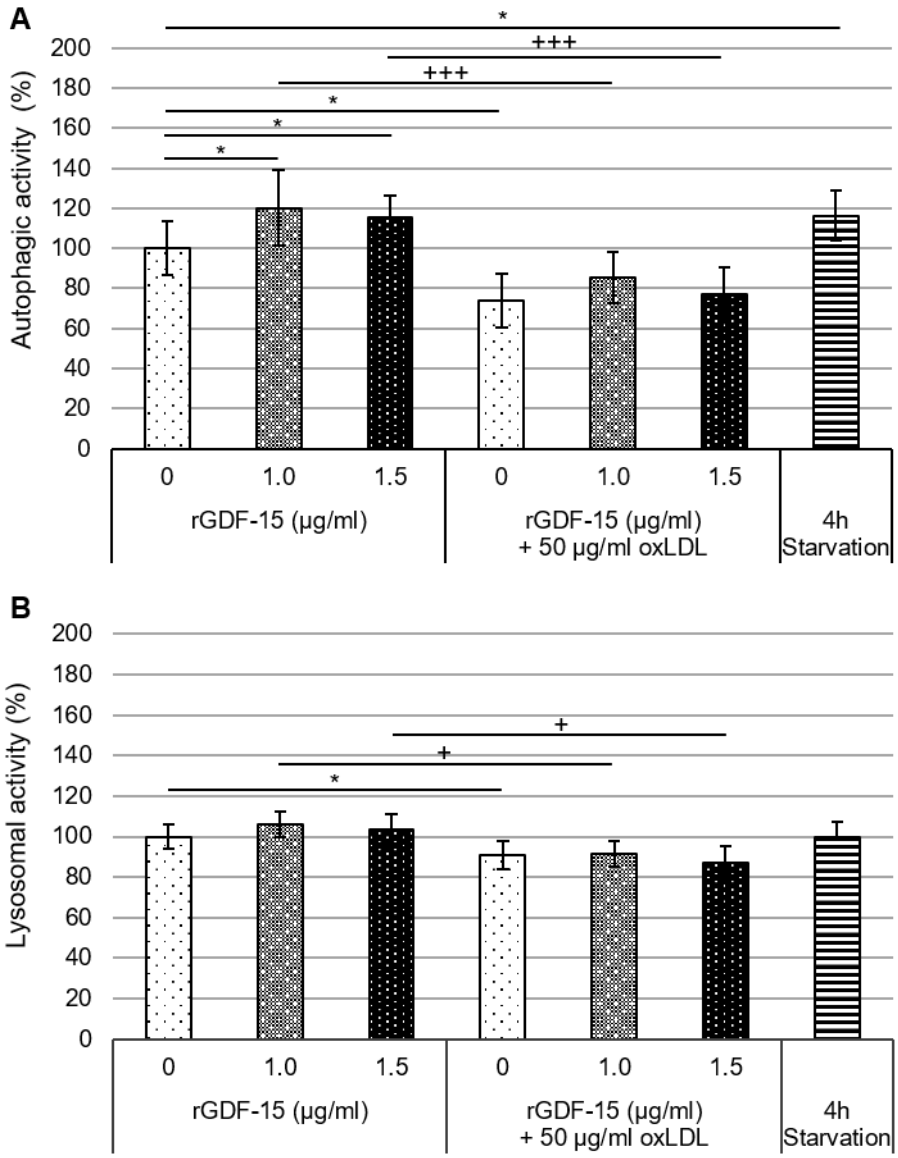


*Figure 23:* **Autophagic and lysosomal activity in THP-1 MΦ after exposure to rGDF-15 with / without oxLDL.** (A) Autophagic activity (in % of THP-1 MΦ incubated in medium = 100%) in THP-1 MΦ determined using blue fluorescent Cell Meter™ Autophagy Assay [$OD_{333/518}$]. Four independent experiments are presented as mean ± SEM. (B) Lysosomal activity (in % of THP-1 MΦ incubated in medium = 100%) in THP-1 MΦ determined using LysoBrite™ Red [$OD_{575/597}$]. Five independent experiments are presented as mean ± SEM. *$p < 0.05$ significance vs. THP-1 MΦ incubated in medium, $^{+}p < 0.01$, $^{+++}p < 0.001$ significance vs. THP-1 MΦ incubated without 50 µg/ml oxLDL. Student-Newman-Keuls test.

In order to investigate the impact of GDF-15 on the autophagy machinery further upstream of the phagophore expansion, mTOR, a marker for the autophagy initiation and Beclin-1, a marker for phagophore nucleation were examined.

Incubation of THP-1 MΦ with 50 µg/ml oxLDL led to 29% ($p < 0.05$) higher p-mTOR/mTOR ratio compared to medium-treated THP-1 MΦ (Figure 24). Upon exposure of THP-1 MΦ to 1.5 µg/ml rGDF-15 a 33% increase in

the p-mTOR / mTOR ratio compared to medium-incubated THP-1 MΦ was not significant (Figure 24). Co-incubation of THP-1 MΦ with rGDF-15 / oxLDL reduced the p-mTOR / mTOR ratio about -33% (1.0 µg/ml rGDF-15 / oxLDL) and -54% (1.5 µg/ml rGDF-15 / oxLDL) compared to oxLDL exposure, nevertheless these changes in the mTOR phosphorylation were not significant (Figure 24). THP-1 MΦ incubated with 80 µg/ml Rapamycin, i.e. a mTOR phosphorylation-inhibitor, showed a -60% ($p < 0.05$) reduction in the p-mTOR / mTOR ratio compared to THP-1 MΦ incubated in medium (Figure 24).

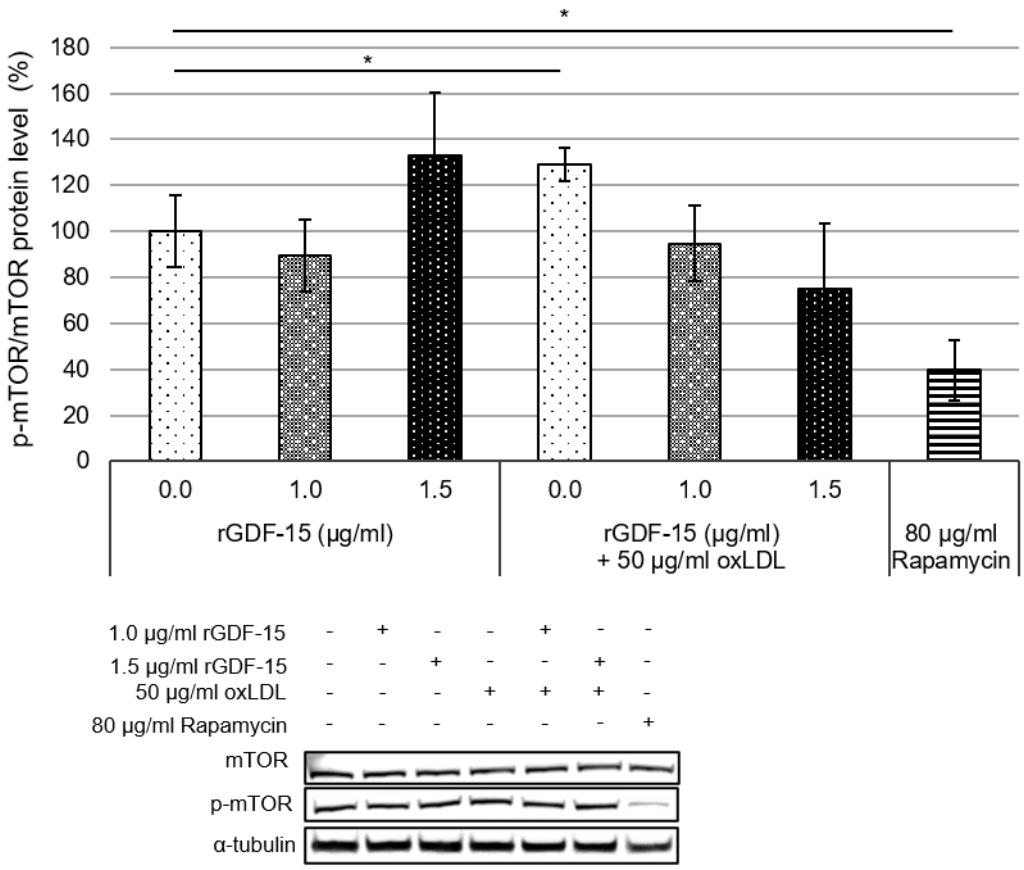


*Figure 24:* **p-mTOR / mTOR protein level in THP-1 MΦ after exposure to rGDF-15 with / without oxLDL.** p-mTOR/mTOR protein level (in % of THP-1 MΦ incubated in medium = 100%) in THP-1 MΦ. Expression was normalized against α-tubulin and quantified with ImageJ. Representative Western Blot images for mTOR, p-mTOR and α-tubulin. Four independent experiments were performed. Data are presented as mean ± SEM. *$p < 0.05$ significance vs. THP-1 MΦ incubated in medium. One Way Anova test.

After exposure of THP-1 MΦ to rGDF-15 or oxLDL no significant changes in the Beclin-1 protein levels compared to medium-incubated THP-1 MΦ were observed. (Figure 25).

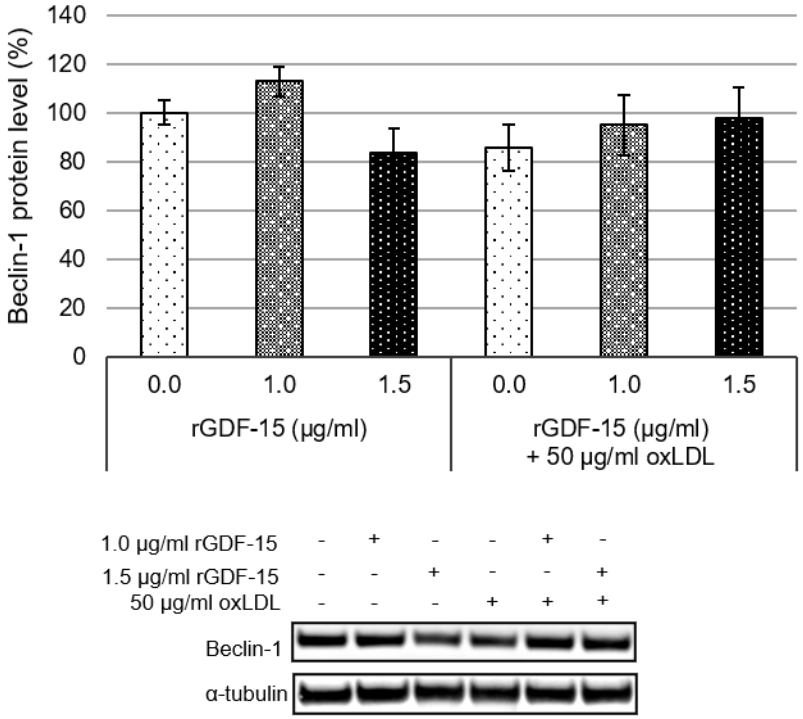


*Figure 25:* **Beclin-1 protein level in THP-1 MΦ after exposure to rGDF-15 with / without oxLDL.** Beclin-1 protein level (in % of THP-1 MΦ incubated in medium = 100%) %) in THP-1 MΦ**.** Expression was normalized against α-tubulin and quantified with ImageJ. Representative Western Blot images for Beclin-1 and α-tubulin. Four independent experiments were performed. Data are presented as mean ± SEM.

# 4 Discussion

## 4.1 GDF-15 in THP-1 MΦ

In the present work, THP-1 MΦ were rendered into foam cells, using oxidized (ox)LDL to investigate GDF-15-dependent MΦ lipid homeostasis and autophagy. This cell line was derived from an one-year old boy with acute monocytic leukaemia (Tsuchiya, Yamabe, et al., 1980). It is published that upon PMA-treatment, the cells become adherent, develop a MΦ-like phenotype and express surface markers like CD11b and CD14, which are known to be expressed in maturating monocytes (Schwende, Fitzke, et al., 1996). THP-1 MΦ are frequently used to study MΦ *in vitro*, since their homogenous genetic background minimizes the degree of variability in the cell phenotype (reviewed in Qin, 2012). This is advantageous for studying the biological function of chemicals with a high variability, such as oxLDL (reviewed in Qin, 2012). Furthermore, since transfection experiments in human primary monocytes and MΦ are often problematic, the downregulation of a protein of interest, using small interfering RNA (siRNA) is highly efficient in THP-1 (reviewed in Qin, 2012).

In this study, the transfection of MΦ with GDF-15 siRNA successfully downregulated the GDF-15-mRNA in medium-incubated siGDF-15 MΦ (-75%) and oxLDL-treated siGDF-15 MΦ (-104%) compared to identically incubated control (nsiGDF-15) MΦ. On the GDF-15 protein level, a reduction from over 50% was achieved for medium- or oxLDL-incubated siGDF-15 MΦ compared to nsiGDF-15 MΦ. Upon oxLDL-exposure an increased GDF-15 mRNA expression (37%) was detected, data which are in line with results from Schlittenhardt et al. (2004). However, the oxLDL-dependent increased GDF-15 expression was not yet detectable on the protein level after 4h oxLDL-exposure. This is discrepant to the data from Schlittenhardt et al. (2004), which also detected a rise in the GDF-15 protein level after exposure to 50 µg/ml oxLDL after 4h. This could be due to the different origin of the cell types used to generate MΦ. Schlittenhardt et. al differentiated peripheral blood mononuclear cells isolated from healthy donors (Schlittenhardt et al., 2004). Whereas here, the THP-1 monocytes originate from an acute monocytic leukemia patient (Tsuchiya et al., 1980). Therefore, it is possible that in THP-1 MΦ, 4h exposure is not sufficient to induce the oxLDL-caused changes in the GDF-15 expression on the protein level. Since the oxLDL-induced upregulation of GDF-15 on the RNA level could be detected after 4h, it is likely that THP-1 MΦ would show an upregulation in the translation with extended exposure time.

The exposure of THP-1 MΦ to 1.0 µg/ml or 1.5 µg/ml rGDF-15 increased the intracellular GDF-15 protein level about 82% and 99%. Also, the co-incubation of rGDF-15 / oxLDL raised the GDF-15 protein level in THP-1 MΦ in a concentration-dependent manner, whereas exposure to oxLDL alone did not significantly change the GDF-15 protein level compared to medium-incubated THP-1 MΦ. Therefore, these experimental settings were chosen to be appropriate to investigate a possible impact of GDF-15 on MΦ lipid homeostasis and autophagy.

## 4.2 GDF-15 and oxLDL independently influence lipid content in THP1 MΦ

The dysregulated lipid metabolism in plaque MΦ is one of the crucial events leading to plaque progression and necrotic core formation (reviewed in Maiolino et al., 2013). Normally, MΦ are able to regulate intracellular lipid content by reverse cholesterol transport, returning excess cholesterol to the liver for recycling or clearance (reviewed in Remmerie & Scott, 2018). In plaque-MΦ this protective mechanism is disturbed, leading to excess lipid accumulation and foam cell formation(Jeong et al., 2017). Previously, the cytokine GDF-15 was described to have regulatory effects on MΦ reverse cholesterol transport (Wu et al., 2014). Thus, in the present study, we tested whether downregulated (siGDF-15) or enhanced (rGDF-15) GDF-15 protein levels influence lipid accumulation and cholesterol levels after incubation of THP-1 MΦ with or without oxLDL.

### 4.2.1 GDF-15 raises lipid droplet-content in THP-1 MΦ

In the present work, THP-1 MΦ treated with 1.0 µg/ml or 1.5 µg/ml rGDF-15 for 4h showed increased, whereas GDF-15-silencing lowered the intracellular lipid accumulation. Surprisingly, THP-1 MΦ cholesterol levels (TC, EC, FC) were not altered upon modified intracellular GDF-15 protein levels. These results seem to be contradictive to findings from Wu et al. (2014), who reported an increased lipid efflux in THP-1 MΦ upon exposure to rGDF-15. They incubated PMA-differentiated THP-1 MΦ with 50 µg/ml oxLDL for 48h to fully differentiate the cells. Thereafter, MΦ were exposed to rGDF-15 in concentrations of 0.5 ng/ml, 1.0 ng/ml, 1.5 ng/ml and 2.0 ng/ml for 0-48h, followed by incubation with radioactive-labelled cholesterol for 72h. After assessing cholesterol levels with liquid scintillation counting, elevated cholesterol efflux was observed at concentrations exceeding 1.0 ng/ml rGDF-15 (Wu et al., 2014). This increased cholesterol efflux was implemented by increased ABCA-1 mRNA and protein expression, induced by rGDF-15 in a time- and dose-dependent manner (Wu et al., 2014). Nevertheless, the experimental setting from Wu et. al (2014) differs from the one implemented in this study.

Here, THP-1 monocytes were differentiated into MΦ by using PMA alone, whereas Wu et al. (2014) used PMA and 50 µg/ml oxLDL for 48h. Also, THP-1 MΦ were separately and for very much longer times exposed to oxLDL and rGDF15, followed by incubation with cholesterol for 72h (Wu et al., 2014). These considerable differences in the experimental setup may explain the contrary findings from Wu et al. (2014), where GDF-15 enhances lipid efflux. Whereas in this study, enhanced GDF-15 levels resulted in increased lipid accumulations. Even though, the GDF-15-dependent changes in the intracellular lipid accumulation were not accompanied by altered cholesterol levels, differences in the lysosomal accumulation could be observed.

In our study, enhanced GDF-15 levels resulted in augmented accumulations of Lamp-1 positive vesicles as well as their and size. These findings are in line with the here observed enhanced lipid accumulations, since MΦ process lipids in their lysosomes to store them in intracellular lipid droplets (Chistiakov et al., 2016). Whereas in our study, the lysosomal activity showed no differences upon enhanced GDF-15 levels. However, the observed changes in the lysosome accumulation could also be due to an increased autophagy activity, which was observed upon rGDF-15-exposure and is discussed in chapter 4.3. Under these circumstances, measuring the ACAT-1 enzyme activity would be helpful to clearly distinguish the reason for the changes in the Lamp-1 accumulation. An increased ACAT-1 activity upon rGDF-15 exposure would indicate that the enhanced Lamp-1 accumulations are, at least in part, due to the monitored augmented lipid accumulation. Additionally, the enzyme activity of LAL would be of interest, because the LAL-activity contributes to the processing of incorporated lipids and regulates the ABCA-1 expression (Bowden et al., 2011). Wu et al. (2014) attributed the GDF-15-enhancing lipid efflux to the activation of the transcription factor Sp1, which is found in the promotor region of the *abca1* gene (Chen et al., 2011). A Sp1-binding side is also present in the promotor region of the *gdf-15* gene (Böttner et al., 1999), as well as the *lipa* gene, encoding LAL (Ries et al., 1998). This would also set our findings in line with the reports from Wu et. al (2014), hinting that GDF-15 is involved in the ABCA-1 as well as the LAL induction at different time points in the signaling cascade. This further hints to GDF-15 as a regulatory cytokine involved in MΦ lipid handling and explains the GDF-15-dependent changes in the lysosome accumulation and lipid accumulation.

### 4.2.2 Exposure (4h) of THP-1 MΦ to oxLDL elevates lipid content without altering cholesterol levels

Histochemical and biochemical studies described the presence of oxLDL in foam cell-rich areas of advanced atherosclerotic lesions in men and rabbit (Rosenfeld et al., 1991; Ylä-Herttuala et al., 1989). Since then, numerous investigations concerning the homeostasis and processing of lipids in MΦ were performed. In the present work, exposure of THP-1 MΦ to 50 µg/ml oxLDL raised the lipid content independent of the GDF-15 status, when compared to medium-incubated THP-1 MΦ. Also, incubation of THP-1 MΦ with a combination of rGDF-15 / oxLDL did not further enhance the lipid accumulation significantly compared to oxLDL alone. Similar results were shown, i.e. in THP-1 MΦ exposed to oxLDL in concentrations between 20 µg/ml and 100 µg/ml for 24 hours, revealing a time- and dose-dependent increase in the lipid content via Oil-Red-O-staining (Liu et al., 2016; Zhou et al., 2016; Yang et al., 2017).

Surprisingly, here THP-1 MΦ showed no changes in the cholesterol level (TC, CE or FC) after exposure to 50 µg/ml oxLDL for 4h compared to medium-incubated THP-1 MΦ. THP-1 MΦ showed increased cholesterol levels after at least 48 h exposure with concentrations of minimum 30 µg/ml oxLDL (Batt, et al., 2004; Ma et al., 2018). In our study, the incubation time for THP-1 MΦ with oxLDL was significantly shorter than in the aforementioned publications. This could explain the unaltered cholesterol levels after 4h oxLDL-exposure. These observations are in line with groups, describing that the processing of oxLDL in MΦ is known to be much slower than e.g. the processing of acLDL (Ouimet et al., 2011; Roma et al., 1990). This explains the in this study non-detectable changes in the cholesterol levels of THP-1 MΦ upon 4h oxLDL-exposure, since oxLDL is still processed to be stored as CE. The reasons for the differences in the MΦ processing of acLDL and oxLDL were investigated by Yancey & Jerome (1998). They compared the loading of THP-1 MΦ with acLDL- or oxLDL-derived cholesterol (both 125 µg/ml, 1-7 days). After 7 days, they found 64% to 88% of the acLDL-cholesterol in cytoplasmic inclusions, meaning lipid droplets, whereas 60% to 90% of the oxLDL-derived cholesterol accumulated in lysosomes (Yancey & Jerome, 1998). The cholesterol esterification was 75% less in THP-1 MΦ enriched with oxLDL compared to THP-1 MΦ enriched with acLDL (Yancey & Jerome, 1998). This impaired lysosomal hydrolysis of oxLDL is due to a reduced lysosomal enzyme activity and is reported multiple times for murine and human MΦ (Emanuel et al., 2014; Hoppe et al., 1994; Jessup et al., 1992; Li et al., 1998; Lougheed et al., 1991; Roma et al., 1992). During lysosomal hydrolysis, oxLDL gets trapped in the lysosome and causes its expansion (Griffin et al., 2005; Lougheed et al., 1999; Yancey & Jerome, 2001).

In the present study, oxLDL-induced lysosomal changes were already detectable after 4h. THP-1 MΦ showed an enhanced accumulation of Lamp-1-positive vesicles, an increase in the size of these Lamp-1-positive vesicles as well as a diminished Lamp-1 fluorescence intensity upon oxLDL-exposure. This agrees with reports, where THP-1 MΦ exposed to 100 µg/ml oxLDL for 3 or 6 days showed large, swollen lysosomes (Jerome et al., 2008). Likewise, the increased size of the lysosomal compartment (Emanuel et al., 2014; Griffin et al., 2005; Lougheed et al., 1999; Yancey & Jerome, 2001) and an increase in the number of acidified vesicles (Lougheed et al., 1999) are already published. Furthermore, our observations of a diminished lysosome activity upon oxLDL-exposure are in accordance with findings of other groups, reporting impaired lysosomal enzyme activity after oxLDL-exposure (Emanuel et al., 2014; Hoppe et al., 1994; Jessup et al., 1992; Li et al., 1998; Lougheed et al., 1991; Roma et al., 1992). Trapped within lysosomes, oxLDL inhibits the ability to maintain an acid pH, mandatory for optimal enzyme function (reviewed in Jerome, 2006). This observed lysosomal pH increase is not due to an oxLDL-induced lysosomal membrane permeability (Emanuel et al., 2014). This type of membrane destabilization would result in cell death induction (Li et al., 2016), but oxLDL-loaded THP-1 MΦ remained viable for an extended period of time (Batt et al., 2004; reviewed in Tabas, 2002). Supposedly, the observed lysosomal pH-change upon oxLDL-exposure was caused by an increase in the FC-proportion in the lysosomal membrane (reviewed in Jerome, 2006; reviewed in Tabas, 2002). Since cellular membranes are composed of different lipids and, depending on the membrane requirements, a certain lipid-ratio is necessary to maintain the proper membrane fluidity, the resulting altered membrane properties inhibit the acidification process (reviewed in Jerome, 2006; reviewed in Tabas, 2002). The lysosomal acidification-process is depending on specialized ATPases, pumping protons into the lysosomal lumen (Crider & Xie, 2003). An altered membrane composition may disturb the transmembrane subunit of the v-ATPase, ultimately resulting in impaired lysosomal enzyme activity (Crider & Xie, 2003). The oxLDL-induced lysosome impairment was not only seen *in vitro,* i.e. ApoE$^{-/-}$ mice on western-diet for 2 month displayed lysosomal dysfunction in aortic-MΦ (Emanuel et al., 2014).

To further investigate, to which extend the applied 50 µg/ml oxLDL get trapped in MΦ lysosomes after 4h, the use of 1,1′-dioctadecyl-3,3,3′3′-tetra-methylindocyanide percholorate (DiI)-labeled oxLDL (DiI-oxLDL) (Xu et al., 2010), together with a lysosomal marker would be suitable to test for a possible trapping of oxLDL in lysosomes. Although the trapping of oxLDL within MΦ-lysosomes is sufficiently reported, the here observed increase in the lipid accumulation, verified by Oil-Red-O-staining, indicates the processing of lipids upon oxLDL-exposure for storage in cellular lipid droplets. Batt et al.

(2004) exposed THP-1 MΦ with oxLDL (30 µg/ml total cholesterol, 48h) and detected an increased level of CE together with a rising amount of intracellular triglycerides (TG). Therefore, measuring the intracellular TG levels together with the enzyme activity of LAL and ACAT-1 would be suitable experiments to complement the present data for further insights into MΦ oxLDL-processing. Furthermore, lysosomes are involved in MΦ lipophagy for lipid breakdown (Ouimet et al., 2011). The present results concerning the aforementioned oxLDL-caused changes on lysosomal activity and morphology could likewise, at least in part, result from the processing of excess lipids through autophagy. The implications of oxLDL on MΦ autophagy and the associated lysosomal changes are further discussed in the following chapter.

## 4.3 GDF-15 influences basal autophagy, but aggravates oxLDL-induced autophagic flux impairment in THP-1 MΦ

Initially discovered and investigated in yeast, in the last decades autophagy gained a lot of attention in the context of human cellular homeostasis. Defective autophagy is associated in the field of neurodegenerative, liver, muscle and cardiac diseases as well as cancer (reviewed in Levine & Kroemer, 2008). Until today, different forms of autophagy were described called macroautophagy, microautophagy or chaperone-mediated autophagy and multiple substrate-specific subforms, such as aggrephagy (aggregated proteins), xenophagy (invading pathogenes), mitophagy (mitochondria) or lipophagy (lipid droplets) (reviewed in Søreng et al., 2018). In the context of atherosclerosis, autophagic flux acts atheroprotective but gets impaired during atherosclerotic lesion progression (Liao et al., 2012; Razani et al., 2012; Zhou et al., 2016). In atherosclerotic plaques, autophagy relevant proteins were found to be mainly localized in MΦ (Razani et al., 2012), which are able to process excessive lipids through autophagy, called lipophagy (Ouimet et al., 2011). However, after prolonged exposure, oxLDL impaired autophagy in THP-1 MΦ (Liu et al., 2016) and peritoneal murine MΦ (Sergin et al., 2016). Interestingly in this context, GDF-15 colocalizes with oxLDL in plaque MΦ (Schlittenhardt et al., 2004) and is associated with MΦ lipid-handling (Wu et al., 2014). For the first time, this work shows the pivotal role of GDF-15 in MΦ autophagic processes and links GDF-15 to MΦ autophagy and lipid handling.

### 4.3.1 GDF-15 facilitates autophagosome formation

In this study, GDF-15-silencing in MΦ (siGDF-15 MΦ) led to an impaired ATG5, ATG12 / ATG5-complex and p62 protein level, as well as fewer p62 accumulations compared to nsiGDF-15 MΦ. This indicates a decreased autophagosome formation and

diminished autophagic flux. THP-1 MΦ exposed to rGDF-15 in concentrations of 1.0 µg/ml or 1.5 µg/ml showed no increment in the ATG5, ATG12 / ATG5-complex and p62 protein levels. However, rGDF-15 enhanced the p62 accumulations as well as the size of the detected p62-positive accumulations. Based on the present results for nsiGDF-15 MΦ, siGDF-15 MΦ and rGDF-15 MΦ, GDF-15 seems to enhance autophagosome maturation, followed by increased autophagic flux. This could be accomplished by stabilizing the ATG5 protein or facilitating ATG12 / ATG5-complex assembly.

These assumptions were confirmed by an autophagy assay, measuring the autophagic flux with Monodansylcadaverine (MDC). This auto-fluorescent substance was described to identify autophagic vesicles (Munafó & Colombo, 2001; Niemann et al., 2000). MDC accumulates upon amino acid deprivation in lipid-rich membranous compartments, which overlap with LC3 and LysoTracker, leading to an intensified fluorescence signal in an acid environment (Munafó & Colombo, 2001; Niemann et al., 2000; Vázquez & Colombo, 2009). This makes MDC a useful marker for autophagosomes and autophagolysosomes. In this study, in siGDF-15 MΦ the autophagic activity decreased compared to nsiGDF-15 MΦ and increased in THP-1 MΦ upon exposure to rGDF-15.

Additionally, the lysosome activity was measured by LysoBrite™ Red, another fluorescent substance that selectively accumulates in lysosomes, supposedly through the pH gradient, where the acid environment enhances the fluorescence. Here, the lysosome activity in THP-1 MΦ was not impaired upon GDF-15-silencing or rGDF-15-exposure. The proper usage and functionality of the autophagy and lysosome assays were assessed with starvation controls, meaning the deprivation of amino acids. This kind of starvation is known to induce autophagy and lysosome activity (Zhou et al., 2013). Here, this was confirmed by the significant enhancement of autophagy and lysosome activity in starved THP-1 MΦ. Hence, GDF-15-silencing or rGDF-15-exposure only affected autophagosome formation in THP-1 MΦ, which would affect the fusion with lysosomes, but not necessarily influence lysosome activity.

Consensual with this thesis, the accumulation and size of Lamp-1-positive vesicle increased upon rGDF-15 exposure, even if the lysosomal activity remained unaltered. This could be due to increased autophagosome and lysosome fusion, which does not necessarily require an increased lysosome activity, when autophagic flux occurs at basal levels. The observed diminished fluorescence of the Lamp-1 signal, indicating a decrease in the Lamp-1 protein level upon rGDF-15 exposure, does not seem to be compatible with an unaffected lysosome activity and increased Lamp-1 accumulation.

Lamp-1 and LysoBrite™ Red are often used indicators for lysosome formation and activity in context of autophagic flux, but there are limitations to these detection systems. LysoBrite™ Red is described to accumulate exclusively in lysosomes due to their acid pH and via proton pumps (AAT Bioquest, Sunnyvale, CA, USA). Depletion of individual v-ATPase subunits disrupts lysosome acidification, but does not affect autophagosome-lysosome fusion, showing that a low lysosomal pH is not a prerequisite for fusion with autophagosomes (Mauvezin et al., 2015). Furthermore, lysosome reformation occurs by recycling lysosomal components from autophagolysosomes. Therefore, Lamp-1-positive tubules protrude and bud off from autophagolysosomal membranes after substrate degradation, to form protolysosomes (Yu et al., 2010). These protolysosomes lack lysosomal acidity, but are positive for different lysosomal membrane markers, becoming acidic after a short period of maturing into complete lysosomes (Yu et al., 2010). Also, there is evidence that Lamp-1 and Lamp-2 labeled organelles might be not exclusively lysosomes. These membrane proteins were found to exist on a wide spectrum of endocytic organelles lacking lysosomal hydrolases (Cheng et al., 2018). Considering this, Lamp-1-detection and lysosome activity assay depending on the GDF-15 level, should be complemented by assessing lysosomal hydrolase activity, *e.g.* by measuring cathepsin B or D.

The hypothesis that GDF-15 influences ATG5 protein-stability and autophagosome elongation, is further supported by the non-impact of rGDF-15 on mTOR and Beclin-1 protein levels, which operate further upstream in autophagy-signaling. Phosphorylation of mTOR, a known mechanism to inhibit autophagy induction, as well as Beclin-1, necessary for autophagosome nucleation (reviewed in Ryter et al., 2013), were not affected by rGDF-15. Therefore, the detected GDF-15 influence on ATG5 and autophagosome elongation cannot be due to GDF-15 operating further upstream in autophagy signaling.

Since the autophagosome formation requires intense membrane remodeling and consumption, there are several cellular compartments (*e.g.* ER, Golgi apparatus, plasma membrane) discussed as possible membrane-contributing source (Dupont et al., 2014). Recently, autophagic structures were identified growing from neutral lipid stores in hepatocytes (Dupont et al., 2014). The triglyceride lipase PNPLA5 was identified to be mandatory for autophagy initiation and autophagic membrane biogenesis. An increase in the cellular lipid droplet content of hepatocytes increased the autophagic capacity, where LC3, ATG16L1 and PNPLA5 were found to colocalize with lipid droplets, initializing the growth of autophagic structures from lipid droplets (Dupont et al., 2014). This lipid droplet-enhanced autophagic capacity was dependent on PNPLA5 and in the

absence of lipid droplet build-up, autophagy still occurred, but at lower levels (Dupont et al., 2014). Since GDF-15 was found to influence the lipid accumulation and autophagosome formation in THP-1 MΦ, investigations of a possible relation between PNPLA5 and GDF-15 would be of great interest.

Another interesting link between MΦ lipid homeostasis and autophagy is the role of the transcription factor Sp1, which is involved in the reverse lipid efflux, as well as found in the gene encoding *gdf-15*. Furthermore, this transcription factor was also associated with autophagy in different cell types. In prostate cancer cells, autophagic flux decreased with Sp1-depletion (Ling, Liu, et al., 2017). Contrary to this, Sp1-deficiency induced autophagy in gastric cancer cells (Xu et al., 2018). This further links GDF-15 to autophagy and lipid homeostasis in MΦ and hints to a regulatory role of GDF-15 in the signalling pathway of both processes.

It is well described, that autophagy gets activated under numerous stress conditions, *e.g.* nutrition deprivation, growth factor withdrawal, oxidative stress, DNA damage or intracellular pathogens (reviewed in Maiuri, et al., 2013 and Moreau et al., 2010). Additionally, autophagy at basal levels occurs continuously as a quality control mechanism to clear and recycle aggregated proteins or dysfunctional organelles (reviewed in Denton et al., 2014). Thereby, basal autophagy maintains cell homeostasis and acts cytoprotective, constituting an initial barrier against apoptosis by promoting cell survival (reviewed in Marino et al., 2014 and Moreau et al., 2010). The switch from anti-apoptotic to pro-apoptotic signaling occurs by cleavage of essential ATG proteins, when cell stress-intensity increases (Yousefi et al., 2006; Rubinstein et al., 2011). In supporting autophagosome formation and increasing autophagic flux at basal levels, GDF-15 seems to act cytoprotectively to maintain a pro-survival signaling.

### 4.3.2 oxLDL inhibits THP-1 MΦ autophagy

Here, we show that THP-1 MΦ displayed no changes in the protein level of ATG5 or ATG12 / ATG5-complex after exposure to 50 µg/ml oxLDL for 4h. GDF-15-silencing resulted in a lower ATG5 protein level after oxLDL-exposure, compared to nsiGDF-15 MΦ exposed to oxLDL. Whereas, the ATG12 / ATG5-complex surprisingly showed no significant reduction in oxLDL-exposed siGDF-15 MΦ. Even though, the difference in the ATG12 / ATG5-complex level between siGDF-15 MΦ and nsiGDF-15 MΦ after oxLDL-exposure is visible but not significant, additional repetitions should verify this observation. However, exposure to oxLDL increased the p62 protein level as well as the p62 accumulations in siGDF-15 MΦ, nsiGDF-15 MΦ and non-transfected THP-1 MΦ compared to medium-incubated siGDF-15 MΦ, nsiGDF-15 MΦ and non-transfected

THP-1 MΦ. Besides, siGDF-15 MΦ exposed to oxLDL had less p62 accumulations than nsiGDF-15 MΦ, even though p62 protein level in siGDF-15 MΦ and nsiGDF-15 MΦ showed no differences. Although these observations indicate an impaired autophagosome formation in siGDF-15 MΦ upon oxLDL-exposure, GDF-15-silencing showed no significant changes compared to nsiGDF-15, when oxLDL was added. Overall, oxLDL impaired the autophagic and lysosomal activity, as already suggested by the increased p62 accumulation. The lacking difference between siGDF-15 MΦ and nsiGDF-15 MΦ, concerning autophagy and lysosome activity, could be explained with an excessive impairing effect of oxLDL on autophagic flux and lysosome activity. Still, the significant decrease in the p62 accumulation and ATG5 protein level comparing siGDF-15 MΦ with nsiGDF-15 MΦ indicate a decrease in the autophagosome formation upon GDF-15-deficiency. The in this study observed impairing effect of oxLDL on MΦ autophagy conforms with other groups, describing the inhibitory effect of higher concentrations of oxLDL on autophagic flux (Fan et al., 2015; Li et al., 2015; Liu et al., 2016; Sergin et al., 2016; Yang et al., 2017; Zhou et al., 2016). Zhou et al. (2016) found that low concentrations of oxLDL (5 µg/ml, 24h) increased the conversion of LC3 I to LC3 II, as well as decreased the p62 protein level, indicating an induction of autophagy to lessen lipid burden. However, at higher concentrations (≥ 20 µg/ml, 24h) oxLDL blocked the LC3I / LC3II conversion and the p62 protein level increased, leading to an impaired autophagic flux (Li et al., 2015; Liu et al., 2016; Yang et al., 2017; Zhou et al., 2016). Similar observations were described by Sergin et al. (2016), where murine MΦ exposed to 50 µg/ml oxLDL for 6h to 24h showed increased p62 accumulations.

In the present study, oxLDL-exposed THP-1 MΦ also displayed enhanced accumulations of Lamp-1-positive vesicles, which also increased in their size, when oxLDL was added. This indicates an enhanced number of lysosomes. However, the performed lysosome activity assay, revealed an impaired lysosomal activity. The increased diameter of Lamp-1 accumulation, but loss of lysosomal activity, upon oxLDL was already described by Emanuel et al. (2014). The here observed diminished lysosomal activity, conforms with results from other groups, where exposure to oxLDL or cholesterol crystals damaged MΦ lysosome membrane-integrity, leading to disruption of lysosomal pH and proteolytic capacity (Li et al., 1998; Duewell et al., 2010; Emanuel et al., 2014; Nihira et al., 2014). Furthermore, murine MΦ showed no co-localization of p62 and Lamp-2 after 24h incubation with oxLDL, which indicates an inhibition of autophagosome and lysosome fusion or disruption of lysosomal membrane integrity. Koga and collegues (2010) described a decreased fusion-efficiency between autophagosomes and lysosomes in murine hepatocytes after 16 weeks on high-fat-diet. This was due to changes in the lipid composition of lysosomal- and autophagic-vacuole

membranes. Interestingly, low-levels of cholesterol *in vitro* and high lipid concentrations *in vivo* had the same cholesterol-lowering effect on the membrane composition of lysosomal- and autophagic-vacuoles (Koga et al., 2010). These changes ultimately resulted in decreased clearance of autophagosomes (Koga et al., 2010). This shows, that the autophagic pathway is highly sensitive to changes in the cellular lipid metabolism. The inhibitory effect of oxLDL on autophagic flux, seems to be by the disruption of lysosomal activity, which leads to accumulation of p62 due to ineffective autophagosome clearance. Here, we were able to show oxLDL-dependent impairments in the autophagic flux and lysosomal activity of THP-1 MΦ. To verify, if exposure to 50 µg/ml oxLDL for 4h disrupts autophagosome and lysosome fusion, investigating the co-localisation of p62 and Lamp-1 would be advantageous. If the co-localisation of p62 / Lamp-1 decreased upon oxLDL-exposure, the observed increase in the accumulation of Lamp-1-positive vesicle and impaired lysosomal activity would be due to the trapping of oxLDL in lysosomes, before it is processed for storage in lipid droplets.

To test whether the disruption of the lysosomal activity is the major inhibitory effect of oxLDL on MΦ autophagy, we tested the phosphorylation-status of autophagy regulator mTOR and the expression of autophagy-relevant protein Beclin-1. Here, we found that THP-1 MΦ showed an increased ratio in the protein level of p-mTOR / mTOR upon oxLDL-exposure. This indicates an inhibition of autophagy induction by mTOR, regulated by oxLDL. The increased phosphorylation of mTOR upon prolonged (10-48 hours) oxLDL-exposure is already described for THP-1 MΦ, human monocytes and murine MΦ (Ma et al., 2018; Sohrabi, Lagache, et al., 2019; Wang, Li, et al., 2014). As positive control for a decrease in the p-mTOR / mTOR ration, we used rapamycin. This agent is a known inducer of autophagy, by inhibiting the kinase activity of mTOR (reviewed in Liu et al., 2019). Here, 80 µg/ml rapamycin significantly decreased the p-mTOR / mTOR ration. The oxLDL-derived inhibition of autophagy-induction would consequently downregulate Beclin-1 protein levels, since it operates downstream of mTOR-signaling in autophagosome nucleation (reviewed in Kang et al., 2011). In this study, the Beclin-1 protein level showed no changes upon oxLDL-exposure, even if phosphorylation of mTOR was induced. Yang et al. (2017) showed slightly diminished Beclin-1 protein levels in THP-1 MΦ upon 24h oxLDL-exposure, using 60 µg/ml oxLDL. Whereas p62 and LC3 II, autophagy-relevant proteins operating downstream in autophagy signaling, were already affected with lower oxLDL concentrations (Yang et al., 2017). Our data are in line with this, showing that oxLDL impairs autophagy, measured by p62 accumulation and autophagy activity assay, even though Beclin-1 expression remained unaltered.

### 4.3.3 rGDF-15 aggravates oxLDL-induced autophagy impairment

In this study, the co-incubation of rGDF-15 / oxLDL enhanced the protein levels of ATG5, ATG12 / ATG5-complex and p62 compared to oxLDL-exposure alone. Furthermore, incubation with 1.5 µg/ml rGDF-15 / oxLDL increased the number and size of p62-positive vesicles, as well as the number and size of Lamp-1-positive vesicles, when compared to oxLDL-exposure alone. The Lamp-1 fluorescence intensity remained depressed after rGDF-15 / oxLDL exposure compared to medium-incubated THP-1 MΦ. This implies a reduction in Lamp-1 protein level, which was already seen after exposure of THP-1 MΦ to rGDF-15 or oxLDL alone. These results suggest an enhanced autophagosome formation upon rGDF-15 / oxLDL exposure, but also an autophagic flux impairment. The unaffected Beclin-1 protein level and mTOR phosphorylation status upon rGDF-15 / oxLDL-exposure indicate that GDF-15 influences autophagosome formation but not the upstream autophagy signaling. In general, autophagy plays a cytoprotective role and autophagic activity intensifies when stress levels, like oxidative stress, increase (Liao et al., 2012; Marino et al., 2014). OxLDL is known to induce defensive autophagy in MΦ to lessen lipid burden, but in higher concentrations and with prolonged exposure, autophagy is impaired (Fan et al., 2015; Liu et al., 2016; Yang et al., 2017; Zhou et al., 2016).

Based on the aforementioned observations, co-incubation with rGDF-15 / oxLDL enhances the autophagosome formation in THP-1 MΦ, indicated by elevated ATG5 protein and ATG12 / ATG5- complex levels. Nevertheless, the inhibitory effect of oxLDL on THP-1 MΦ autophagy prevails upon exposure to rGDF-15 / oxLDL. This was shown by the increased p62 and Lamp-1 accumulations, as well as the decreased autophagy and lysosome activity, indicative of an impaired autophagic flux. OxLDL is reported to affect lysosomal activity and to decrease fusion efficiency between autophagosomes and lysosomes (Sergin et al., 2016), which conforms with the results showing decreased Lamp-1 protein levels and lysosome activity.

Taken together, GDF-15 enhances autophagosome formation and autophagy activity. However, in addition with oxLDL an enhanced GDF-15 protein level aggravates accumulation of autophagic vacuoles and autophagic flux impairment. Since it is known that impaired autophagy triggers cell apoptosis (Liao et al., 2012; Liu et al., 2016), additional experiments would be to investigate the cell apoptosis and necrosis upon rGDF-15 / oxLDL exposure, to verify the aforementioned conclusions concerning the effects of GDF-15 on MΦ autophagy.

## 4.4 Conclusions – Role of GDF-15 in MΦ autophagy

This work is the first one to demonstrate the pivotal role of GDF-15 in MΦ autophagy, using the human cell line THP-1 as a model for investigating MΦ autophagy. By influencing the autophagy-relevant proteins ATG5 and the ATG12 / ATG5-complex, GDF-15 promotes autophagosome formation. Thereby, GDF-15 increases autophagic flux, as shown by enhanced p62 and Lamp-1 accumulation as well as an increased autophagy activity. This process is illustrated in Figure 26 A, demonstrating the involvement of GDF-15 in autophagic processes during basal autophagy in MΦ. Furthermore, GDF-15 was found to enhance lipid accumulation in MΦ. This effect could be related to its role in MΦ autophagy, being an effect of lipophagy induction. Further investigations, concerning this GDF-15-effect on lipid homeostasis need to be executed to complement our current understanding concerning the involvement of GDF-15 in MΦ autophagy and lipid homeostasis.

However, based on its role in MΦ autophagy, GDF-15 seems to aggravate oxLDL-induced autophagy impairment during excess lipid stimuli. Figure 26 B illustrates the effect of oxLDL on MΦ autophagy. After receptor-mediated uptake, oxLDL is processed in lysosomes, leading to the storage of esterified cholesterol and triglycerides in lipid droplets. During excess lipid stimuli, MΦ are able to process lipids through lipophagy, breaking down lipid droplets for export. Nevertheless, excess lipid accumulation is also known to inhibit autophagic degradation, leading to the accumulation of autophagic vacuoles. In promoting the autophagosome formation, GDF-15 aggravates oxLDL-induced accumulation of autophagic vacuoles.

In the last years, a lot of promising therapeutic approaches in the field of atherosclerosis were investigated, using autophagy induction to reverse or slow down atherosclerotic progression. Even if further investigations are required to fully unravel the role of GDF-15 in MΦ autophagy and lipid homeostasis, the current insights reveal a promising potential for new therapeutic strategies e.g. in atherosclerosis.

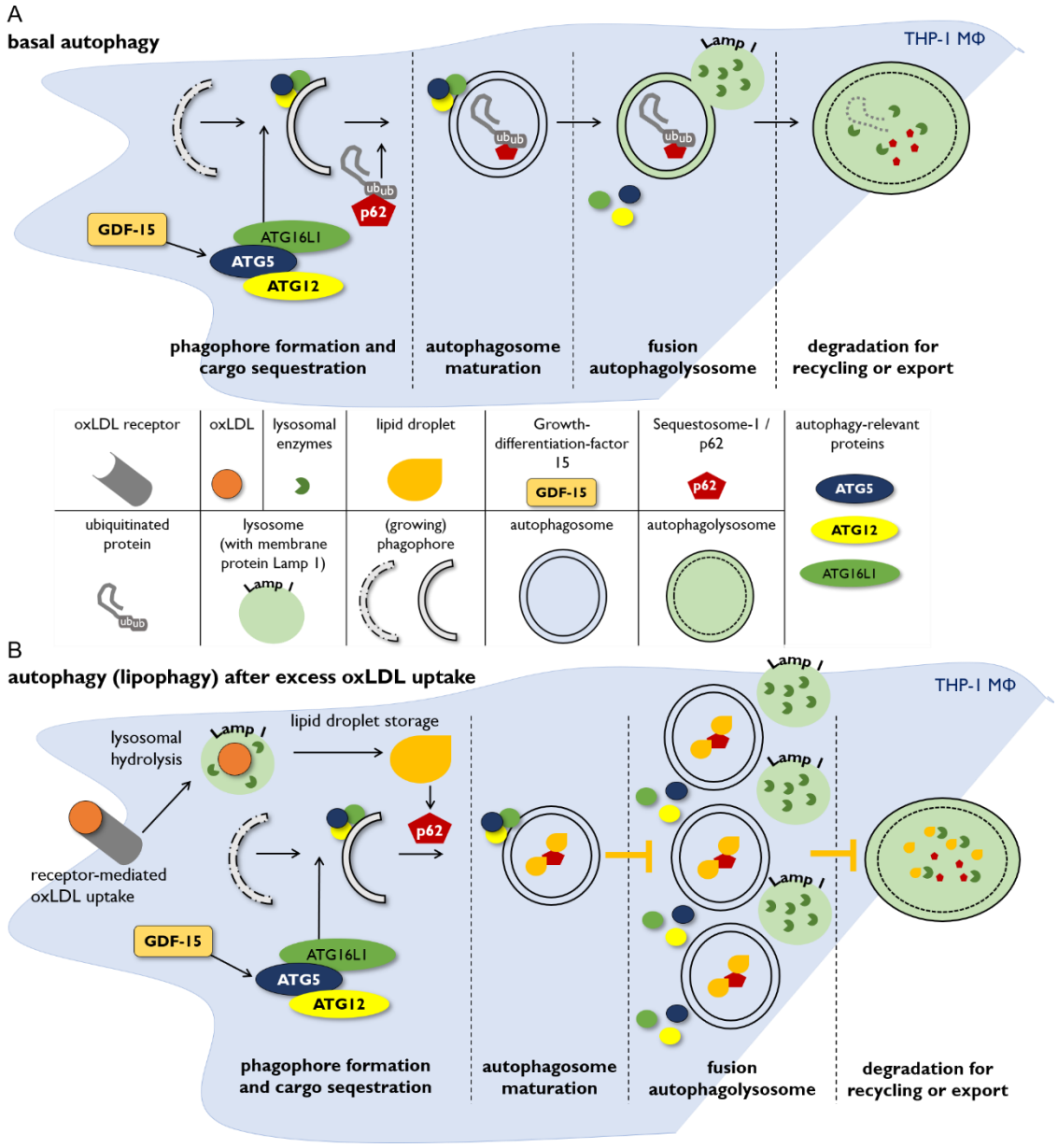


*Figure 26:* **Basal autophagy and autophagy after excess oxLDL-uptake in THP-1 MΦ**. Model of (A) basal autophagy and (B) autophagy (lipophagy) after excess oxLDL-uptake in THP-1 MΦ. (A) Under normal conditions, basal autophagy promotes cell survival by degrading misfolded, aggregated or defective proteins or organelles. GDF-15 supports autophagosome formation by influencing ATG5 stability or ATG5 / ATG12-complex formation. p62 chaperones for degradation marked, ubiquitinated proteins or organelles to the building phagophore and is sequestered along with its cargo within the maturated autophagosome. After fusion of the autophagosome with a lysosome, p62 and its cargo are degraded within the newly formed autophagolysosome by lysosomal enzymes. Afterwards, the released components are available for the cell or get exported. (B) After receptor-mediated uptake, oxLDL is enzymatically hydrolyzed in lysosomes and the emerging free cholesterol is stored in its esterified form within lipid droplets. To prevent foam cell formation, due to excess oxLDL uptake, lipid droplet breakdown is mediated through autophagy, called lipophagy. Thereby, lipid droplets, in whole or in part, are sequestered with p62 into autophagosomes. After fusion with a lysosome, lipids are enzymatically hydrolyzed to export the emerging free cholesterol out of the cell. Excess oxLDL-uptake blocks the lipophagy by blocking fusion of autophagolysosome, leading to accumulation of autophagosomes. Due to its enhancing effect on autophagosome formation, GDF-15 aggravates oxLDL-induced accumulation of autophagic vesicles (Ackermann et al., 2019b; modified).

# 5 Summary / Zusammenfassung

## 5.1 Summary

Cardiovascular diseases are the leading cause of death, representing more than 30% of all global deaths. Risk factors for developing atherosclerotic alterations are hypertension, diabetes, obesity, nicotine or alcohol abuse, which are widespread among industrial nations. Atherosclerotic alterations concern human arteries, where infiltration of modified lipids triggers an immune response, initiating the transmigration of monocytic cells and smooth muscle cells to remove this subendothelial accumulated lipids. In this context, autophagic processes were found highly active in atherosclerotic plaques, especially in lesional macrophages (MΦ). Supporting the MΦ reverse cholesterol transport, autophagy aids to resolve the subendothelial lipid accumulation, promoting plaque reduction and plaque stability. Furthermore, the cytokine Growth-Differentiation-Factor-15 (GDF-15) was found strongly expressed in lesional MΦ, where it is implicated in reverse cholesterol transport as well. These findings suggest a potential link between autophagy and GDF-15 in MΦ lipid homeostasis. This possible implication of GDF-15 in macrophages autophagy and lipid homeostasis was investigated in the present work.

Therefore, we diminished or increased GDF-15 protein levels in human THP-1 MΦ, using small interfering RNAs and recombinant GDF-15 protein. Exposing THP-1 MΦ to oxLDL was used to induce foam cell formation. Subsequently, intracellular lipid accumulation and cholesterol levels, autophagy-relevant proteins, as well as autophagic and lysosomal activity were investigated.

Aiming to investigate the basal autophagy in macrophages, we altered the GDF-15 protein level without exposing THP-1 MΦ to oxLDL. Diminishing the GDF-15 protein level in THP-1 MΦ led to decreased intracellular lipid accumulations, whereas cholesterol levels remained unaltered. Furthermore, the ATG5 and p62 protein levels decreased, as well as the ATG12 / ATG5-complex levels. Additionally, the p62 accumulation and the autophagy activity were diminished. Since ATG5 and ATG12 are mandatory for the autophagosome formation and p62 accumulation represents autophagic vesicles, these observations indicated to a diminished autophagosome formation, which explained the observed reduction in the autophagy activity. An increased GDF-15 protein level did not influence ATG5 and p62 protein levels or the ATG12 / ATG5-complex. However, it enhanced the p62 and Lamp-1 accumulations and increased the autophagy activity, whereas the lysosome activity remained unaltered. Thus, we concluded that GDF-15 possibly stabilizes the ATG5 protein level or facilitates the ATG12 / ATG5-complex assembly, leading to enhanced build-up in autophagic vesicles and thereby increasing the autophagy activity. To test, whether GDF-15 may operate further upstream in the

autophagy signaling pathway, we investigated the Beclin-1 protein level and phosphorylation status of mTOR. Amplified GDF-15 protein levels did not influence Beclin-1 or phosphorylation status of mTOR, which confirmed our conclusion about the impact of GDF-15 on MΦ autophagy being linked to ATG5 protein and/or ATG12 / ATG5-complex.

In exposing THP-1 MΦ to oxLDL, we induced foam cell formation. Upon oxLDL-exposure, THP-1 MΦ showed increased lipid accumulation, whereas the cholesterol levels remained unaltered. The p62 and Lamp-1 accumulation were increased, whereas the autophagic and lysosomal activities were diminished. These results were in line with already published data, where oxLDL was reported to induce lipid accumulation and to lead to lysosome expansion and to disturb lysosomal activity. Likewise, our observations of impaired autophagy activity and accumulation of autophagic vesicles have already been described.

In proceeding to investigate GDF-15-depending autophagy in foam cells, we exposed THP-1 MΦ with altered GDF-15 protein levels to oxLDL. The combination of an enhanced GDF-15 protein level in THP-1 MΦ and exposure to oxLDL increased the ATG5 and p62 protein levels and the ATG12 / ATG5-complex. Furthermore, increased GDF-15 protein levels in foam cells amplified the p62 and Lamp-1 accumulation, compared to oxLDL-exposure alone. Whereas an enhanced or diminished GDF-15 protein level in combination with oxLDL-exposure had no additional influence on the autophagy and lysosome activity, which remained repressed just like after exposure to oxLDL alone. Conclusively, we found that increased GDF-15 protein levels aggravated the oxLDL-induced accumulation of autophagic vesicles, whereas vice versa decreased GDF-15 protein levels diminished the oxLDl-induced accumulation of autophagic vesicles.

This work is the first one to reveal the crucial role of GDF-15 on MΦ autophagy: GDF-15 acts protective during basal autophagy, whereas during excess lipid stimuli, this GDF-15 influence on autophagosome formation aggravates the lipid-induced accumulation of autophagic vesicles. These observations identify GDF-15 as an important regulator in macrophage autophagy and lipid homeostasis, revealing its potential for new therapeutic strategies e.g. in atherosclerosis and cardiovascular diseases or stroke.

## 5.2 Zusammenfassung

Herz-Kreislauf-Erkrankungen sind die häufigste Todesursache mit mehr als 30% aller Todesfälle weltweit. Risikofaktoren für die Entwicklung arteriosklerotischer Veränderungen sind Bluthochdruck, Diabetes, Fettleibigkeit, Nikotin- oder Alkoholmissbrauch, welche in den Industrie-Nationen weit verbreitet sind. Arteriosklerotische Veränderungen betreffen menschliche Arterien, bei denen die Infiltration modifizierter Lipide eine Immunantwort auslöst. Diese Immunantwort führt zur Transmigration monozytärer Zellen und glatter Muskelzellen, um diese subendothelialen Lipidansammlungen zu entfernen. In diesem Zusammenhang wurde eine erhöhte Autophagie-Aktivität in arteriosklerotischen Plaques, insbesondere in Plaque-Makrophagen (MΦ) nachgewiesen. Diese erhöhte Autophagie-Aktivität trägt unter anderem zum Export von Cholesterin und somit zur Auflösung der subendothelialen Lipidansammlungen bei. Dadurch fördert Autophagie die Plaque-Reduktion und die Plaque-Stabilität. Darüber hinaus ist das Zytokin Wachstums-Differenzierungs-Faktor-15 (GDF-15) in Plaque- MΦ stark exprimiert, wo es am Export von Cholesterin beteiligt ist. Diese Beobachtungen deuten auf eine mögliche Verbindung zwischen Autophagie und GDF-15 in der Lipidhomöostase der MΦ hin, welche in der vorliegenden Arbeit untersucht wurde.

Dazu wurde das GDF-15-Proteinlevel in humanen THP-1-Makrophagen vermindert oder erhöht. Erreicht wurde dies durch die Verwendung von small interfering RNAs oder rekombinantem GDF-15-Protein. Die Bildung von Schaumzellen wurde dabei durch Stimulation der THP-1-MΦ mit oxLDL induzieren. Anschließend wurden die intrazelluläre Lipidakkumulation und der Cholesterinspiegel, Autophagie-relevante Proteine sowie die Autophagie- und Lysosomen-Aktivität untersucht.

Zur Untersuchung der basalen Autophagie in MΦ wurde das GDF-15-Proteinlevel modifiziert, ohne zunächst die Schaumzellbildung durch oxLDL zu induzieren. Die Verminderung des GDF-15-Proteinlevels führte zu einer verminderten intrazellulären Lipidanreicherung, während der Cholesterinspiegel unverändert blieb. Darüber hinaus erniedrigte sich das ATG5-Proteinlevel, das ATG12 / ATG5-Komplex-Level, sowie das p62-Proteinlevel, die p62-Akkumulationen und eine Verminderung in der Autophagie-Aktivität waren messbar. Da ATG5 und ATG12 essentiell für die Autophagosomenbildung sind und p62-Akkumulationen die Bildung von Autophagie-Vesikeln widerspiegeln, deuteten diese Beobachtungen auf eine verminderte Autophagosomenbildung hin, was wiederum die gemessene Verminderung in der Autophagie-Aktivität erklärt. Eine Erhöhung des GDF-15-Proteinlevels in THP-1- MΦ hatte keinen Einfluss auf das ATG5- und p62-Proteinlevel, oder die Bildung des ATG12 / ATG5-Komplex. Allerdings verstärkte es die p62- und

Lamp-1-Akkumulationen und erhöhte die Autophagie-Aktivität, während die Lysosomen-Aktivität unverändert blieb. Dies führte zu der Schlussfolgerung, dass GDF-15 möglicherweise das ATG5-Proteinlevel stabilisiert oder die Bildung des ATG12 / ATG5-Komplex erleichtert, was die verstärkte Bildung und Anreicherung von Autophagie-Vesikeln, sowie die erhöhte Autophagie-Aktivität erklären würde. Ein erhöhtes GDF-15-Proteinlevel zeigte keine Auswirkungen auf das Beclin-1 Proteinlevel oder den Phosphorylierungsstatus von mTOR. Somit festigte sich die Schlussfolgerung bezüglich des Einflusses von GDF-15 auf die Stabilisierung von ATG5 und/oder die Komplexbildung von ATG12 / ATG5.

Durch die oxLDL-Stimulation wurde die Schaumzellbildung in THP-1 MΦ induziert. Nach oxLDL-Stimulation zeigten THP-1 MΦ eine erhöhte Lipidakkumulation, während die Cholesterinwerte unverändert blieben. Die p62- und Lamp-1-Akkumulation nahm zu, während die Autophagie- und Lysosomen-Aktivität abnahm. Diese Ergebnisse standen im Einklang mit bereits publizierten Daten, in denen oxLDL eine Lipidakkumulation induzierte und zu einer Ausdehnung der Lysosomen führte, sowie die lysosomale Aktivität störte. Ebenso ist die hier nachgewiesene, gestörte Autophagie-Aktivität und die Akkumulation von Autophagie-Vesikeln bereits publiziert.

Zur Untersuchung der GDF-15-abhängigen Autophagie in Schaumzellen, wurden THP-1-MΦ mit modifiziertem GDF-15-Proteinlevel ebenfalls oxLDL-exponiert. Die Kombination eines erhöhten GDF-15 Proteinlevels führte in oxLDL-exponierten THP-1 MΦ zu einer Erhöhung des ATG5- und p62-Proteinlevels, sowie einer vermehrten ATG12 / ATG5-Komplex-Bildung. Darüber hinaus führte ein erhöhtes GDF-15 Proteinlevel in Kombination mit oxLDL zu vermehrten p62- und Lamp-1-Akkumulationen, verglichen mit alleiniger oxLDL-Stimulation. Eine Erhöhung oder Verminderung des GDF-15 Proteinlevels hatte keinen weiteren Einfluss auf die Autophagie- und die Lysosomen-Aktivität, welche beide weiterhin vermindert blieben, wie bereits nach alleiniger oxLDL-Stimulation feststellbar. Zusammenfassend konnten wir nachweisen, dass ein erhöhtes GDF-15 Proteinlevel die oxLDL-induzierte Akkumulation von Autophagie-Vesikeln verschlimmert, während umgekehrt ein erniedrigtes GDF-15 Proteinlevel die oxLDL-verursachte Akkumulation von Autophagie-Vesikeln erniedrigt.

Somit wurde in der vorliegenden Arbeit erstmals die entscheidende regulatorische Rolle von GDF-15 in der MΦ-Autophagie nachgewiesen. Durch Beeinflussung der Autophagosomen-Bildung wirkt GDF-15 während der basalen Autophagie schützend. Bei überschüssigem Lipid-Stimulus verschärft GDF-15 jedoch die lipidinduzierte Akkumulation von Autophagie-Vesikeln. Diese Erkenntnisse lassen sich möglicherweise

für neue therapeutische Strategien z.B. bei Arteriosklerose, kardiovaskulären Erkrankungen oder Schlaganfällen nutzen.

# 6 References

Ackermann, K., Bonaterra, G. A., Kinscherf, R., & Schwarz, A. (2019a). Data on autophagy markers in human macrophages exposed to oxLDL and growth differentiation factor-15. *Data in Brief*, *23*, 103728. https://doi.org/10.1016/j.dib.2019.103728

Ackermann, K., Bonaterra, G. A., Kinscherf, R., & Schwarz, A. (2019b). Growth differentiation factor-15 regulates oxLDL-induced lipid homeostasis and autophagy in human macrophages. *Atherosclerosis*, *281*, 128–136. https://doi.org/10.1016/j.atherosclerosis.2018.12.009

Adela, R., & Banerjee, S. K. (2015). GDF-15 as a Target and Biomarker for Diabetes and Cardiovascular Diseases: A Translational Prospective. *Journal of Diabetes Research*, *2015*, 490842. https://doi.org/10.1155/2015/490842

Baetta, R., Granata, A., Canavesi, M., Ferri, N., Arnaboldi, L., Bellosta, S., Pfister, P., & Corsini, A. (2009). Everolimus inhibits monocyte/macrophage migration in vitro and their accumulation in carotid lesions of cholesterol-fed rabbits. *Journal of Pharmacology and Experimental Therapeutics*, *328*(2), 419–425. https://doi.org/10.1124/jpet.108.144147

Batt, K. V., Avella, M., Moore, E. H., Jackson, B., Suckling, K. E., & Botham, K. M. (2004). Differential effects of low-density lipoprotein and chylomicron remnants on lipid accumulation in human macrophages. *Experimental Biology and Medicine*, *229*(6), 528–537. https://doi.org/10.1177/153537020422900611

Bento, C. F., Renna, M., Ghislat, G., Puri, C., Ashkenazi, A., Vicinanza, M., Menzies, F. M., & Rubinsztein, D. C. (2016). Mammalian Autophagy: How Does It Work? *Annual Review of Biochemistry*, *85*(1), 685–713. https://doi.org/10.1146/annurev-biochem-060815-014556

Beutner, F., Brendel, D., Teupser, D., Sass, K., Baber, R., Mueller, M., Ceglarek, U., & Thiery, J. (2012). Effect of everolimus on pre-existing atherosclerosis in LDL-receptor deficient mice. *Atherosclerosis*, *222*(2), 337–343. https://doi.org/10.1016/j.atherosclerosis.2012.03.003

Biazik, J., Ylä-Anttila, P., Vihinen, H., Jokitalo, E., & Eskelinen, E.-L. (2015). Ultrastructural relationship of the phagophore with surrounding organelles. *Autophagy*, *11*(3), 439–451. https://doi.org/10.1080/15548627.2015.1017178

Bobryshev, Y. V., Ivanova, E. A., Chistiakov, D. A., Nikiforov, N. G., & Orekhov, A. N. (2016). Macrophages and Their Role in Atherosclerosis: Pathophysiology and Transcriptome Analysis. *BioMed Research International*, *2016*(Figure 1), 9582430. https://doi.org/10.1155/2016/9582430

Bonaterra, G. A., Zügel, S., Thogersen, J., Walter, S. A., Haberkorn, U., Strelau, J., & Kinscherf, R. (2012). Growth differentiation factor-15 deficiency inhibits atherosclerosis progression by regulating interleukin-6-dependent inflammatory response to vascular injury. *Journal of the American Heart Association*, *1*(6). https://doi.org/10.1161/JAHA.112.002550

Bootcov, M. R., Bauskin, A. R., Valenzuela, S. M., Moore, A. G., Bansal, M., He, X. Y., Zhang, H. P., Donnellan, M., Mahler, S., Pryor, K., Walsh, B. J., Nicholson, R. C., Fairlie, W. D., Por, S. B., Robbins, J. M., & Breit, S. N. (1997). MIC-1, a novel macrophage inhibitory cytokine, is a divergent member of the TGF-beta superfamily. *Proceedings of the National Academy of Sciences of the United States of America*, *94*(21), 11514–11519. https://doi.org/10.1073/pnas.94.21.11514

Böttner, M, Suter-Crazzolara, C., Schober, A., & Unsicker, K. (1999). Expression of a novel member of the TGF-beta superfamily, growth/differentiation factor-15/macrophage-inhibiting cytokine-1 (GDF-15/MIC-1) in adult rat tissues. *Cell and Tissue Research*, *297*(1), 103–110. Retrieved from http://www.ncbi.nlm.nih.gov/pubmed/10398887

Böttner, Martina, Laaff, M., Schechinger, B., Rappold, G., Unsicker, K., & Suter-Crazzolara, C. (1999). Characterization of the rat, mouse, and human genes of growth/differentiation factor-15/macrophage inhibiting cytokine-1 (GDF-15/MIC-1). *Gene*, *237*(1), 105–111. https://doi.org/10.1016/S0378-1119(99)00309-1

Bowden, K. L., Bilbey, N. J., Bilawchuk, L. M., Boadu, E., Sidhu, R., Ory, D. S., Du, H., Chan, T., & Francis, G. A. (2011). Lysosomal Acid Lipase Deficiency Impairs Regulation of ABCA1 Gene and Formation of High Density Lipoproteins in Cholesteryl Ester Storage Disease. *Journal of Biological Chemistry*, *286*(35), 30624–30635. https://doi.org/10.1074/jbc.M111.274381

Brown, D. A., Breit, S. N., Buring, J., Fairlie, W. D., Bauskin, A. R., Liu, T., & Ridker, P. M. (2002). Concentration in plasma of macrophage inhibitory cytokine-1 and risk of cardiovascular events in women: A nested case-control study. *Lancet*, *359*(9324), 2159–2163. https://doi.org/10.1016/S0140-6736(02)09093-1

Brown, D. A., Stephan, C., Ward, R. L., Law, M., Hunter, M., Bauskin, A. R., Amin, J., Jung, K., Diamandis, E. P., Hampton, G. M., Russell, P. J., Giles, G. G., & Breit, S. N. (2006). Measurement of serum levels of macrophage inhibitory cytokine 1 combined with prostate-specific antigen improves prostate cancer diagnosis. *Clinical Cancer Research*, *12*(1), 89–96. https://doi.org/10.1158/1078-0432.CCR-05-1331

Cecconi, F., & Levine, B. (2008). The Role of Autophagy in Mammalian Development: Cell Makeover Rather than Cell Death. *Developmental Cell*, *15*(3), 344–357. https://doi.org/10.1016/j.devcel.2008.08.012

Chen, X., Zhao, Y., Guo, Z., Zhou, L., Okoro, E. U., & Yang, H. (2011). Transcriptional regulation of ATP-binding cassette transporter A1 expression by a novel signaling pathway. *The Journal of Biological Chemistry*, *286*(11), 8917–8923. https://doi.org/10.1074/jbc.M110.214429

Cheng, X. T., Xie, Y. X., Zhou, B., Huang, N., Farfel-Becker, T., & Sheng, Z. H. (2018). Characterization of LAMP1-labeled nondegradative lysosomal and endocytic compartments in neurons. *Journal of Cell Biology*, *217*(9), 3127–3139. https://doi.org/10.1083/jcb.201711083

Chistiakov, D. A., Bobryshev, Y. V., & Orekhov, A. N. (2016). Macrophage-mediated cholesterol handling in atherosclerosis. *Journal of Cellular and Molecular Medicine*, *20*(1), 17–28. https://doi.org/10.1111/jcmm.12689

Chistiakov, D. A., Melnichenko, A. A., Myasoedova, V. A., Grechko, A. V., & Orekhov, A. N. (2017). Mechanisms of foam cell formation in atherosclerosis. *Journal of Molecular Medicine*, *95*(11), 1153–1165. https://doi.org/10.1007/s00109-017-1575-8

Christian, P., Sacco, J., & Adeli, K. (2013). Autophagy: Emerging roles in lipid homeostasis and metabolic control. *Biochimica et Biophysica Acta - Molecular and Cell Biology of Lipids*, *1831*(4), 819–824. https://doi.org/10.1016/j.bbalip.2012.12.009

Chrysovergis, K., Wang, X., Kosak, J., Lee, S.-H., Kim, J. S., Foley, J. F., Travlos, G., Singh, S., Baek, S. J., & Eling, T. E. (2014). NAG-1/GDF-15 prevents obesity by increasing thermogenesis, lipolysis and oxidative metabolism. *International Journal of Obesity*, *38*(12), 1555–1564. https://doi.org/10.1038/ijo.2014.27

Chun, Y., & Kim, J. (2018). Autophagy: An Essential Degradation Program for Cellular Homeostasis and Life. *Cells*, *7*(12), 278. https://doi.org/10.3390/cells7120278

Crider, B. P., & Xie, X. S. (2003). Characterization of the functional coupling of bovine brain vacuolar-type H+-translocating ATPase. Effect of divalent cations, phospholipids, and subunit H (SFD). *Journal of Biological Chemistry*, *278*(45), 44281–44288. https://doi.org/10.1074/jbc.M307372200

Daniels, L. B., Clopton, P., Laughlin, G. A., Maisel, A. S., & Barrett-Connor, E. (2011). Growth-differentiation factor-15 is a robust, independent predictor of 11-year mortality risk in community-dwelling older adults: The rancho bernardo study. *Circulation*, *123*(19), 2101–2110. https://doi.org/10.1161/CIRCULATIONAHA.110.979740

de Jager, S. C. a, Bermúdez, B., Bot, I., Koenen, R. R., Bot, M., Kavelaars, A., de Waard, V., Heijnen, C. J., Muriana, F. J. G., Weber, C., van Berkel, T. J. C., Kuiper, J., Lee, S.-J., Abia, R., & Biessen, E. a L. (2011). Growth differentiation factor 15 deficiency protects against atherosclerosis by attenuating CCR2-mediated macrophage chemotaxis. *The Journal of Experimental Medicine*, *208*(2), 217–225. https://doi.org/10.1084/jem.20100370

De Meyer, G. R. Y., & Martinet, W. (2009). Autophagy in the cardiovascular system. *Biochimica et Biophysica Acta - Molecular Cell Research*, *1793*(9), 1485–1495. https://doi.org/10.1016/j.bbamcr.2008.12.011

De Meyer, I., Martinet, W., & De Meyer, G. R. Y. (2012). Therapeutic strategies to deplete macrophages in atherosclerotic plaques. *British Journal of Clinical Pharmacology*, *74*(2), 246–263. https://doi.org/10.1111/j.1365-2125.2012.04211.x

Denton, D., Xu, T., & Kumar, S. (2014). Autophagy as a pro-death pathway. *Immunology and Cell Biology*, *93*(1), 35–42. https://doi.org/10.1038/icb.2014.85

Dikic, I., & Elazar, Z. (2018). Mechanism and medical implications of mammalian autophagy. *Nature Reviews Molecular Cell Biology*, *19*(6), 349–364. https://doi.org/10.1038/s41580-018-0003-4

Duewell, P., Kono, H., Rayner, K. J., Sirois, C. M., Vladimer, G., Bauernfeind, F. G., Abela, G. S., Franchi, L., Nuñez, G., Schnurr, M., Espevik, T., Lien, E., Fitzgerald, K. a, Rock, K. L., Moore, K. J., Wright, S. D., Hornung, V., & Latz, E. (2010). NLRP3 inflammasomes are required for atherogenesis and activated by cholesterol crystals. *Nature*, *464*(7293), 1357–1361. https://doi.org/10.1038/nature08938

Dupont, N., Chauhan, S., Arko-Mensah, J., Castillo, E. F., Masedunskas, A., Weigert, R., Robenek, H., Proikas-Cezanne, T., & Deretic, V. (2014). Neutral Lipid Stores and Lipase PNPLA5 Contribute to Autophagosome Biogenesis. *Current Biology*, *24*(6), 609–620. https://doi.org/10.1016/j.cub.2014.02.008

Eggers, K. M., Kempf, T., Lind, L., Sundström, J., Wallentin, L., Wollert, K. C., & Siegbahn, A. (2012). Relations of growth-differentiation factor-15 to biomarkers reflecting vascular pathologies in a population-based sample of elderly subjects. *Scandinavian Journal of Clinical and Laboratory Investigation*, *72*(1), 45–51. https://doi.org/10.3109/00365513.2011.626072

Emanuel, R., Sergin, I., Bhattacharya, S., Turner, J. N., Epelman, S., Settembre, C., Diwan, A., Ballabio, A., & Razani, B. (2014). Induction of lysosomal biogenesis in atherosclerotic macrophages can rescue lipid-induced lysosomal dysfunction and downstream sequelae. *Arteriosclerosis, Thrombosis, and Vascular Biology*, *34*(9), 1942–1952. https://doi.org/10.1161/ATVBAHA.114.303342

Emmerson, P. J., Duffin, K. L., Chintharlapalli, S., & Wu, X. (2018). GDF15 and Growth Control. *Frontiers in Physiology*, *9*(November), 1–7. https://doi.org/10.3389/fphys.2018.01712

Evans, T. D., Sergin, I., Zhang, X., & Razani, B. (2017). Target acquired: Selective autophagy in cardiometabolic disease. *Science Signaling*, *10*(468), 1–18. https://doi.org/10.1126/scisignal.aag2298

Fairlie, W. D., Moore, a G., Bauskin, a R., Russell, P. K., Zhang, H. P., & Breit, S. N. (1999). MIC-1 is a novel TGF-beta superfamily cytokine associated with macrophage activation. *Journal of Leukocyte Biology*, *65*(1), 2–5.

Fan, X., Wang, J., Hou, J., Lin, C., Bensoussan, A., Chang, D., Liu, J., & Wang, B. (2015). Berberine alleviates ox-LDL induced inflammatory factors by up-regulation of autophagy via AMPK/mTOR signaling pathway. *Journal of Translational Medicine*, *13*, 1–11. https://doi.org/10.1186/s12967-015-0450-z

Fernandez-Ruiz, I., Puchalska, P., Narasimhulu, C. A., Sengupta, B., & Parthasarathy, S. (2016). Differential lipid metabolism in monocytes and macrophages: influence of cholesterol loading. *Journal of Lipid Research*, *57*(4), 574–586. https://doi.org/10.1194/jlr.M062752

Foxx, K. K., Roberts, R. L., & Waxdal, M. J. (2008). *Human OxLDL™ Technical Note 3*. Retrieved from www.kalenbiomed.com

Frostegard, J., Nilsson, J., Haegerstrand, A., Hamsten, A., Wigzell, H., & Gidlund, M. (1990). Oxidized low density lipoprotein induces differentiation and adhesion of human monocytes and the monocytic cell line U937. *Proceedings of the National Academy of Sciences of the United States of America*, *87*(3), 904–908.

Galis, Z. S., Sukhova, G. K., Lark, M. W., & Libby, P. (1994). Increased expression of matrix metalloproteinases and matrix degrading activity in vulnerable regions of human atherosclerotic plaques. *The Journal of Clinical Investigation*, *94*(6), 2493–2503. https://doi.org/10.1172/JCI117619

Galle, J., & Wanner, C. (n.d.). Oxidized LDL and Lp(a): Preparation, Modification, and Analysis. In *Free Radical and Antioxidant Protocols* (Vol. 108, pp. 119–130). https://doi.org/10.1385/0-89603-472-0:119

Ghosh, S., Zhao, B., Bie, J., & Song, J. (2010). Macrophage cholesteryl ester mobilization and atherosclerosis. *Vascular Pharmacology*, *52*(1–2), 1–10. https://doi.org/10.1016/j.vph.2009.10.002

Gisterå, A., & Hansson, G. K. (2017). The immunology of atherosclerosis. *Nature Reviews. Nephrology*, *13*(6), 368–380. https://doi.org/10.1038/nrneph.2017.51

Glass, C. K., & Witztum, J. L. (2001). Atherosclerosis. *Cell*, *104*(4), 503–516. https://doi.org/10.1016/S0092-8674(01)00238-0

Hansen, M., Rubinsztein, D. C., & Walker, D. W. (2018). Autophagy as a promoter of longevity: insights from model organisms. *Nature Reviews Molecular Cell Biology*, *19*(9), 579–593. https://doi.org/10.1038/s41580-018-0033-y

Hoppe, G., O'Neil, J., & Hoff, H. F. (1994). Inactivation of lysosomal proteases by oxidized low density lipoprotein is partially responsible for its poor degradation by mouse peritoneal macrophages. *Journal of Clinical Investigation*, *94*(4), 1506–1512. https://doi.org/10.1172/JCI117490

Jeong, S. J., Lee, M. N., & Oh, G. T. (2017). The Role of Macrophage Lipophagy in Reverse Cholesterol Transport. *Endocrinology and Metabolism (Seoul, Korea)*, *32*(1), 41–46. https://doi.org/10.3803/EnM.2017.32.1.41

Jerome, W. G. (2006). Advanced Atherosclerotic Foam Cell Formation Has Features of an Acquired Lysosomal Storage Disorder. *Rejuvenation Research*, *9*(2), 245–255. https://doi.org/10.1089/rej.2006.9.245

Jerome, W. G., Cox, B. E., Griffin, E. E., & Ullery, J. C. (2008). Lysosomal Cholesterol Accumulation Inhibits Subsequent Hydrolysis of Lipoprotein Cholesteryl Ester. *Microscopy and Microanalysis*, *14*(02), 138–149. https://doi.org/10.1017/S1431927608080069

Jessup, W., Mander, E. L., & Dean, R. T. (1992). The intracellular storage and turnover of apolipoprotein B of oxidized LDL in macrophages. *Biochimica et Biophysica Acta (BBA)/Lipids and Lipid Metabolism*, *1126*(2), 167–177. https://doi.org/10.1016/0005-2760(92)90287-6

Johnen, H., Kuffner, T., Brown, D. A., Wu, B. J., Stocker, R., & Breit, S. N. (2012). Increased expression of the TGF-b superfamily cytokine MIC-1/GDF15 protects ApoE-/- mice from the development of atherosclerosis. *Cardiovascular Pathology*, *21*(6), 499–505. https://doi.org/10.1016/j.carpath.2012.02.003

Kang, R., Zeh, H. J., Lotze, M. T., & Tang, D. (2011). The Beclin 1 network regulates autophagy and apoptosis. *Cell Death and Differentiation*, *18*(4), 571–580. https://doi.org/10.1038/cdd.2010.191

Kim, J., Kundu, M., Viollet, B., & Guan, K. L. (2011). AMPK and mTOR regulate autophagy through direct phosphorylation of Ulk1. *Nature Cell Biology*, *13*(2), 132–141. https://doi.org/10.1038/ncb2152

Kim, J. M., Kosak, J. P., Kim, J. K., Kissling, G., Germolec, D. R., Zeldin, D. C., Bradbury, J. A., Baek, S. J., & Eling, T. E. (2013). NAG-1/GDF15 transgenic mouse has less white adipose tissue and a reduced inflammatory response. *Mediators of Inflammation*, *2013*. https://doi.org/10.1155/2013/641851

Kim, K. H., Kim, S. H., Han, D. H., Jo, Y. S., Lee, Y. H., & Lee, M. S. (2018). Growth differentiation factor 15 ameliorates nonalcoholic steatohepatitis and related metabolic disorders in mice. *Scientific Reports*, *8*(1), 1–14. https://doi.org/10.1038/s41598-018-25098-0

Kinscherf, R., Claus, R., Wagner, M., Gehrke, C., Kamencic, H., Hou, D., Nauen, O., Schmiedt, W., Kovacs, G., Pill, J., Metz, J., & Deigner, H. P. (1998). Apoptosis caused by oxidized LDL is manganese superoxide dismutase and p53 dependent. *FASEB Journal : Official Publication of the Federation of American Societies for Experimental Biology*, *12*(6), 461–467

Koga, H., Kaushik, S., & Cuervo, A. M. (2010). Altered lipid content inhibits autophagic vesicular fusion. *The FASEB Journal*, *24*(8), 3052–3065. https://doi.org/10.1096/fj.09-144519

Kurdi, A., De Meyer, G. R. Y., & Martinet, W. (2016). Potential therapeutic effects of mTOR inhibition in atherosclerosis. *British Journal of Clinical Pharmacology*, *82*(5), 1267–1279. https://doi.org/10.1111/bcp.12820

Lawton, L. N., Bonaldo, M. F., Jelenc, P. C., Qiu, L., Baumes, S. A., Marcelino, R. A., de Jesus, G. M., Wellington, S., Knowles, J. A., Warburton, D., Brown, S., & Soares, M. B. (1997). Identification of a novel member of the TGF-beta superfamily highly expressed in human placenta. *Gene*, *203*(1), 17–26. https://doi.org/10.1016/S0378-1119(97)00485-X

Levine, B., & Kroemer, G. (2008). Autophagy in the Pathogenesis of Disease. *Cell*, *132*(1), 27–42. https://doi.org/10.1016/j.cell.2007.12.018

Li, G., Peng, J., Liu, Y., Li, X., Yang, Q., Li, Y., Tang, Z., Wang, Z., Jiang, Z., & Wei, D. (2015). Oxidized Low-Density Lipoprotein Inhibits THP-1-Derived Macrophage Autophagy via TET2 Down-regulation. *Lipids*, *50*(2), 177–183. https://doi.org/10.1007/s11745-014-3977-5

Li, M., Gao, P., & Zhang, J. (2016). Crosstalk between Autophagy and Apoptosis: Potential and Emerging Therapeutic Targets for Cardiac Diseases. *International Journal of Molecular Sciences*, *17*(3), 332. https://doi.org/10.3390/ijms17030332

Li, W., Sultana, N., Siraj, N., Ward, L. J., Pawlik, M., Levy, E., Jovinge, S., Bengtsson, E., & Yuan, X. M. (2016). Autophagy dysfunction and regulatory cystatin C in macrophage death of atherosclerosis. *Journal of Cellular and Molecular Medicine*, *20*(9), 1664–1672. https://doi.org/10.1111/jcmm.12859

Li, W., Yuan, X. M., Olsson, A. G., & Brunk, U. T. (1998). Uptake of oxidized LDL by macrophages results in partial lysosomal enzyme inactivation and relocation. *Arteriosclerosis, Thrombosis, and Vascular Biology*, *18*(2), 177–184. https://doi.org/10.1161/01.ATV.18.2.177

Liao, X., Sluimer, J. C., Wang, Y., Subramanian, M., Brown, K., Pattison, J. S., Robbins, J., Martinez, J., & Tabas, I. (2012). Macrophage Autophagy Plays a Protective Role in Advanced Atherosclerosis. *Cell Metabolism*, *15*(4), 545–553. https://doi.org/10.1016/j.cmet.2012.01.022

Libby, P., Buring, J. E., Badimon, L., Hansson, G. K., Deanfield, J., Bittencourt, M. S., Tokgözoğlu, L., & Lewis, E. F. (2019). Atherosclerosis. *Nature Reviews Disease Primers*, *5*(1), 56. https://doi.org/10.1038/s41572-019-0106-z

Libby, P., Ridker, P. M., & Hansson, G. K. (2011). Progress and challenges in translating the biology of atherosclerosis. *Nature*, *473*(7347), 317–325. https://doi.org/10.1038/nature10146

Lin, J. F., Wu, S., Hsu, S. Y., Yeh, K. H., Chou, H. H., Cheng, S. T., Wu, T. Y., Hsu, W. T., Yang, C. C., & Ko, Y. L. (2014). Growth-differentiation factor-15 and major cardiac events. *American Journal of the Medical Sciences*, *347*(4), 305–311. https://doi.org/10.1097/MAJ.0b013e318291cd4e

Ling, Z., Liu, D., Zhang, G., Liang, Q., Xiang, P., Xu, Y., Han, C., & Tao, T. (2017). miR-361-5p modulates metabolism and autophagy via the Sp1-mediated regulation of PKM2 in prostate cancer. *Oncology Reports*, *38*(3), 1621–1628. https://doi.org/10.3892/or.2017.5852

Liu, H. H., Cao, Y. J., Tong, T., Shi, J. J., Zhang, Y. L., Yang, Y. P., & Liu, C. F. (2015). Autophagy in atherosclerosis: A phenomenon found in human carotid atherosclerotic plaques. *Chinese Medical Journal*, *128*(1), 69–74. https://doi.org/10.4103/0366-6999.147815

Liu, X., Tang, Y., Cui, Y., Zhang, H., & Zhang, D. (2016). Autophagy is associated with cell fate in the process of macrophage-derived foam cells formation and progress. *Journal of Biomedical Science*, *23*(1), 57. https://doi.org/10.1186/s12929-016-0274-z

Liu, Y., Yang, F., Zou, S., & Qu, L. (2019). Rapamycin: A bacteria-derived immunosuppressant that has anti-atherosclerotic effects and its clinical application. *Frontiers in Pharmacology*, *9*(JAN), 1–15. https://doi.org/10.3389/fphar.2018.01520

Lougheed, M., Moore, E. D. W., Scriven, D. R. L., & Steinbrecher, U. P. (1999). Uptake of oxidized LDL by macrophages differs from that of acetyl LDL and leads to expansion of an acidic endolysosomal compartment. *Arteriosclerosis, Thrombosis, and Vascular Biology*, *19*(8), 1881–1890. https://doi.org/10.1161/01.ATV.19.8.1881

Lougheed, M., & Steinbrecher, U. P. (1996). Mechanism of uptake of copper-oxidized low density lipoprotein in macrophages is dependent on its extent of oxidation. *Journal of Biological Chemistry*, *271*(20), 11798–11805. https://doi.org/10.1074/jbc.271.20.11798

Lougheed, M., Zhang, H., & Steinbrecher, U. P. (1991). Oxidized low density lipoprotein is resistant to cathepsins and accumulates within macrophages. *Journal of Biological Chemistry*, *266*(22), 14519–14525.

Lusis, A. J. (2000). Atherosclerosis. *Nature*, *407*(6801), 233–241. https://doi.org/10.1038/35025203

Ma, Y., Huang, Z., Zhou, Z., He, X., Wang, Y., Meng, C., Huang, G., & Fang, N. (2018). A novel antioxidant Mito-Tempol inhibits ox-LDL-induced foam cell formation through restoration of autophagy flux. *Free Radical Biology and Medicine*, *129*(May), 463–472. https://doi.org/10.1016/j.freeradbiomed.2018.10.412

Macia, L., Tsai, V. W. W., Nguyen, A. D., Johnen, H., Kuffner, T., Shi, Y. C., Lin, S., Herzog, H., Brown, D. A., Breit, S. N., & Sainsbury, A. (2012). Macrophage inhibitory cytokine 1 (MIC-1/GDF15) decreases food intake, body weight and improves glucose tolerance in mice on normal & obesogenic diets. *PLoS ONE*, *7*(4), 1–8. https://doi.org/10.1371/journal.pone.0034868

Maiolino, G., Rossitto, G., Caielli, P., Bisogni, V., Rossi, G. P., & Calò, L. A. (2013). The role of oxidized low-density lipoproteins in atherosclerosis: The myths and the facts. *Mediators of Inflammation*, *2013*. https://doi.org/10.1155/2013/714653

Maiuri, M. C., Grassia, G., Platt, A. M., Carnuccio, R., Ialenti, A., & Maffia, P. (2013). Macrophage autophagy in atherosclerosis. *Mediators of Inflammation*, *2013*. https://doi.org/10.1155/2013/584715

Marino, G., Niso-Santano, M., Baehrecke, E. H., & Kroemer, G. (2014). Self-consumption: the interplay of autophagy and apoptosis. *Nat Rev Mol Cell Biol*, *15*(2), 81–94. https://doi.org/10.1038/nrm3735

Martinet, W., & De Meyer, G. R. Y. (2009). Autophagy in Atherosclerosis. *Circulation Research*, *104*(3), 304–317. https://doi.org/10.1161/CIRCRESAHA.108.188318

Martinet, W., Verheye, S., & De Meyer, G. R. Y. (2007). Everolimus-induced mTOR inhibition selectively depletes macrophages in atherosclerotic plaques by autophagy. *Autophagy*, *3*(3), 241–244. https://doi.org/3711 [pii]

Mauvezin, C., Nagy, P., Juhász, G., & Neufeld, T. P. (2015). Autophagosome-lysosome fusion is independent of V-ATPase-mediated acidification. *Nature Communications*, *6*(May). https://doi.org/10.1038/ncomms8007

McLaren, J. E., Michael, D. R., Ashlin, T. G., & Ramji, D. P. (2011). Cytokines, macrophage lipid metabolism and foam cells: Implications for cardiovascular disease therapy. *Progress in Lipid Research*, *50*(4), 331–347. https://doi.org/10.1016/j.plipres.2011.04.002

Mehrpour, M., Esclatine, A., Beau, I., & Codogno, P. (2010). Overview of macroautophagy regulation in mammalian cells. *Cell Research*, *20*(7), 748–762. https://doi.org/10.1038/cr.2010.82

Moore, K. J., Sheedy, F. J., & Fisher, E. A. (2013). Macrophages in atherosclerosis: a dynamic balance. *Nature Reviews Immunology*, *13*(10), 709–721. https://doi.org/10.1038/nri3520

Moore, K. J., & Tabas, I. (2011). Macrophages in the Pathogenesis of Atherosclerosis. *Cell*, *145*(3), 341–355. https://doi.org/10.1016/j.cell.2011.04.005

Moreau, K., Luo, S., & Rubinsztein, D. C. (2010). Cytoprotective roles for autophagy. *Current Opinion in Cell Biology*, *22*(2), 206–211. https://doi.org/10.1016/j.ceb.2009.12.002

Mueller, M. A., Beutner, F., Teupser, D., Ceglarek, U., & Thiery, J. (2008). Prevention of atherosclerosis by the mTOR inhibitor everolimus in LDLR-/- mice despite severe hypercholesterolemia. *Atherosclerosis*, *198*(1), 39–48. https://doi.org/10.1016/j.atherosclerosis.2007.09.019

Mullican, S. E., Lin-Schmidt, X., Chin, C.-N., Chavez, J. A., Furman, J. L., Armstrong, A. A., Beck, S. C., South, V. J., Dinh, T. Q., Cash-Mason, T. D., Cavanaugh, C. R., Nelson, S., Huang, C., Hunter, M. J., & Rangwala, S. M. (2017). GFRAL is the receptor for GDF15 and the ligand promotes weight loss in mice and nonhuman primates. *Nature Medicine*, *23*(10), 1150–1157. https://doi.org/10.1038/nm.4392

Munafó, D. B., & Colombo, M. I. (2001). A novel assay to study autophagy: Regulation of autophagosome vacuole size by amino acid deprivation. *Journal of Cell Science*, *114*(20), 3619–3629.

Niemann, A., Takatsuki, A., & Elsässer, H. P. (2000). The lysosomotropic agent monodansylcadaverine also acts as a solvent polarity probe. *Journal of Histochemistry and Cytochemistry*, *48*(2), 251–258. https://doi.org/10.1177/002215540004800210

Nihira, K., Miki, Y., Ono, K., Suzuki, T., & Sasano, H. (2014). An inhibition of p62/SQSTM1 caused autophagic cell death of several human carcinoma cells. *Cancer Science*, *105*(5), 568–575. https://doi.org/10.1111/cas.12396

Ouimet, M. (2013). Autophagy in obesity and atherosclerosis: Interrelationships between cholesterol homeostasis, lipoprotein metabolism and autophagy in macrophages and other systems. *Biochimica et Biophysica Acta*, *1831*(6), 1124–1133. https://doi.org/10.1016/j.bbalip.2013.03.007

Ouimet, M., Franklin, V., Mak, E., Liao, X., Tabas, I., & Marcel, Y. L. (2011). Autophagy regulates cholesterol efflux from macrophage foam cells via lysosomal acid lipase. *Cell Metabolism*, *13*(6), 655–667. https://doi.org/10.1016/j.cmet.2011.03.023

Park, Y. M. (2014). CD36, a scavenger receptor implicated in atherosclerosis. *Experimental & Molecular Medicine*, *46*(6), e99–e99. https://doi.org/10.1038/emm.2014.38

Pirillo, A., Norata, G. D., & Catapano, A. L. (2013). LOX-1, OxLDL, and Atherosclerosis. *Mediators of Inflammation*, *2013*(Figure 1), 1–12. https://doi.org/10.1155/2013/152786

Preusch MR, Baeuerle M, Albrecht C, Blessing E, Bischof M, Katus HA, B. F. (2013). GDF-15 protects from macrophage accumulation in a mousemodel of advanced atherosclerosis. *Eur J Med Res.*, *24*(18), 9. https://doi.org/doi: 10.1186/2047-783X-18-19

Qin, Z. (2012). The use of THP-1 cells as a model for mimicking the function and regulation of monocytes and macrophages in the vasculature. *Atherosclerosis*, *221*(1), 2–11. https://doi.org/10.1016/j.atherosclerosis.2011.09.003

Razani, B., Feng, C., Coleman, T., Emanuel, R., Wen, H., Hwang, S., Ting, J. P., Virgin, H. W., Kastan, M. B., & Semenkovich, C. F. (2012). Autophagy links inflammasomes to atherosclerotic progression. *Cell Metabolism*, *15*(4), 534–544. https://doi.org/10.1016/j.cmet.2012.02.011

Remmerie, A., & Scott, C. L. (2018). Macrophages and lipid metabolism. *Cellular Immunology*, *330*(February), 27–42. https://doi.org/10.1016/j.cellimm.2018.01.020

Ries, S., Büchler, C., Langmann, T., Fehringer, P., Aslanidis, C., & Schmitz, G. (1998). Transcriptional regulation of lysosomal acid lipase in differentiating monocytes is mediated by transcription factors Sp1 and AP-2. *Journal of Lipid Research*, *39*(11), 2125–2134.

Rohatgi, A., Patel, P., Das, S. R., Ayers, C. R., Khera, A., Martinez-Rumayor, A., Berry, J. D., McGuire, D. K., & De Lemos, J. A. (2012). Association of growth differentiation factor-15 with coronary atherosclerosis and mortality in a young, multiethnic population: Observations from the dallas heart study. *Clinical Chemistry*, *58*(1), 172–182. https://doi.org/10.1373/clinchem.2011.171926

Roma, P., Bernini, F., Fogliatto, R., Bertulli, S. M., Negri, S., Fumagalli, R., & Catapano, A. L. (1992). Defective catabolism of oxidized LDL by J774 murine macrophages. *Journal of Lipid Research*, *33*(6), 819–829.

Roma, P., Catapano, A. L., Bertulli, S. M., Varesi, L., Fumagalli, R., & Bernini, F. (1990). Oxidized LDL increase free cholesterol and fail to stimulate cholesterol esterification in murine macrophages. *Biochemical and Biophysical Research Communications*, *171*(1), 123–131. https://doi.org/10.1016/0006-291x(90)91365-y

Rosenfeld, M. E., Khoo, J. C., Miller, E., Parthasarathy, S., Palinski, W., & Witztum, J. L. (1991). Macrophage-derived foam cells freshly Isolated from rabbit atherosclerotic lesions degrade modified lipoproteins, promote oxidation of low-density lipoproteins, and contain oxidation-specific lipid-protein adducts. *Journal of Clinical Investigation*, *87*(1), 90–99. https://doi.org/10.1172/JCI115006

Ross, R., Glomset, J., & Harker, L. (1977). Response to injury and atherogenesis. *The American Journal of Pathology*, *86*(3), 675–684. Retrieved from http://www.ncbi.nlm.nih.gov/pubmed/842616

Rubinstein, A. D., Eisenstein, M., Ber, Y., Bialik, S., & Kimchi, A. (2011). The autophagy protein atg12 associates with antiapoptotic Bcl-2 family members to promote mitochondrial apoptosis. *Molecular Cell*, *44*(5), 698–709. https://doi.org/10.1016/j.molcel.2011.10.014

Ryter, S. W., Cloonan, S. M., & Choi, A. M. K. (2013). Autophagy: A critical regulator of cellular metabolism and homeostasis. *Molecules and Cells*, *36*(1), 7–16. https://doi.org/10.1007/s10059-013-0140-8

Schlittenhardt, D., Schober, A., Strelau, J., Bonaterra, G. A., Schmiedt, W., Unsicker, K., Metz, J., & Kinscherf, R. (2004). Involvement of growth differentiation factor-15/macrophage inhibitory cytokine-1 (GDF-15/MIC-1) in oxLDL-induced apoptosis of human macrophages in vitro and in arteriosclerotic lesions. *Cell and Tissue Research*, *318*(2), 325–333. https://doi.org/10.1007/s00441-004-0986-3

Schober, A., Bottner, M., Strelau, J., Kinscherf, R., Bonaterra, G. A., Barth, M., Schilling, L., Fairlie, W. D., Breit, S. N., & Unsicker, K. (2001). Expression of growth differentiation factor-15/macrophage inhibitory cytokine-1 (GDF-15/MIC-1) in the perinatal, adult, and injured rat brain. *Journal of Comparative Neurology*, *439*(1), 32–45.

Schwende, H., Fitzke, E., Ambs, P., & Dieter, P. (1996). Differences in the state of differentiation of THP-1 cells induced by phorbol ester and 1,25-dihydroxyvitamin D3. *Journal of Leukocyte Biology*, *59*(4), 555–561. Retrieved from http://www.ncbi.nlm.nih.gov/entrez/query.fcgi?db=pubmed&cmd=Retrieve&dopt=AbstractPlus&list_uids=8613704%5Cnpapers2://publication/uuid/47FAEFCF-2DEA-4A6F-B05D-E69A29C95E8C

Sergin, I., Bhattacharya, S., Emanuel, R., Esen, E., Stokes, C. J., Evans, T. D., Arif, B., Curci, J. A., & Razani, B. (2016). Inclusion bodies enriched for p62 and polyubiquitinated proteins in macrophages protect against atherosclerosis. *Science Signaling*, *9*(409), ra2–ra2. https://doi.org/10.1126/scisignal.aad5614

Sergin, I., Evans, T. D., Zhang, X., Bhattacharya, S., Stokes, C. J., Song, E., Ali, S., Dehestani, B., Holloway, K. B., Micevych, P. S., Javaheri, A., Crowley, J. R., Ballabio, A., Schilling, J. D., Epelman, S., Weihl, C. C., Diwan, A., … Razani, B. (2017). Exploiting macrophage autophagy-lysosomal biogenesis as a therapy for atherosclerosis. *Nature Communications*, *8*, 1–20. https://doi.org/10.1038/ncomms15750

Sergin, I., & Razani, B. (2014). Self-eating in the plaque: what macrophage autophagy reveals about atherosclerosis. *Trends in Endocrinology & Metabolism*, *25*(5), 225–234. https://doi.org/10.1016/j.tem.2014.03.010

Singh, R., & Cuervo, A. M. (2012). Lipophagy: Connecting Autophagy and Lipid Metabolism. *International Journal of Cell Biology*, *2012*, 1–12. https://doi.org/10.1155/2012/282041

Singh, R., Kaushik, S., Wang, Y., Xiang, Y., Novak, I., Komatsu, M., Tanaka, K., Cuervo, A. M., & Czaja, M. J. (2009). Autophagy regulates lipid metabolism. *Nature*, *458*(7242), 1131–1135. https://doi.org/10.1038/nature07976

Sohrabi, Y., Lagache, S. M. M., Schnack, L., Godfrey, R., Kahles, F., Bruemmer, D., Waltenberger, J., & Findeisen, H. M. (2019). mTOR-Dependent Oxidative Stress Regulates oxLDL-Induced Trained Innate Immunity in Human Monocytes. *Frontiers in Immunology*, *9*(JAN), 1–14. https://doi.org/10.3389/fimmu.2018.03155

Søreng, K., Neufeld, T. P., & Simonsen, A. (2018). Membrane Trafficking in Autophagy. In *International Review of Cell and Molecular Biology* (Vol. 336, pp. 1–92). https://doi.org/10.1016/bs.ircmb.2017.07.001

Tabas, I. (2002). Consequences of cellular cholesterol accumulation : Basic concepts and physiological implications *Journal of Clinical Investigation*, *110*(7), 905–911. https://doi.org/10.1172/JCI200216452.The

Tegos, T. J., Kalodiki, E., Sabetai, M. M., & Nicolaides, A. N. (2001). The genesis of atherosclerosis and risk factors: A review. *Angiology*, *52*(2), 89–98. https://doi.org/10.1177/000331970105200201

Tran, T., Yang, J., Gardner, J., & Xiong, Y. (2018). GDF15 deficiency promotes high fat diet-induced obesity in mice. *PLOS ONE*, *13*(8), e0201584. https://doi.org/10.1371/journal.pone.0201584

Tsai, V. W. W., Macia, L., Johnen, H., Kuffner, T., Manadhar, R., Jørgensen, S. B., Lee-Ng, K. K. M., Zhang, H. P., Wu, L., Marquis, C. P., Jiang, L., Husaini, Y., Lin, S., Herzog, H., Brown, D. A., Sainsbury, A., & Breit, S. N. (2013). TGF-b Superfamily Cytokine MIC-1/GDF15 Is a Physiological Appetite and Body Weight Regulator. *PLoS ONE*, *8*(2), 0–8. https://doi.org/10.1371/journal.pone.0055174

Tsai, V. W., Zhang, H. P., Manandhar, R., Lee-Ng, K. K. M., Lebhar, H., Marquis, C. P., Husaini, Y., Sainsbury, A., Brown, D. A., & Breit, S. N. (2018). Treatment with the TGF-b superfamily cytokine MIC-1/GDF15 reduces the adiposity and corrects the metabolic dysfunction of mice with diet-induced obesity. *International Journal of Obesity*, *42*(3), 561–571. https://doi.org/10.1038/ijo.2017.258

Tsuchiya, S., Yamabe, M., Yamaguchi, Y., Kobayashi, Y., Konno, T., & Tada, K. (1980). Establishment and characterization of a human acute monocytic leukemia cell line (THP-1). *International Journal of Cancer. Journal International Du Cancer*, *26*(2), 171–176. https://doi.org/10.1002/ijc.2910260208

Vasiliou, V., Vasiliou, K., & Nebert, D. W. (2009). Human ATP-binding cassette (ABC) transporter family. *Human Genomics*, *3*(3), 281–290. https://doi.org/10.1186/1479-7364-3-3-281

Vázquez, C. L., & Colombo, M. I. (2009). Chapter 6 Assays to Assess Autophagy Induction and Fusion of Autophagic Vacuoles with a Degradative Compartment, Using Monodansylcadaverine (MDC) and DQ-BSA. In *Methods in Enzymology* (Vol. 451, pp. 85–95). https://doi.org/10.1016/S0076-6879(08)03606-9

Verheye, S., Martinet, W., Kockx, M. M., Knaapen, M. W. M., Salu, K., Timmermans, J. P., Ellis, J. T., Kilpatrick, D. L., & De Meyer, G. R. Y. (2007). Selective Clearance of Macrophages in Atherosclerotic Plaques by Autophagy. *Journal of the American College of Cardiology*, *49*(6), 706–715. https://doi.org/10.1016/j.jacc.2006.09.047

Walsh, B. J., Gooley, A. A., Williams, K. L., & Breit, S. N. (1995). Identification of macrophage activation associated proteins by two-dimensional gel electrophoresis and microsequencing. *Journal of Leukocyte Biology*, *57*(3), 507–512. https://doi.org/10.1002/jlb.57.3.507

Wang, X., Li, L., Niu, X., Dang, X., Li, P., Qu, L., Bi, X., Gao, Y., Hu, Y., Li, M., Qiao, W., Peng, Z., & Pan, L. (2014). mTOR enhances foam cell formation by suppressing the autophagy pathway. *DNA and Cell Biology*, *33*(4), 198–204. https://doi.org/10.1089/dna.2013.2164

Williams, K. J., & Tabas, I. (1995). The response-to-retention hypothesis of early atherogenesis. *Arteriosclerosis, Thrombosis, and Vascular Biology*, *15*(5), 551–561. https://doi.org/10.1161/01.atv.15.5.551

Wollert, K. C., Kempf, T., & Wallentin, L. (2016). Growth Differentiation Factor 15 as a Biomarker in Cardiovascular Disease. *Clinical Chemistry*, *000*, 1–14. https://doi.org/10.1373/clinchem.2016.255174

Wu, J. F., Wang, Y., Zhang, M., Tang, Y. Y., Wang, B., He, P. P., Lv, Y. C., Ouyang, X. P., Yao, F., Tan, Y. L., Tang, S. L., Tang, D. P., Cayabyab, F. S., Zheng, X. L., Zhang, D. W., Zeng, G. F., & Tang, C. K. (2014). Growth differentiation factor-15 induces expression of ATP-binding cassette transporter A1 through PI3-K/PKC??/SP1 pathway in THP-1 macrophages. *Biochemical and Biophysical Research Communications*, *444*(3), 325–331. https://doi.org/10.1016/j.bbrc.2014.01.048

Xu, S., Huang, Y., Xie, Y., Lan, T., Le, K., Chen, J., Chen, S., Gao, S., Xu, X., Shen, X., Huang, H., & Liu, P. (2010). Evaluation of foam cell formation in cultured macrophages: an improved method with Oil Red O staining and DiI-oxLDL uptake. *Cytotechnology*, *62*(5), 473–481. https://doi.org/10.1007/s10616-010-9290-0

Xu, X., Pan, C., Yang, X., Zhou, L., Zheng, Z., & Li, D. (2018). SP1 reduces autophagic flux through activating p62 in gastric cancer cells. *Molecular Medicine Reports*, *17*(3), 4633–4638. https://doi.org/10.3892/mmr.2018.8400

Yancey, P. G., & Jerome, W. G. (1998). Lysosomal sequestration of free and esterified cholesterol from oxidized low density lipoprotein in macrophages of different species. *Journal of Lipid Research*, *39*(7), 1349–1361.

Yang, X., Wei, J., He, Y., Jing, T., Li, Y., Xiao, Y., Wang, B., Wang, W., Zhang, J., & Rong Lin, and. (2017). SIRT1 inhibition promotes atherosclerosis through impaired autophagy. *Oncotarget*, *8*(31), 51447–51461. https://doi.org/10.18632/oncotarget.17691

Ylä-Herttuala, S., Palinski, W., Rosenfeld, M. E., Parthasarathy, S., Carew, T. E., Butler, S., Witztum, J. L., & Steinberg, D. (1989). Evidence for the presence of oxidatively modified low density lipoprotein in atherosclerotic lesions of rabbit and man. *The Journal of Clinical Investigation*, *84*(4), 1086–1095. https://doi.org/10.1172/JCI114271

Yousefi, S., Perozzo, R., Schmid, I., Ziemiecki, A., Schaffner, T., Scapozza, L., Brunner, T., & Simon, H.-U. (2006). Calpain-mediated cleavage of Atg5 switches autophagy to apoptosis. *Nature Cell Biology*, *8*(10), 1124–1132. https://doi.org/10.1038/ncb1482

Yu, L., McPhee, C. K., Zheng, L., Mardones, G. A., Rong, Y., Peng, J., Mi, N., Zhao, Y., Liu, Z., Wan, F., Hailey, D. W., Oorschot, V., Klumperman, J., Baehrecke, E. H., & Lenardo, M. J. (2010). Termination of autophagy and reformation of lysosomes regulated by mTOR. *Nature*, *465*(7300), 942–946. https://doi.org/10.1038/nature09076

Yu, X. H., Fu, Y. C., Zhang, D. W., Yin, K., & Tang, C. K. (2013). Foam cells in atherosclerosis. *Clinica Chimica Acta*, *424*, 245–252. https://doi.org/10.1016/j.cca.2013.06.006

Zhang, Y.-L., Cao, Y.-J., Zhang, X., Liu, H.-H., Tong, T., Xiao, G.-D., Yang, Y.-P., & Liu, C.-F. (2010). The autophagy-lysosome pathway: a novel mechanism involved in the processing of oxidized LDL in human vascular endothelial cells. *Biochemical and Biophysical Research Communications*, *394*(2), 377–382. https://doi.org/10.1016/j.bbrc.2010.03.026

Zhou, F., Liu, D., Ning, H., Yu, X., & Guan, X. (2016). The roles of p62/SQSTM1 on regulation of matrix metalloproteinase-9 gene expression in response to oxLDL in atherosclerosis. *Biochemical and Biophysical Research Communications*, *472*(3), 451–458. https://doi.org/10.1016/j.bbrc.2016.01.065

Zhou, J., Tan, S. H., Nicolas, V., Bauvy, C., Yang, N. Di, Zhang, J., Xue, Y., Codogno, P., & Shen, H. M. (2013). Activation of lysosomal function in the course of autophagy via mTORC1 suppression and autophagosome-lysosome fusion. *Cell Research*, *23*(4), 508–523. https://doi.org/10.1038/cr.2013.11

Zhu, Y. N., Fan, W. J., Zhang, C., Guo, F., Li, W., Wang, Y. F., Jiang, Z. S., & Qu, S. L. (2017). Role of autophagy in advanced atherosclerosis (Review). *Molecular Medicine Reports*, *15*(5), 2903–2908. https://doi.org/10.3892/mmr.2017.6403

# 7 Appendix

## a. Data of two additional rGDF-15 concentrations on the ATG5, ATG12 / ATG5-complex and p62 protein level

Besides the concentrations of 1.0 µg/ml and 1.5 µg/ml rGDF-15, we also tested rGDF-15 in the concentration of 20 ng/ml and 2.0 µg/ml. Therefore, 2 µg/ml rGDF-15 was applied along with 1.0 or 1.5 µg/ml in the experimental setting depicted in Figure 4 B. Since 20 ng/ml rGDF-15 was tested along with transfected THP-1 MΦ (Figure 4 A), we exposed nsiGDF-15 MΦ to 20 ng/ml rGDF-15 with or without 50 µg/ml oxLDL for 4h and normalized against nsiGDF-15 MΦ exposed to medium alone. On the ATG5 protein level, rGDF-15 in the concentrations of 20 ng/ml or 2.0 µg/ml had no significant influence (Figure 27 A, D). On the ATG12 / ATG5-complex level, exposure to 2.0 µg/ml rGDF-15 / oxLDL significantly enhanced the complex build-up, compared to 2.0 µg/ml rGDF-15 alone (Figure 27 B). Though, 2.0 µg/ml rGDF-15 did not further amplify the ATG12 / ATG5-complex build-up upon oxLDL-exposure, compared to 1.5 µg/ml rGDF-15 co-incubated with oxLDL. 20 ng/ml rGDF-15 did not show any significant alterations in the ATG12 / ATG5 complex build up (Figure 27 E).

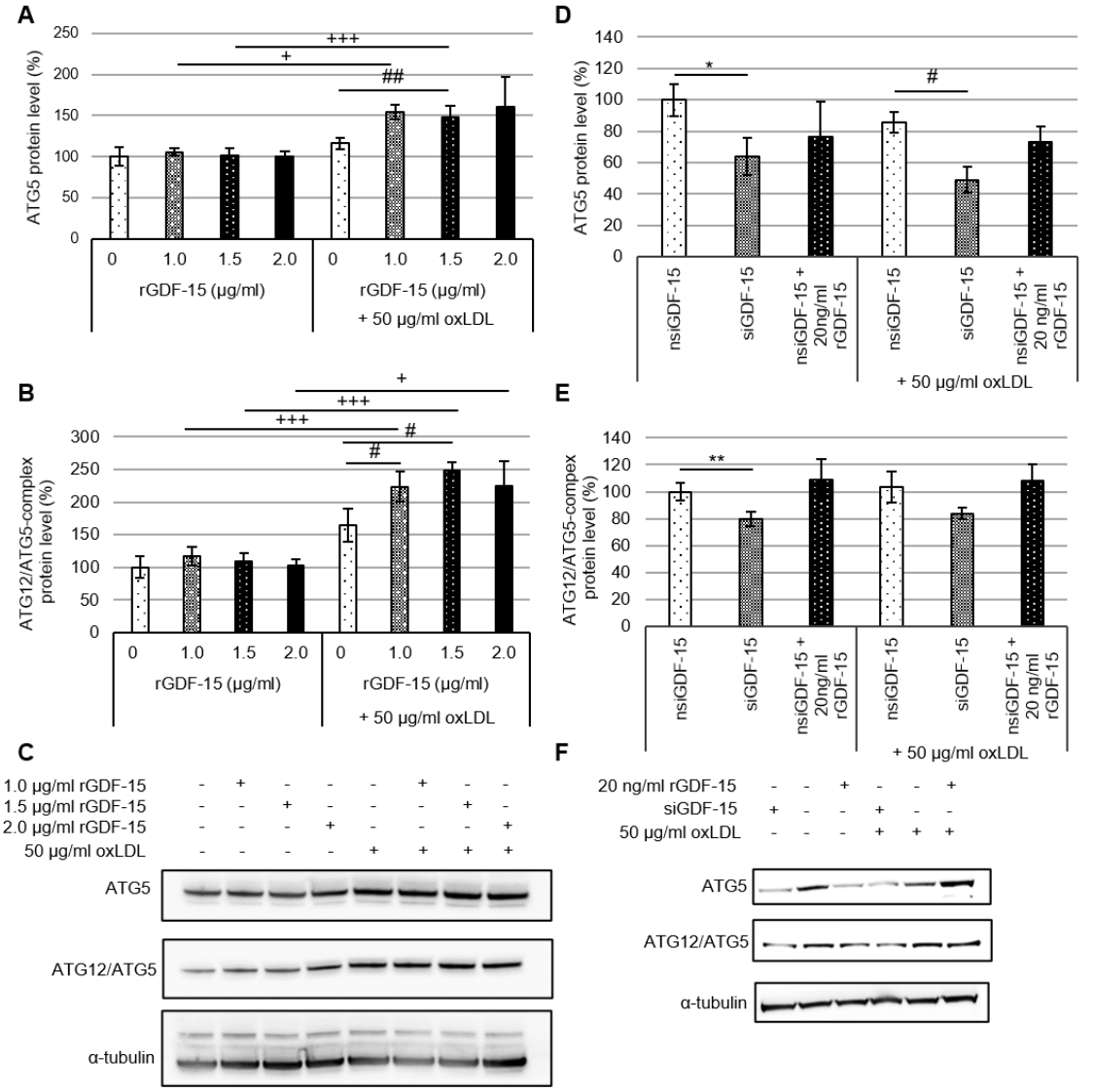


*Figure 27:* **ATG5 protein and ATG12 / ATG5-complex protein levels in THP-1 MΦ, nsiGDF-15 MΦ and siGDF-15 MΦ after exposure to rGDF-15 with / without oxLDL.** (A) ATG5 and (B) ATG12 / ATG5-complex protein levels (in % of THP-1 MΦ incubated in medium = 100%) in THP-1 MΦ. Expression was normalized against α-tubulin and quantified with ImageJ. (C) Representative Western Blot images for ATG5, ATG12 / ATG5-complex and α-tubulin. Six independent experiments are presented as mean ± SEM. $^{\#}p < 0.05$, $^{\#\#}p < 0.01$ significance vs. THP-1 MΦ + 50 µg/ml oxLDL, $^{+}p<0.05$, $^{+++}p < 0.01$ significance vs. THP-1 MΦ incubated without 50 µg/ml oxLDL. (D) ATG5 and (E) ATG12 / ATG5-complex protein levels (in % of nsiGDF-15 MΦ incubated in medium = 100%) in nsiGDF-15 / siGDF-15 THP-1 MΦ. ATG5 and ATG12 / ATG5-complex protein was normalized against α-tubulin and quantified with ImageJ. (F) Representative Western Blot images. Four independent experiments were performed. Data are presented as mean ± SEM. $^{*}p < 0.05$, $^{**}p < 0.01$ significance vs. nsiGDF-15 MΦ incubated in medium, $^{\#}p < 0.05$ significance vs. nsiGDF-15 MΦ + 50 µg/ml oxLDL. Student-Newman-Keuls test (ATG5) and Holm-Sidak test (ATG12 / ATG5-complex). Data published in Ackermann et al., 2019a.

On the p62 protein level, 2.0 µg/ml rGDF-15 had no significant influence (Figure 28 A). The p62 protein level was enhanced in nsiGDF-15 MΦ exposed to 20 ng/ml rGDF-15 / 50 µg/ml oxLDL, compared to nsiGDF-15 MΦ exposed to 20 ng/ml rGDF-15 alone (Figure 28 C). This observed significance is more likely caused by oxLDL, than by 20 ng/ml rGDF-15. Based on these observations, we decided to not further persue to investigate the influence of rGDF-15 in the concentations of 20 ng/ml and 2.0 µg/ml.

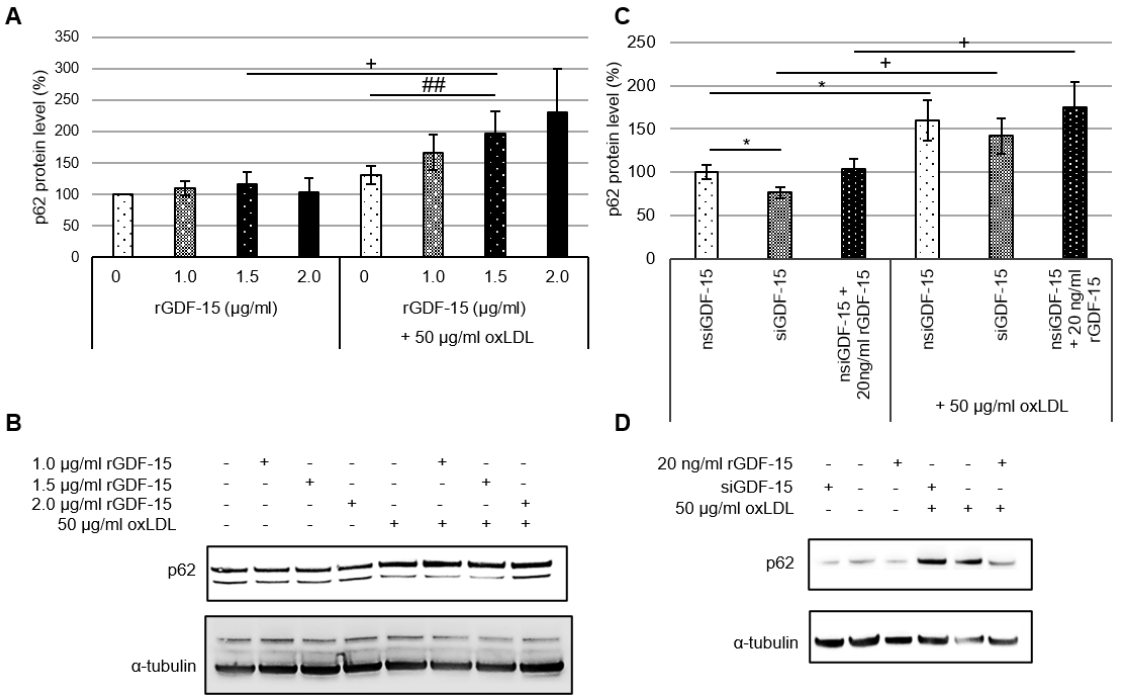


*Figure 28:* **p62 protein level in THP-1 MΦ, nsiGDF-15 MΦ and siGDF-15 MΦ after exposure to rGDF-15 with / without oxLDL.** (A) Total p62 protein level (in % of THP-1 MΦ incubated in medium = 100%) in THP-1 MΦ. Expression was normalized against α-tubulin and quantified with ImageJ. Six independent experiments were performed (B) Representative Western Blot images for p62 and α-tubulin. Data are presented as mean ± SEM. $^{\#\#}p < 0.01$ significance vs. THP-1 MΦ + 50 µg/ml oxLDL, $^{+}p < 0.05$ significance vs. THP-1 MΦ incubated without 50 µg/ml oxLDL. Student-Newman-Keuls test (C) p62 protein level (in % of nsiGDF-15 MΦ incubated in medium = 100%) in nsiGDF-15 / siGDF-15 THP-1 MΦ. Expression was normalized against α-tubulin and quantified with ImageJ. Nine independent experiments were performed. (D) Representative Western Blot images for p62 and α-tubulin. Data are presented as mean ± SEM. $^{*}p < 0.05$ significance vs. nsiGDF-15 MΦ incubated in medium, $^{+}p < 0.05$, significance vs. siGDF-15 MΦ or nsiGDF-15 + 20 ng/ml rGDF-15 incubated without oxLDL. Student-Newman-Keuls test. Data published in Ackermann et al., 2019a.

## b. Verzeichnis der akademischen Lehrer/-innen

1. Bachelorstudiengang Biowissenschaften an der Goethe-Universität Frankfurt am Main

Meine akademischen Lehrenden in Frankfurt am Main waren folgende Damen und Herren

- Auerhoff
- Auner
- Brüggemann
- Büchel
- Droba
- Engels
- Entian
- Gaese
- Grünewald
- Herteler
- Jacoby
- Klussmann-Kolb
- Kössl
- Merker
- Müller
- Oehlmann
- Osiewacz
- Plath
- Podlech
- Prinzinger
- Russ
- Scharf
- Schleiff
- Schmidt
- Schrenk
- Soppa
- Starzinski-Powitz
- Streit
- Thalau
- Tiede
- Türkay
- Volknandt
- Wiltschko
- Wittig

2. Masterstudiengang Humanbiologie mit Schwerpunkt Zellbiologie an der Philipps-Universität Marburg

Meine akademischen Lehrenden in Marburg waren folgende Damen und Herren

- Elsässer
- Greene
- Hänze
- Jakob
- Kinscherf
- Lauth
- Lill
- Mandic
- Pankuweit
- Wanzel
- Yu
- Wittig

## c. Danksagung

Ich bedanke mich ganz herzlich bei Prof. Dr. Ralf Kinscherf für die Möglichkeit die Dissertation in seiner Arbeitsgruppe zu schreiben, für die Bereitstellung eines so spannenden Themas und seine Unterstützung während der gesamten Bearbeitungsphase.

Besonderer Dank gilt Dr. Anja Schwarz für die exzellente Betreuung. Danke für die Hilfestellung bei methodischen und inhaltlichen Fragen, die konstruktiven und lehrreichen Gespräche, die Geduld und vor allem für die zahlreichen motivierenden Worte.

Bei Andrea Cordes, Nadine Heinrich, Elke Völck-Badouin und Claudia Keppler bedanke ich mich für die Unterstützung im Labor. Bei allen Fragen habt Ihr mir immer weitergeholfen und auch häufig mit Zellen ausgeholfen.

Der gesamten Arbeitsgruppe danke ich für die Unterstützung und Hilfsbereitschaft. Ich habe mich sehr wohl bei Euch gefühlt und gerne mit Euch zusammengearbeitet.

Besonderer Dank gilt meinen Eltern, die mich in allem was ich tue immer unterstützt haben.

Danke an Manuel für seine Geduld, seine Office-Kenntnisse und das gemeinsame Lachen.